Journal of Paleontology, page 1 of 42

0022-3360/19/1937-2337
doi: 10.1017/jpa.2018.95

JOURNAL OF PALEONTOLOGY
A PUBLICATION OF THE Paleontological SOCIETY

New small-bodied ornithopods (Dinosauria, Neornithischia) from the Early Cretaceous Wonthaggi Formation (Strzelecki Group) of the Australian-Antarctic rift system, with revision of *Qantassaurus intrepidus* Rich and Vickers-Rich, 1999

Matthew C. Herne,[1,2] Jay P. Nair,[2] Alistair R. Evans,[3] and Alan M. Tait[4]

[1]School of Environmental and Rural Science, University of New England, Armidale 2351, New South Wales, Australia <ornithomatt@gmail.com>
[2]School of Biological Sciences, The University of Queensland, Brisbane, Queensland 4072, Australia <jayraptor@gmail.com>
[3]School of Biological Sciences, Monash University, Melbourne, Victoria 3800, Australia <alistair.evans@monash.edu>
[4]School of Earth, Atmosphere & Environment, Monash University, Melbourne, Victoria 3800, Australia <alan.tait@monash.edu>

Abstract.—The Flat Rocks locality in the Wonthaggi Formation (Strzelecki Group) of the Gippsland Basin, southeastern Australia, hosts fossils of a late Barremian vertebrate fauna that inhabited the ancient rift between Australia and Antarctica. Known from its dentary, *Qantassaurus intrepidus* Rich and Vickers-Rich, 1999 has been the only dinosaur named from this locality. However, the plethora of vertebrate fossils collected from Flat Rocks suggests that further dinosaurs await discovery. From this locality, we name a new small-bodied ornithopod, *Galleonosaurus dorisae* n. gen. n. sp. from craniodental remains. Five ornithopodan genera are now named from Victoria. *Galleonosaurus dorisae* n. gen. n. sp. is known from five maxillae, from which the first description of jaw growth in an Australian dinosaur is provided. The holotype of *Galleonosaurus dorisae* n. gen. n. sp. is the most complete dinosaur maxilla known from Victoria. Micro-CT imagery of the holotype reveals the complex internal anatomy of the neurovascular tract and antorbital fossa. We confirm that *Q. intrepidus* is uniquely characterized by a deep foreshortened dentary. Two dentaries originally referred to *Q. intrepidus* are reassigned to *Q.* ?*intrepidus* and a further maxilla is referred to cf. *Atlascopcosaurus loadsi* Rich and Rich, 1989. A further ornithopod dentary morphotype is identified, more elongate than those of *Q. intrepidus* and *Q.* ?*intrepidus* and with three more tooth positions. This dentary might pertain to *Galleonosaurus dorisae* n. gen. n. sp. Phylogenetic analysis recovered Cretaceous Victorian and Argentinian nonstyracosternan ornithopods within the exclusively Gondwanan clade Elasmaria. However, the large-bodied taxon *Muttaburrasaurus langdoni* Bartholomai and Molnar, 1981 is hypothesised as a basal iguanodontian with closer affinities to dryomorphans than to rhabdodontids.

UUID: http://zoobank.org/4af87bb4-b687-42f3-9622-aa806a6b4116

Introduction

A rich assemblage of isolated body fossils and rare associated skeletal remains of small-bodied ornithopods has been recovered from Early Cretaceous rocks of the Australian-Antarctic rift system, strata of which crop out in sea cliffs and wave-cut shore platforms along the southern coast of Victoria, southeastern Australia (Fig. 1.1, 1.2). Four small-bodied ornithopods have been named from this region, including *Atlascopcosaurus loadsi* Rich and Rich, 1989, *Leaellynasaura amicagraphica* Rich and Rich, 1989, and *Diluvicursor pickeringi* Herne et al., 2018, all of which are from the lower Albian of the Eumeralla Formation in the Otway Basin (Fig. 1.2); and *Qantassaurus intrepidus* Rich and Vickers-Rich, 1999 from the Wonthaggi Formation in the Gippsland Basin (Fig. 1.2), which has been considered Valanginian–middle Barremian in age (Wagstaff and McEwen Mason, 1989). Of these four taxa, *Atlascopcosaurus loadsi*, *L. amicagraphica*, and *Q. intrepidus* are known from craniodental remains, whereas *Diluvicursor pickeringi* is known from a partial postcranium.

In addition to the named Victorian taxa, several isolated femora from the Eumeralla and Wonthaggi formations were referred to *Fulgurotherium australe* von Huene, 1932 (Rich and Rich, 1989; Rich and Vickers-Rich, 1999), a femoral-based taxon from the Albian Griman Creek Formation in the Lightning Ridge region of northern New South Wales (Molnar and Galton, 1986). However, *Fulgurotherium australe* has been reassessed as a nomen dubium (Agnolin et al., 2010). Another femur (NMV P156980) collected from Cape Paterson in the Wonthaggi Formation (Fig. 1.2), approximately double the size of the largest Victorian femora assigned to *Fulgurotherium australe* (see Rich and Vickers-Rich, 1999; Herne, 2014), was informally termed 'Victorian Hypsilophodontid Femur Type 2' (Rich and Rich, 1989).

Excavated at the Slippery Rock site at the fossil vertebrate locality of Dinosaur Cove (Fig. 1.2), the holotype of *Leaellynasaura*

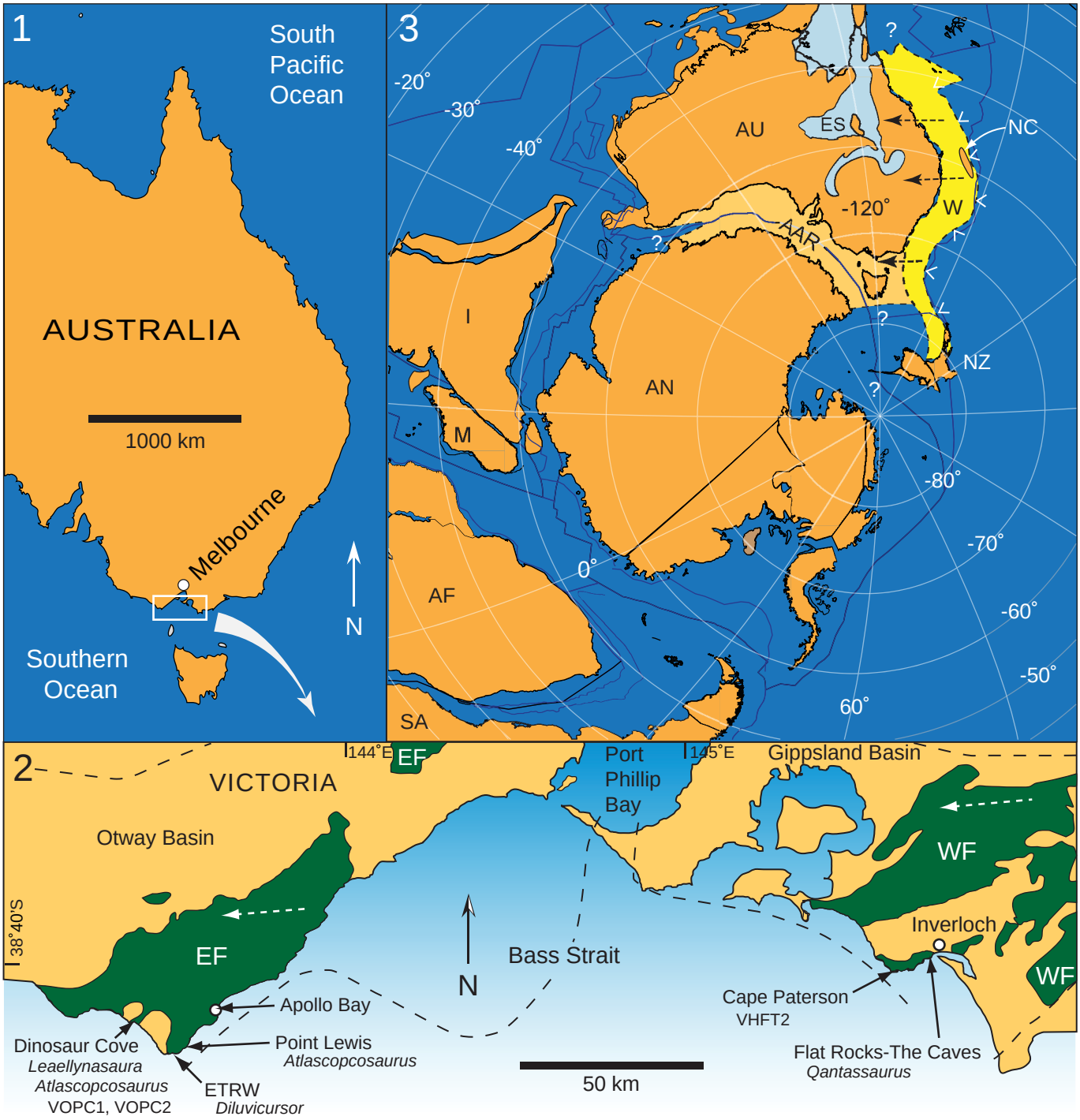

Figure 1. Maps of Australia, southern Victoria and Gondwana: (**1**) present-day eastern Australia indicating region of interest; (**2**) inset from (**1**) showing upper Barremian–lower Albian ornithopod localities and associated geology; (**3**) reconstruction of Gondwana during the late Barremian (~ 125 Ma) using GPlates (www.gplates.org). Dashed lines in (**2**) indicate basin boundaries. Geological information in (**2**) based on Bryan et al. (1997, 2000). V-shaped symbols in (**3**) indicate direction and position of plate subduction, based on Wandres and Bradshaw (2005). Australian paleoshoreline in (**3**) based on Heine et al. (2015). Dashed arrows in (**2–3**) indicate paleoflow direction. AAR = Australian-Antarctic rift; AF = Africa; AN = Antarctica; AU = Australia; I = India; EF = Eumeralla Formation; ES = epeiric Eromanga Sea (in region of Eromanga Basin); ETRW = Eric the Red West; M = Madagascar; NC = New Caledonia; NZ = New Zealand; SA = South America; VHFT2 = Victorian Hypsilophodontid Femur Type 2; VOPC1 = Victorian ornithopod postcranium 1 (NMV P185992/P185993); VOPC2 = Victorian ornithopod postcranium 2 (NMV P186047); W = Whitsunday Large Siliceous Igneous Province (Bryan et al., 1997); WF = Wonthaggi Formation.

amicagraphica (NMV P185991) comprises a left-side cheek fragment of a juvenile individual, including the maxilla (Rich and Rich, 1989) but lacks a dentary. A cranial table (NMV P185990) and two partial postcranial specimens (NMV P185992, P185993; confirmed as belonging to a single individual; Herne, 2009; Herne et al., 2016, fig. 5) were originally referred to *L. amicagraphica*, as scattered parts of the holotypic individual (Rich and Rich, 1989; Rich and Vickers-Rich, 2000). However,

https://doi.org/10.1017/jpa.2018.95

these referrals have also been questioned (Herne et al., 2016). For this reason, the referrals of several isolated femora and another partial postcranium (NMV P186047) to *L. amicagraphica* from Dinosaur Cove (sensu Rich and Rich, 1989; Rich and Vickers-Rich, 1999; Rich et al., 2010) have also been questioned (Herne et al., 2016).

Discovered at the locality of Point Lewis in the Eumeralla Formation (Fig. 1.2), the holotype of *Atlascopcosaurus loadsi* (NMV P166409) consists of a partial left maxillary fragment. In addition to the *Atlascopcosaurus loadsi* holotype, another left maxillary fragment from Point Lewis (NMV P157390), as well as a left maxillary fragment (NMV P157970) and several isolated maxillary teeth from Dinosaur Cove, were also referred to the taxon. Two isolated dentary fragments (NMV P182967, P186847) and two isolated dentary teeth (notably NMV P177934) were also referred to *Atlascopcosaurus loadsi* (Rich and Rich, 1989; see also Herne et al., 2016). However, because none of these *Atlascopcosaurus loadsi*-referred dentary and dentary tooth specimens were found in association with a maxilla, we consider these assignments inconclusive.

Discovered at the locality of Eric the Red West in the Eumeralla Formation (Fig. 1.2), *Diluvicursor pickeringi* comprises the holotypic partial hind-region postcranium (NMV P221080) and a referred, isolated caudal vertebra (Herne et al., 2018). With future discoveries, this taxon could be found synonymous with any one of the Victorian taxa previously named from craniodental remains. However, the significance of *Diluvicursor pickeringi* as a rare, articulated Australian ornithopod skeleton, clearly differing from two other partial postcrania from the Eumeralla Formation (i.e., NMV P185992/P185993, P186047), were considered by Herne et al. (2018) as justification for erecting the taxon.

Discovered during excavations at the Flat Rocks site in the Wonthaggi Formation (Figs. 1.2, 2), *Qantassaurus intrepidus* is known from the three isolated dentaries (Rich and Vickers-Rich, 1999)—that of the holotype (NMV P199075) and two additional specimens (NMV P198962, P199087). Originally referred to Hypsilophodontidae, the *Q. intrepidus* dentary was diagnosed by a combination of three features: possession of 10 cheek teeth; foreshortened morphology; and anteriorly convergent dorsal and ventral margins (sensu Rich and Vickers-Rich, 1999). Agnolin et al. (2010) reassessed *Q. intrepidus* as a non-dryomorphan ornithopod, agreeing that the foreshortened dentary with anteriorly convergent alveolar and ventral margins presented a combination of features that distinguished *Q. intrepidus* from other ornithopods.

A plethora of isolated body fossils have been collected from the Flat Rocks site, which among the dinosaur materials, some have been identified as ankylosaurian, avian, and nonavian theropodan bones and teeth (Close et al., 2009; Barrett et al., 2010; Benson et al., 2012; see also Poropat et al., 2018). However, *Qantassaurus intrepidus* has been the only ornithopod named from the Wonthaggi Formation. The partial maxilla of an ornithopod (NMV P186440) was further reported by Rich and Vickers-Rich (1999) from a cliffed coastal headland site called The Caves ~200 m from the Flat Rocks excavations (Figs. 1.2, 2). However, Rich and Vickers-Rich (1999) were uncertain whether NMV P186440 was assignable to *Atlascopcosaurus loadsi* or *Q. intrepidus*. In this investigation, we describe new craniodental materials of ornithopods from the Flat Rocks locality (=Flat Rocks and The Caves sites), revise *Q. intrepidus*, reassess the diversity and phylogenetic relationships of the Victorian ornithopods, and update the distribution of Australian ornithopods.

Geological setting

Most of the specimens of interest to this investigation were collected from the Flat Rocks site (=Dinosaur Dreaming Field Site; Seegets-Villiers, 2012), which consists of a series of ~1 m deep excavations on the coastal, wave-eroded rock platform within the Bunurong Marine National Park, 2.2 km southwest of the town of Inverloch in Victoria, southeastern Australia (38.660792°S, 145.681009°E, GDA94 [Intergovernmental Committee on Surveying and Mapping, 2014]; Seegets-Villiers, 2012), ~112 km southeast of the city of Melbourne (Figs. 1–2). One additional specimen (NMV P186440; reported by Rich and Vickers-Rich, 1999) discovered in a large boulder that had fallen from the sea cliff at The Caves (38.662792°S, 145.680108°E, Map Grid of Australia, 1994; see also Kool, 2010, p. 60), ~230 m southwest of the Flat Rocks site (Figs. 1.2, 2) is also of interest to this study. The Flat Rocks site is located within the undifferentiated upper section of the Strzelecki Group in the Gippsland Basin (see Tosolini et al., 1999), which has been informally termed the Wonthaggi Formation (Constantine and Holdgate, 1993; see also Chiupka, 1996), the name used herein (Fig. 1.2).

The predominantly volcanogenic sediments of the Wonthaggi and Eumeralla formations (Fig. 1.2) in the Gippsland and Otway basins, respectively, were deposited during the Early Cretaceous as thick (to 3,000 m) depocenters within the extensional rift valley that formed between Australia and Antarctica, coinciding with the fragmentation of Gondwana (Willcox and Stagg, 1990; Bryan et al., 1997; Tosolini et al., 1999; Hall and Keetley, 2009). The Gippsland and Otway basins, however, are most likely a single basin system (VandenBerg et al., 2006). The sediments were sourced from the Whitsunday Silicic Large Igneous Province (WSLIP) that was situated along the eastern margin of the Australian Plate (Bryan et al., 1997; Bryan, 2007; Fig. 1.3). In addition, quartzose grit and gravel admixtures were sourced from older basement rocks that formed the rift margins (based on Felton, 1997). The Wonthaggi Formation has been described as comprising multistorey sheet-flood to braided river-like fluvial channel complexes to 200 m thick, interspersed with overbank sequences up to 100 m thick (Bryan et al., 1997). However, new research (unpublished data, Tait, Hall, and Herne, 2018) further suggests that the Wonthaggi and Eumeralla formations could be the product of a large-scale meandering river system with associated vegetated flood plains.

Sediments at the Flat Rocks site (Fig. 2) comprise interbedded volcaniclastic sandstones and mudstone conglomerates within the basal meter of a fluvial sandbody ~24 m thick (see also Seegets-Villiers, 2012). This sandbody is hereafter termed the 'Flat Rocks Sandstone.' The erosive base of the Flat Rocks Sandstone has a relief of ~0.5 m at the dig site, cut into thinly interbedded mudstones and very fine-grained sandstones, thin coals, and paleosols with in situ tree stumps deposited on a fluvial floodplain (see also Seegets-Villiers, 2012). The fossil-bearing sandstones and conglomerates also contain copious

https://doi.org/10.1017/jpa.2018.95

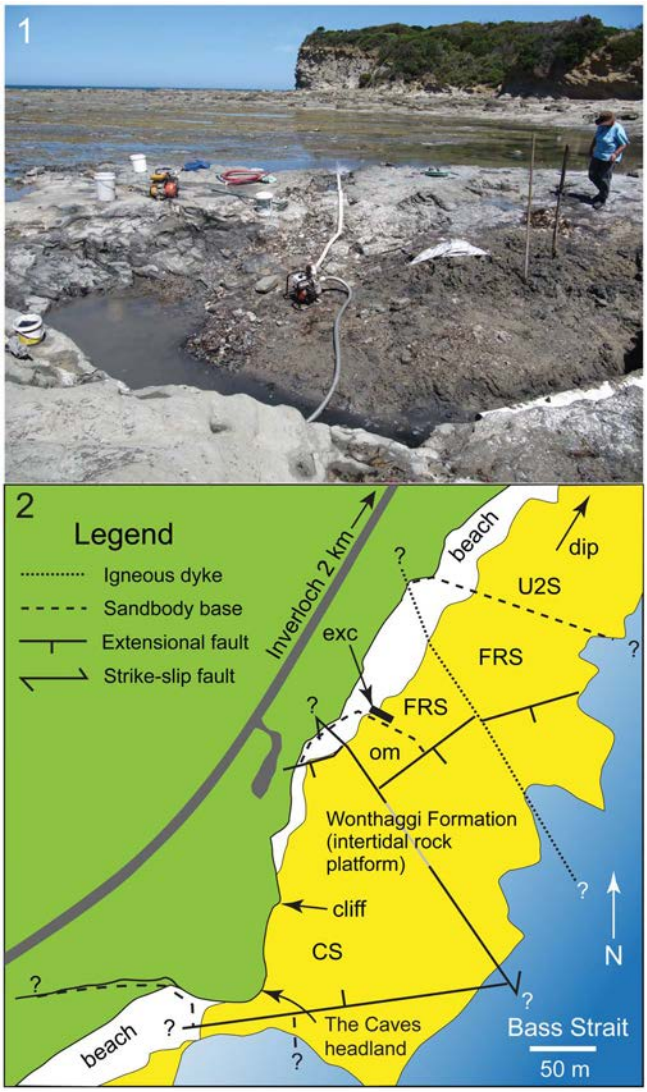

Figure 2. Flat Rocks locality in the Bunurong Marine National Park of the Strzelecki region, Victoria, southeastern Australia: (**1**) view looking southwest showing the Flat Rocks excavation (foreground), wave eroded rock platform (midground), and The Caves headland (background), which is ~ 230 m southwest of the Flat Rocks excavation; (**2**) map showing site positions, topographic and geostructural features, and estimated boundaries of sandstone units. ? = unknown extension of feature; CS = The Caves Sandstone; exc = excavations; FRS = Flat Rocks Sandstone; om = overbank mudstone; U2S = Unit 2 Sandstone.

fossilized plant fragments up to small log-sized, which are now coalified and flattened, as well as contemporaneous charcoal (see also Seegets-Villiers, 2012). The mudstone clasts range to cobble-size and include pale gray types, lithologically identical to the paleosol mudstones, and pale brown types thought to represent riverbank or abandoned channel deposits. The brown mudstone contains freshwater bivalve shell fossils, including two unionoidean species (Thompson and Stilwell, 2010). The bedding within the sandbody becomes thinner upward and the grain size becomes finer starting from medium to coarse sand at the unit base. Thus, the Flat Rocks Sandstone is potentially a single storey unit deposited by lateral accretion of a meandering river >24 m deep (considering postdepositional compaction). The fossil-bearing sediments were deposited as bedload by high-speed flow at the base of the river, with the alignment of elongate plant fragments and prograding bedforms indicating a local current direction toward ~240° (sensu Seegets-Villiers, 2012, fig. 2.12). The boulders at the foot of the cliffed headland site (The Caves; Fig. 2) result from undercutting of the cliff by waves, or from weathering. The sandstone at The Caves could be a down-faulted section of the Flat Rocks Sandstone, although this assessment has yet to be verified. However, for the purposes of this investigation, we informally term the unit in this region 'The Caves Sandstone' (Fig. 2).

Detailed taphonomic investigation of the fossil vertebrate remains from the Flat Rocks site was conducted by Seegets-Villiers (2012). The specimens consist of isolated, reworked, multispecific whole bones and bone fragments that accumulated under conditions of in-channel hydraulic flow on low-angle prograding bedforms on the channel floor. Many bones from the locality had been subject to surficial weathering, possibly including heating and charring by fire (Seegets-Villiers, 2012). Various degrees of in-channel abrasion suggest the bones differed in periods of transport, with some undergoing multiple stages of reworking (Seegets-Villiers, 2012). Thus, the accumulation can be considered time-averaged (e.g., Behrensmeyer, 1982). Most of the vertebrate fossils in this deposit comprise disassociated bones and bone fragments. However, NMV P186440—collected at The Caves site and reported by Rich and Vickers-Rich (1999, fig. 2) as a maxilla—constitutes an associated cranial fragment, rarely found in Victoria.

Palynological work previously suggested that the region of the Wonthaggi Formation encompassing the Flat Rocks locality was middle Valanginian–middle Barremian in age (following Wagstaff and McEwen Mason, 1989). However, renewed palynological investigations (personal communication, B. Wagstaff, 2018) suggest that the Flat Rocks locality falls within the upper part of the *Foraminisporis wonthaggiensis* (Cookson and Dettmann, 1958) spore-pollen zone of Helby et al. (1987), indicating a late Barremian age (~125–127.2 Ma, following Cohen et al., 2013). Using GPlates (v. 2.0.0; www.gplates.org), the position of the Flat Rocks locality at 125 Ma is estimated at ~72°S, 119°E (Fig. 1.3).

Materials and methods

Craniodental remains of ornithischians from the collections of Museums Victoria (NMV) and other comparative materials (Table S1) were examined first-hand in this investigation, from which new assignments were made and the diversity and phylogenetic relationships of the Victorian ornithopods were revised. The specimens were documented using digital photography, vernier callipers, and a microscope-mounted camera-lucida attachment. New NMV specimens were mechanically prepared (by L. Kool, Monash University, and D. Pickering, Museums Victoria). Additional anatomical data and imagery for the maxilla NMV P229196 utilized micro-Computed Tomography (μCT) scans (Zeiss Xradia XRM Versa520 X-Ray Microtomography: voxel size 45.61 μm; power 10 W; voltage 140 kV). The scans were digitally modelled and volume-rendered using Avizo software, v. 9 (FEI, Berlin). The production of figures utilized Adobe Illustrator and Photoshop software, CS4 (www.adobe.com). Nomenclature for the dentition used in the Systematic paleontology section and phylogenetic dataset is outlined in

https://doi.org/10.1017/jpa.2018.95

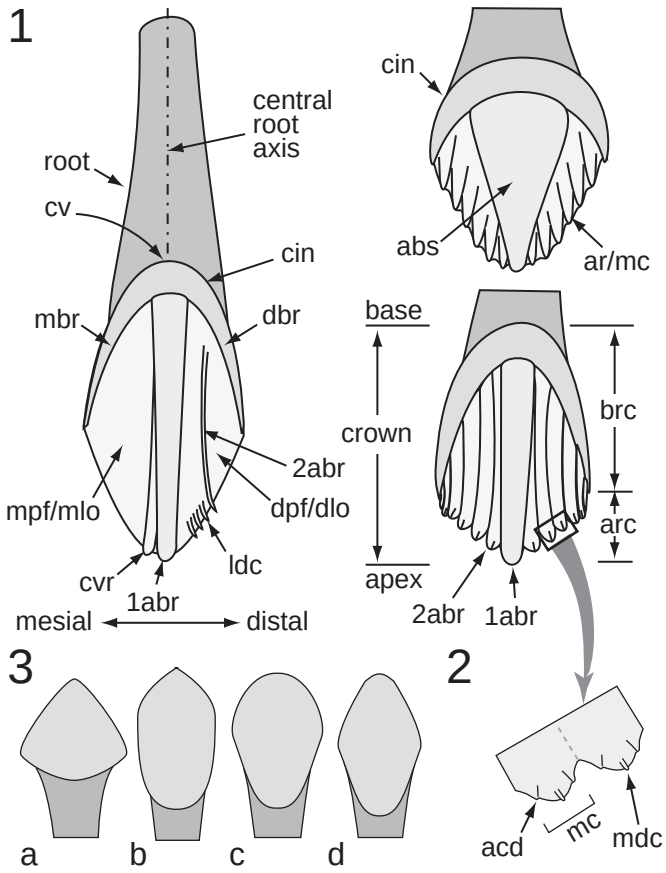

Figure 3. Ornithischian dental nomenclature: (**1**) crown ornamentation features; (**2**) portion of crown surface indicated by large arrow in (**1**), showing location of accessory denticles relative to the median denticle on the apical cusp (typically lingual maxillary and labial dentary faces); (**3**) variation in crown shape: subtriangular (a), urn-shaped (b), spatulate (c), and rhomboidal/lanceolate (d). 1abr = primary apicobasal ridge; 2abr = secondary apicobasal ridge; abs = apicobasal swelling; acd = accessory denticle; ar = apical ridge; arc = apical region of crown; brc = basal region of crown; cin = cingulum (= dbr + mbr); cv = cingular vertex; cvr = convergent (accessory) ridge; dbr = distal bounding ridge; dlo = distal lobe; dpf = distal paracingular fossa; ldc = lingulate denticle; mbr = mesial bounding ridge; mc = mamillated cusp; mdc = median denticle; mlo = mesial lobe; mpf = mesial paracingular fossa.

Figure 3 and Table 1. The phylogenetic relationships of the Australian taxa of interest were hypothesized from a cladistic analysis using TNT 1.5 (Goloboff and Catalano, 2016). The Systematic paleontology section follows the phylogenetic framework resulting from the cladistic analysis, and referrals in open nomenclature follow the criteria of Bengston (1988). The phylogenetic definitions of clades predominantly follow Madzia et al. (2018; see Text S1) and the relative stratigraphic ages of taxa of interest are provided in Text S1.

Repository and institutional abbreviations.—CD = New Zealand Geological Survey Collection, Lower Hutt, New Zealand; CM = Carnegie Museum of Natural History, Pittsburgh, Pennsylvania, USA; MB.R. = Collection of Fossil Reptilia, Museum für Naturkunde, Berlin, Germany; MCF-PVPH = Museo Carmen Funes-Paleontología de Vertebrados, Plaza Huincul, Neuquén Province, Argentina; MUCPv = Museo de Geologia y Paleontologia de la Universidad Nacional del Comahue, Paleontologia de Vertebrados, Neuquén Province, Argentina; NMV = Museums Victoria, Melbourne, Victoria, Australia; NHMUK = The Natural History Museum, London, UK; QM = Queensland Museum, Brisbane, Queensland, Australia; RBINS = Royal Belgian Institute of Natural Sciences, Brussels, Belgium; SAM-PK = South African Museum (Karoo Palaeontology collection), Cape Town, South Africa; UBB = Catedra de Geologie, Facultatea de Biologie şi Geologie, Universitatea din Babes-Bolyai, Cluj-Napoca, Romania; YPM VP = Yale Peabody Museum (Vertebrate Paleontology), New Haven, Connecticut, USA.

Systematic paleontology

Dinosauria Owen, 1842
Ornithischia Seeley, 1888
Neornithischia Cooper, 1985
Cerapoda Sereno, 1986
Ornithopoda Marsh, 1881
Genus *Galleonosaurus* new genus

Type species.—*Galleonosaurus dorisae* n. gen. n. sp., by monotypy.

Diagnosis.—As for the type species.

Etymology.—From *galleon* (Latinization of the English for a type of large sailing ship) + *saurus* (New Latin from the Greek *sauros* for lizard), in reference to the appearance of the maxilla to the upturned hull of a galleon.

Occurrence.—Flat Rocks locality in the Inverloch region of Victoria, southeastern Australia (Fig. 1); Flat Rocks Sandstone and The Caves Sandstone, upper Barremian of the Wonthaggi Formation in the Gippsland Basin.

Remarks.—Prior to the recognition of *Galleonosaurus* n. gen., *Atlascopcosaurus loadsi* and *Leaellynasaura amicagraphica* were the only Victorian ornithopods identified from maxillary remains (Rich and Rich, 1989). The maxillae of *Atlascopcosaurus loadsi* are highly incomplete and the only known maxilla of *L. amicagraphica* (that of the holotype, NMV P185991) is damaged, and due to its diminutive size, difficult to study. The maxillae of *Galleonosaurus* n. gen., as well as the complete palatine and fragment of the lacrimal, now provide new information from which the anatomy of the other Victorian ornithopods can be better understood. The holotype of *Galleonosaurus dorisae* n. gen. n. sp. (NMV P229196) represents the most complete maxilla of a dinosaur currently known from Victoria.

Galleonosaurus dorisae new species
Figures 4–8, 10–13, 15–16, 17.4; Table 2

Holotype.—NMV P229196, a complete left maxilla with partial dentition.

Diagnosis.—Small-bodied, noniguanodontian ornithopod characterized by five potential autapomorphies: (1) ascending ramus of maxilla has two slot-like foramina on the anterior

https://doi.org/10.1017/jpa.2018.95

Table 1. Terminology used for ornithischian cheek tooth crown descriptions.

Morphology (abbreviation)	Description
Accessory (apicobasal) ridge	All full apicobasal ridges on the labial and lingual crown surfaces, equivalent to secondary ridges (2abr) when a primary ridge (1abr) is present.
Accessory denticle (adc)	Denticle on an apicobasal ridge mesial or distal to the central apical denticle and contributing to a multidenticulate cusp.
Apical region of crown (arc)	Region of the crown apical to the marginal bounding ridges.
Apical ridge	Marginal ridge terminating in a mamillated tip, failing to extend to the crown base or marginal bounding ridge, and typically merging with the crown surface.
Apicobasal ridge (abr)	Ridge extending from the crown apex to the base, but not specifically definable as primary, secondary, or tertiary.
Apicobasal swelling (abs)	Prominent ridge markedly expanding in the basal direction. Crowns with apicobasal swelling typically lack full apicobasal ridges.
Basal region of crown (brc)	Region of the crown defined by the marginal bounding ridges.
Cingular vertex (cv)	Point of merger of the mesial and distal bounding ridges, or where the marginal bounding ridges are absent, the basalmost point of the cingulum.
Cingulum (cin)	Swollen region of the crown base distinguishing the enamelled crown from the root. On some crowns, the surface of the cingulum can merge with the root. The cingulum can be formed from the two marginal bounding ridges, however on some crown surfaces (e.g., the lingual surfaces of maxillary crowns), marginal bounding ridges might not be developed.
Convergent apicobasal ridge (cvr)	Secondary ridge converging with a margin of the primary ridge in the basal direction.
Denticle (dcl)	A cusp or fine ridge (can be transverse and blade-like) formed at the apical termination of a marginal ridge or apicobasal ridge, or projecting from the surface of a ridge.
Distal bounding ridge (dbr)	Distal marginal ridge of the cingulum.
Distal paracingular fossa (dpf)/mesial lobe (dlo)	Fossa forming a channel on the crown lobe distal to the primary ridge and bordered by the distal bounding ridge.
Lingulate denticle (ldc)	Tongue-shaped marginal denticle that can be supported or unsupported by an accessory apicobasal ridge, and can be formed on the mesial and distal bounding ridges.
Mesial bounding ridge (mbr)	Mesial marginal ridge of the cingulum.
Mesial paracingular fossa (mpf)/mesial lobe (mlo)	Fossa forming a channel on the crown lobe mesial to the primary ridge and bordered by the mesial bounding ridge.
Primary apicobasal ridge (1abr)	Prominent apicobasal ridge with subparallel to parallel margins. Crowns with a primary apicobasal ridge typically possess accessory (secondary) apicobasal ridges.
Secondary apicobasal ridge (2abr)	Apicobasal ridge of less 'strength' (less mesiodistal width and prominence) than the primary apicobasal ridge (see also accessory apicobasal ridge).
Tertiary apicobasal ridge (3abr)	Apicobasal ridge developed on the surfaces of primary and secondary apicobasal ridges.

margin that communicate with the neurovascular tract; (2) neurovascular tract bifurcates internally to exit at two anteroventral maxillary foramina; (3) lingual margin of maxillary tooth roots in midregion of tooth row form an S-bend at their bases; (4) posterior third of maxilla on some, but not all, specimens deflects posterolaterally at an abrupt kink; and (5) lateral end of palatine lateral ramus forms a hatchet-shaped flange.

Occurrence.—Flat Rocks locality in the Inverloch region of Victoria, southeastern Australia (Fig. 1); Flat Rocks Sandstone and The Caves Sandstone, upper Barremian of the Wonthaggi Formation in the Gippsland Basin.

Description.—The taxon is known from five isolated left maxillae with dentition, an isolated right maxillary tooth, the palatine, and a partial lacrimal. The most complete of the maxillae, the holotype (NMV P229196), retains four fully erupted teeth (Figs. 4, 5). Marginally larger than the holotype but incomplete, NMV P186440 (Figs. 4, 6) preserves the posterior region of the maxilla with six tooth positions (five crowns fully erupted), the complete left palatine, and a ventrolateral fragment of the lacrimal, preserved in situ. NMV P208178 is ~73% of the holotype in size and retains five erupted crowns (Fig. 4). The two smallest maxillae (NMV P209977, P212845) lack erupted dentition (Figs. 4, 7, 8). Because the complete lacrimal is presently unknown, the anteroposterior and dorsoventral extent of the antorbital fossa and external antorbital fenestra are also unknown.

Maxilla.—Two maxillary forms are apparent. On NMV P229196 (the holotype), P208178, and P212845, an abrupt kink causes the posterior third of these maxillae to angle posterolaterally outward (Figs. 5, 8). This kink coincides with a bulge on the medial surface at the anterior end of the facet for the palatine, and resembles the kink on the maxilla of *Camptosaurus dispar* Marsh, 1879 (YPM VP 1886; Fig. 9). However, in the latter taxon, deflection is relatively less. On one of the smallest maxillae (NMV P209977; Fig. 7.1, 7.2), the kink is absent and could also be absent on the largest maxilla (NMV P186440; Fig. 6.1, 6.2, 6.7, 6.8), although noting that the latter specimen is incomplete anteriorly (see further comments under Variation, below). The largest complete maxillae (NMV P229196, P208178) each contain 15 alveoli, and the smallest maxillae (NMV P209977, NMV P212845) contain 13 and 14 alveoli, respectively. Viewed ventrally, the maxillary teeth are arranged en echelon, with one replacement crown present per alveolus (Figs. 5, 6). Staggered tooth replacement occurs across groups of two tooth families. The tooth row is laterally concave with the alveoli in the middle of the tooth row obliquely angled relative to the anteroposterior tooth row axis. The anterior alveoli outturn laterally relative to the lateral margin of the maxilla (Fig. 5), as in *Camptosaurus dispar* (YPM VP 1886; Fig. 9) and *Dysalotosaurus lettowvorbecki* Pompeckj, 1920 (Janensch, 1955, table 11), and similar to these taxa, no substantial diastema is developed. As a result, the anterior alveolus locates in the anteroventral process that abuts the posterolateral end of the premaxilla (Figs. 5, 7, 8). In *Leaellynasaura amicagraphica*, the anterior alveoli are oriented parallel to the lateral margin of the maxilla (Fig. 10.5).

https://doi.org/10.1017/jpa.2018.95

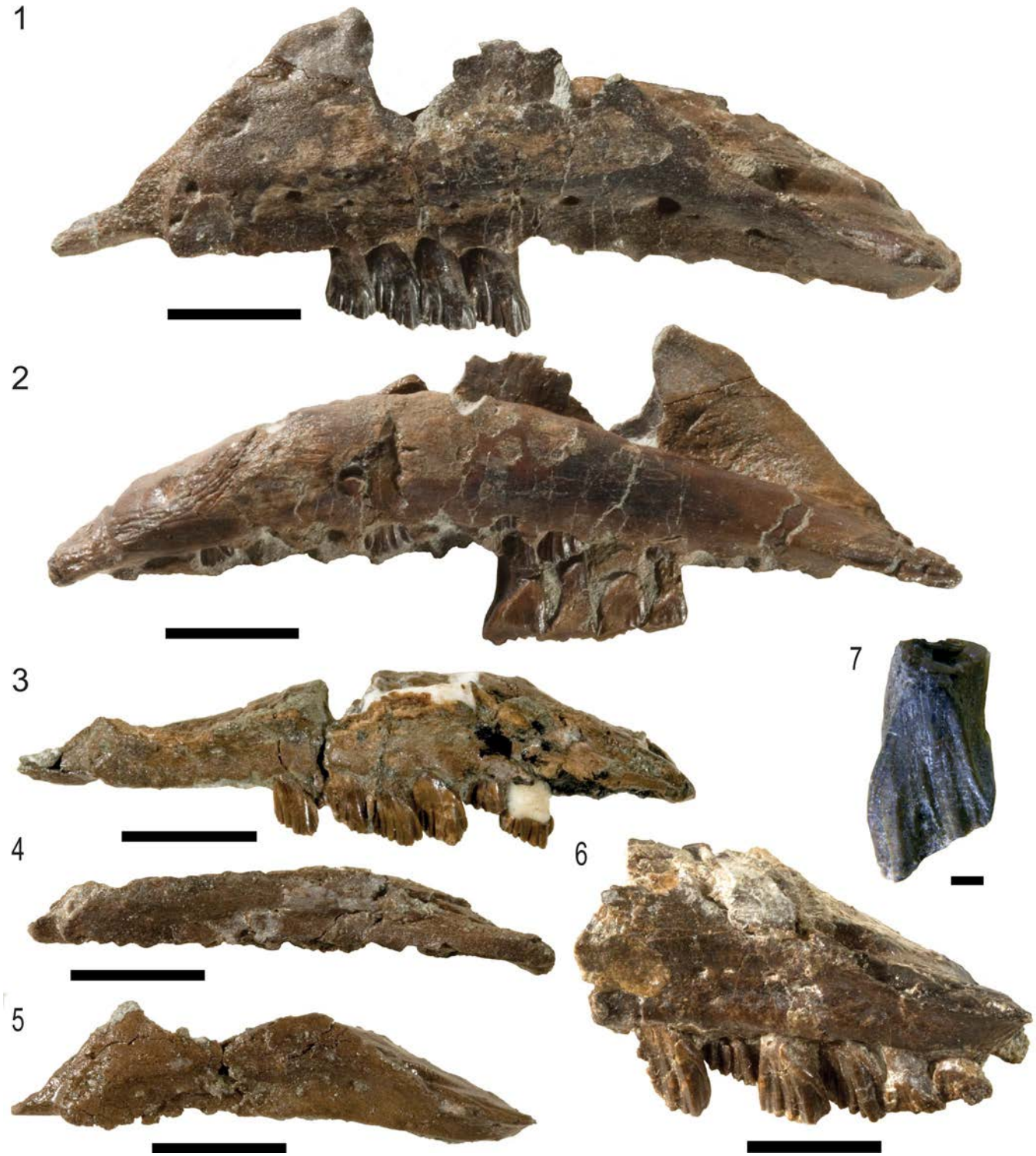

Figure 4. Specimens of *Galleonosaurus dorisae* n. gen. n. sp. from the Flat Rocks Sandstone in the upper Barremian, Wonthaggi Formation, Gippsland Basin, southeastern Australia: (**1–2**) holotype (NMV P229196), left maxilla in lateral (**1**) and medial (**2**) views; (**3**) NMV P208178, left maxilla in lateral view; (**4**) NMV P212845, left maxilla in lateral view; (**5**) NMV P209977, left maxilla in lateral view; (**6**) NMV P186440, left maxilla in lateral view; (**7**) NMV 208113, right maxillary tooth in labial view. Scale bars = 10 mm (**1–6**); 1 mm (**7**).

The ventral region of an anteroposteriorly extensive antorbital fossa is formed by the maxilla (Figs. 5–8, 11, 12). The supralveolar lamina forms the lateral wall of the maxilla and the buccal ridge formed by this lamina is shallowly rounded dorsoventrally (Figs. 5.6, 6.11, 7, 8, 11, 12). Buccal emargination, measured midway along the tooth row in ventral view, approximately equals the labiolingual width of one crown on the holotype (Fig. 5) and two crowns on the smallest maxillae (NMV P209977, P212845; Figs. 7, 8). Buccal emargination on the maxilla of *Leaellynasaura amicagraphica* is shallower

https://doi.org/10.1017/jpa.2018.95

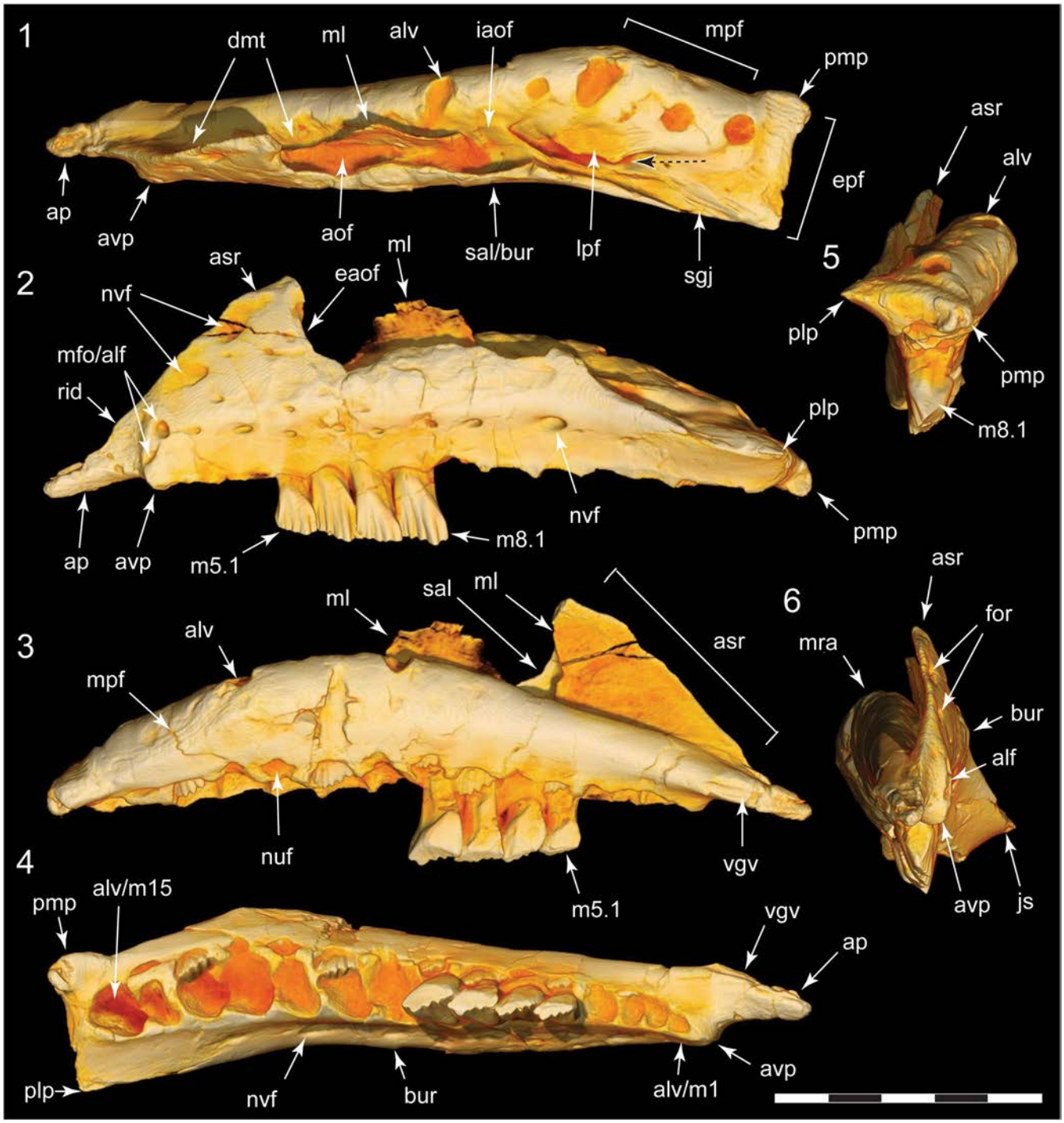

Figure 5. *Galleonosaurus dorisae* n. gen. n. sp., digital 3D models of holotypic left maxilla (NMV P229196), derived from µCT scans in dorsal (**1**), lateral (**2**), medial (**3**), ventral (**4**), posterior (**5**), and anterior (**6**) views. Dashed arrow in (**1**) indicates line of neurovascular tract and posterodorsal foramen. alf = anterolateral fossa; alv = alveolus; aof = antorbital fossa; ap = anterior (premaxillary) process; asr = ascending ramus of maxilla; avp = anteroventral process; bur = buccal ridge; dmt = dorsal maxillary trough; eaof = region of external antorbital fossa; epf = ectopterygoid flange; for = foramen; iaof = region of internal antorbital fossa; js = jugal shelf; lpf = sutural flange for the lateral palatine ramus; m# = maxillary tooth position (from anterior end) and replacement number; mfo = anterior maxillary foramina; ml = medial lamina; mpf = medial palatine facet; mra = maxillary ramus; nuf = nutrient foramen; nvf = neurovascular foramen; plp = posterolateral process; pmp = posteromedial process; rid = ridge (crista); sal = supralveolar lamina; sgj, sutural grove for jugal; vgv = vomer groove. Scale bar increments = 5 mm.

(approximately two-thirds of the crown width at the deepest point along the tooth row; Fig. 10.5). Similarly to *L. amicagraphica*, the buccal ridge is protrusive in *Atlascopcosaurus loadsi*, however, buccal emargination is at least as deep as in *Galleonosaurus dorisae* n. gen. n. sp. or possibly deeper (Fig. 10).

Viewed laterally (Figs. 4–8), the alveolar margin is shallowly concave and the anterior margin of the ascending ramus is convex. The premaxillary process is spinose and slightly inset medially from the lateral surface of the maxilla by the anteroventral process at the base of the ascending ramus (Figs. 5, 7, 8).

https://doi.org/10.1017/jpa.2018.95

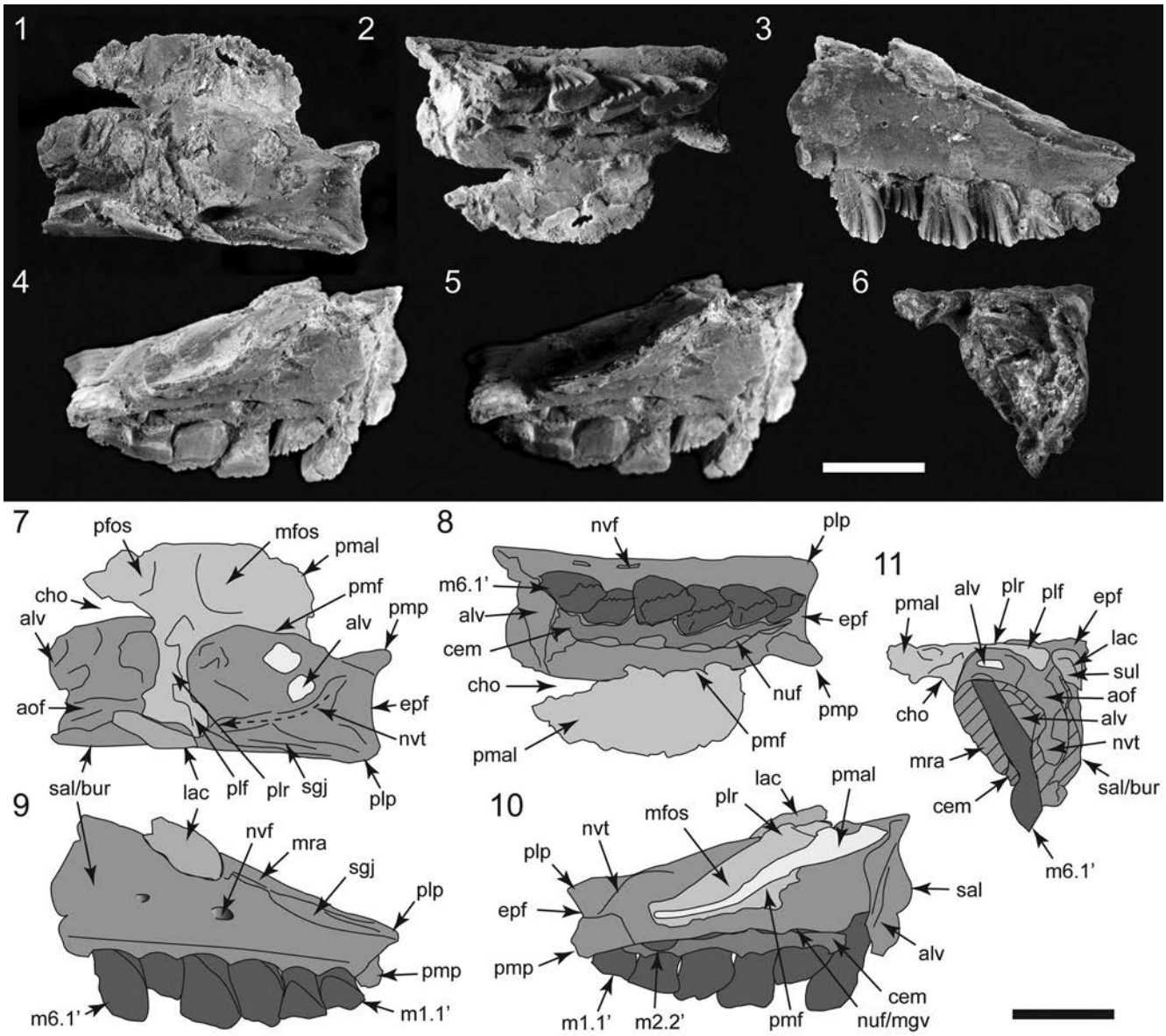

Figure 6. *Galleonosaurus dorisae* n. gen. n. sp. (NMV P186440), left cranial fragment in dorsal (**1**), ventral (**2**), lateral (**3**), medial (**4**), medial (**5**, bottom lighting), and anterior (**6**) views, and schematics (**7–11**) of (**1–4, 6**), respectively. Specimen has been ammonium chloride coated. Dashed arrow in (**7**) indicates line of neurovascular tract and posterodorsal foramen. alv = alveolus; aof = antorbital fossa; bur = buccal ridge; cem = cementum; cho = choana; epf = ectopterygoid flange; lac = lacrimal; m#' = maxillary tooth position (from posterior end) and replacement number; mfos = muscular fossa; mgv = medial groove; mra = maxillary ramus; nuf = nutrient foramen; nvf = neurovascular foramen; nvt = neurovascular tract; pfos = pneumatic fossa; plf = palatine lateral flange; plp = posterolateral process; plr = palatine lateral ramus; pmal = palatine medial ala; pmf = palatine maxillary flange; pmp = posteromedial process; sal = supralveolar lamina; sgj = sutural grove for jugal; sul = sulcus on lacrimal fragment. Scale bars = 10 mm.

A groove on the medial margin of the premaxillary process could have accommodated the vomer. A shallow cleft-like fossa containing neurovascular foramina is present anteriorly on the ventrolateral margin of the maxilla, dorsal to the anteroventral process (Figs. 5, 7, 8, 11), as in *Changchunsaurus parvus* Zan et al., 2005 (Jin et al., 2010), *Jeholosaurus shangyuanensis* Xu, Wang, and You, 2000 (Barrett and Han, 2009), *Tenontosaurus tilletti* Ostrom, 1970 (Thomas, 2015, fig. 2) and *Zalmoxes robustus* Nopcsa, 1900 (NHMUK R3395; unpublished data, Herne, 2009). A fossa on the anterolateral margin of the maxilla has been considered an ornithopodan synapomorphy (Butler et al., 2008). Along the anterior margin of the ascending ramus, the medial lamina forms a thin, buttress-like crista with a straight anterodorsal edge connecting the dorsal edge of the premaxillary process (Figs. 5, 7). A fortuitous break through the ascending ramus on the holotype (during its preparation) indicated that the ascending ramus is formed from both the thicker supralveolar and far thinner medial laminae (Fig. 12), as in *Lesothosaurus diagnosticus* Galton, 1978 (Porro et al., 2015). A thin seam of sediment infill indicates that these two laminae are unfused. In places, the medial lamina is <150 μm thick and its medial surface in the region of the ascending ramus is roughened, forming a shallow fossa (Figs. 5, 12). The external antorbital fenestra is bordered anteriorly by the ascending ramus (Figs. 5, 12). Although the full form of the external antorbital fenestra cannot be assessed, because the ventral

https://doi.org/10.1017/jpa.2018.95

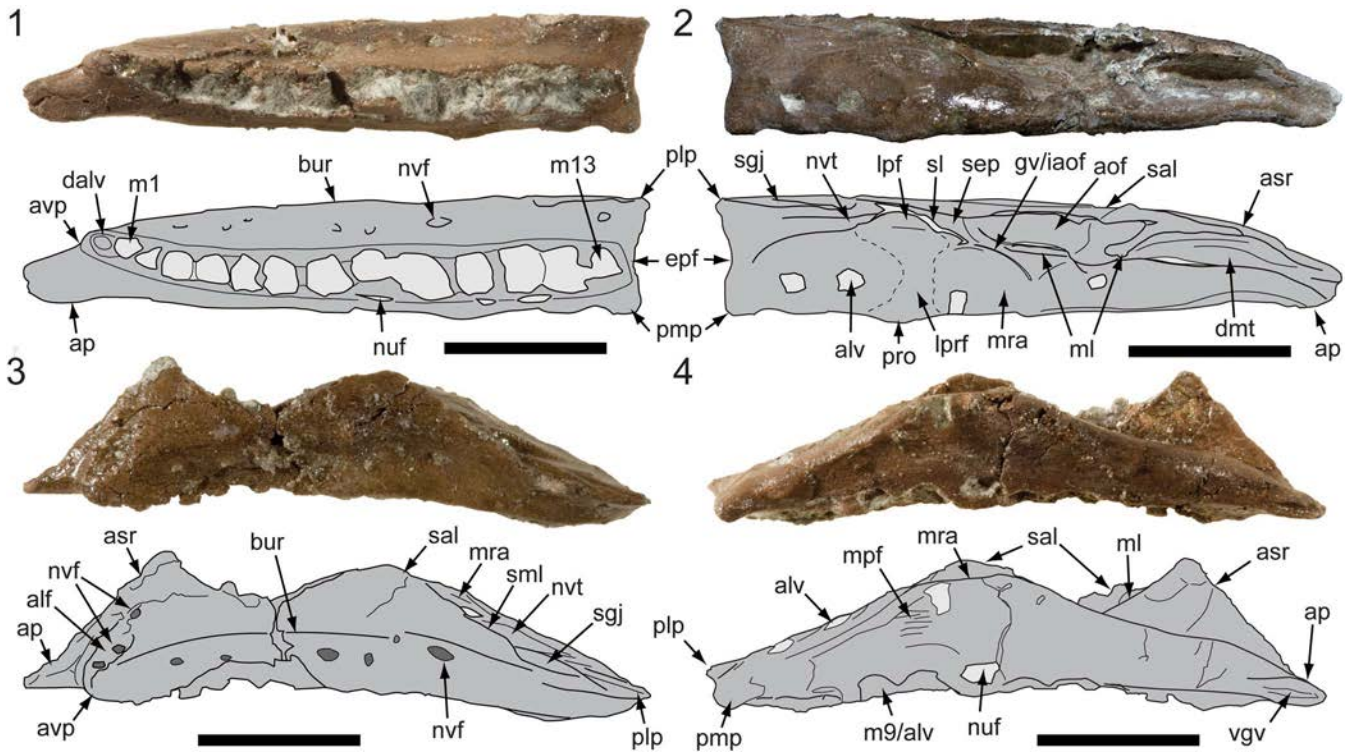

Figure 7. *Galleonosaurus dorisae* n. gen. n. sp. (NMV P209977), left maxillae and schematics in ventral (**1**), dorsal (**2**), lateral (**3**), and medial (**4**) views. Dashed lines in (**2**) indicate approximate margins of the palatine facet. alf = anterolateral fossa; alv = alveolus; aof = antorbital fossa; ap = anterior (premaxillary) process; asr = ascending ramus of maxilla; avp = anteroventral process; bur = buccal ridge; dalv = developing alveolus; dmt = dorsal maxillary trough; epf = ectopterygoid flange; gv = groove; iaof = region of internal antorbital fossa; lpf = sutural flange for the lateral palatine ramus; lprf = facet for the lateral ramus of the palatine; m# = maxillary tooth position (from anterior end) and replacement number; ml = medial lamina; mpf = medial palatine facet; mra = maxillary ramus; nuf = nutrient foramen; nvf = neurovascular foramen; nvt = neurovascular tract; plp = posterolateral process; pmp = posteromedial process; pro = protuberance; sal = supralveolar lamina; sep = septum; sgj = sutural grove for jugal; sl = slot; sml = sutural margin for lacrimal; vgv = vomer groove. Scale bars = 10 mm.

margin formed by the supralveolar lamina is degraded on all of the specimens, its ventral margin is positioned dorsally, well above the buccal ridge.

Medially (Fig. 6), the maxillary ramus is differentiated from the alveolar parapet by a medial groove, along which elongate nutrient foramina ('special foramina' of Edmund, 1957) align with the alveoli. The developing crowns and roots are encased in cementum (suggested by grayer contrast in the μCT imagery; Fig. 11). The dorsal surface of the maxillary ramus is penetrated by the alveoli (Figs. 5–8, 10, 11), as in *Zalmoxes robustus*, which was previously considered unique in that taxon (Weishampel et al., 2003).

Viewed dorsoventrally, the posterior margin of the ectopterygoid flange is straight to shallowly concave and oriented orthogonally to the axis of the tooth row (Figs. 5–7). A knob- to spike-like posteromedial process projects from the posteromedial corner of the flange. The posteromedial process is separate from the maxillary ramus, which might also occur in *Camptosaurus dispar* (YPM VP 1886; Fig. 9). We are presently uncertain whether a separate posteromedial process is commonly developed in other taxa. The posterolateral process is weakly developed, as in *Leaellynasaura amicagraphica*, and contrasts with that of *Atlascopcosaurus loadsi*, which is more pronounced (Fig. 10). The dorsal surface of the ectopterygoid flange is striated and horizontal in posterior view (Fig. 5). Viewed medially, the dorsal surface of the maxillary ramus is convex and dorsoventrally deepest roughly midway along the ramus (Figs. 5, 7, 8). A deeply striated sutural surface for the medial flange of the palatine is developed posterior to the medial bulge that coincides with the anterior end of the medial palatine facet (Figs. 5, 7). A slotted sutural facet for the jugal and lacrimal is developed dorsally on the posterolateral edge of the maxilla (Figs. 5–8, 10, 11). Viewed laterally, the jugolacrimal margin is sinuous (Figs. 5, 6). The overall line of these margins slopes posteroventrally at ~30° relative to the alveolar margin, as in *Atlascopcosaurus loadsi* (Fig. 13) and *L. amicagraphica* (see Herne, 2014, fig. 5.3). This margin is more steeply angled in *Hypsilophodon foxii* Huxley, 1870 (Galton, 1974, figs. 2–3) and the anterior end of the sutural margin for the jugal on the maxilla of *Gasparinisaura cincosaltensis* Coria and Salgado, 1996 is distinctly stepped (Coria and Salgado, 1996, fig. 2).

The dorsal and internal structures of the maxilla are complex. Micro-CT imagery (Fig. 11) reveals regions of the antorbital fossa hidden by the matrix and the internal passage of the neurovascular system. The neurovascular tract (= neurovascular canal of Witmer, 1997; maxillary canal of Thomas, 2015) extends the length of the maxillary ramus (Fig. 11.2) and would have conveyed the maxillary division of the trigeminal nerve (cn V_2; see Witmer, 1995, 1997; Benoit et al., 2016; Barker et al., 2017). Posteriorly, the neurovascular tract forms a shallow channel on the dorsal surface of the maxilla medial to the sutural groove for the jugal (Figs. 5–8, 11). The neurovascular tract enters the internal region of the maxilla at the posterodorsal foramen (Figs. 5.1, 6.7, 11.1), which is roofed dorsally

https://doi.org/10.1017/jpa.2018.95

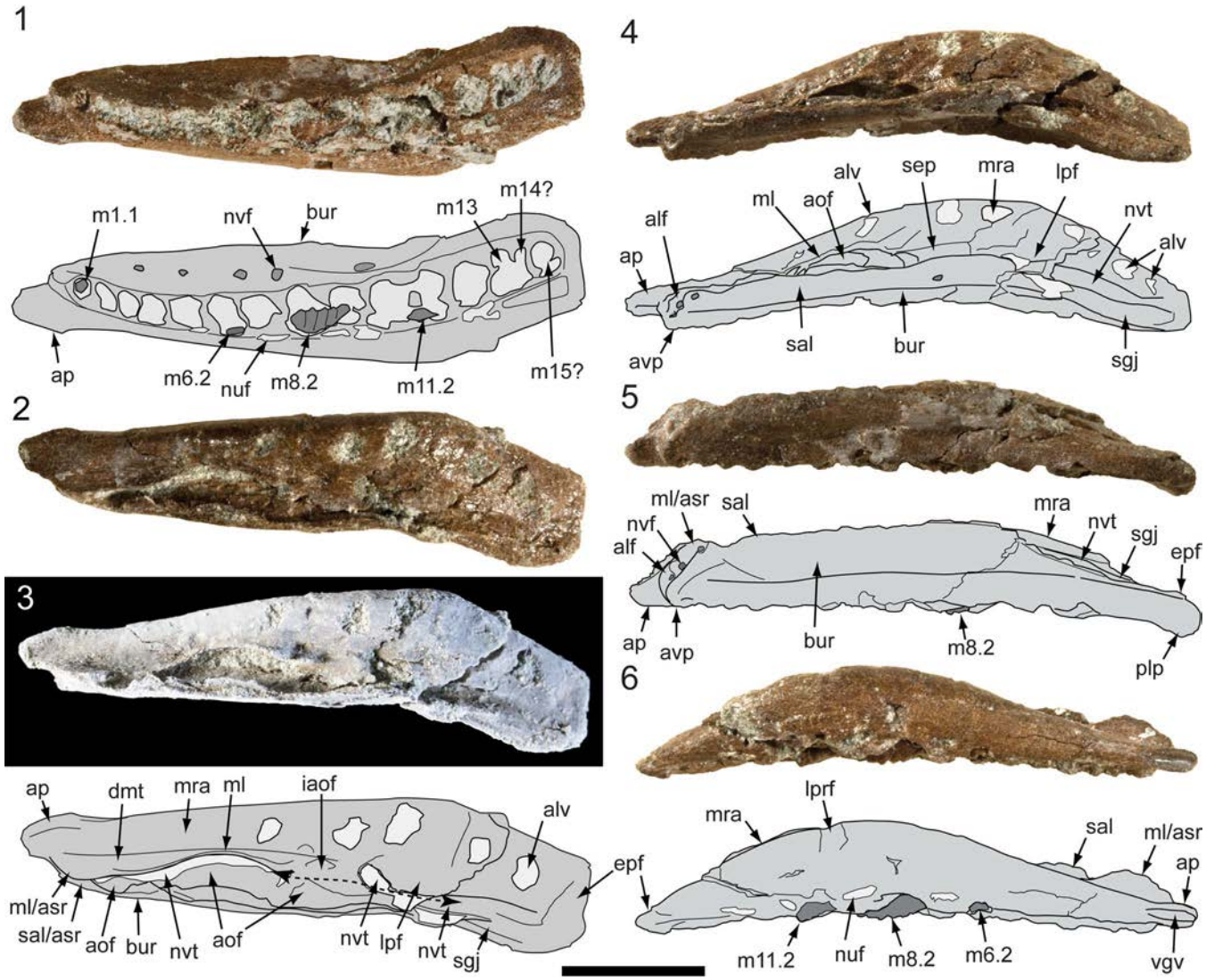

Figure 8. *Galleonosaurus dorisae* n. gen. n. sp. (NMV P212845), left maxillae and schematics in ventral (**1**), dorsal (**2, 3**), dorsolateral (**4**), lateral (**5**), and medial (**6**) views. Specimen in (**3**) has been ammonium chloride coated; dashed line in schematic indicates presumed internal path of the neurovascular tract. alf = anterolateral fossa; alv = alveolus; aof = antorbital fossa; ap = anterior (premaxillary) process; asr = ascending ramus of maxilla; avp = anteroventral process; bur = buccal ridge; dmt = dorsal maxillary trough; epf = ectopterygoid flange; iaof = region of internal antorbital fossa; lpf = sutural flange for the lateral palatine ramus; lprf = facet for the lateral ramus of the palatine; m# = maxillary tooth position (from anterior end) and replacement number; ml = medial lamina; mra = maxillary ramus; nuf = nutrient foramen; nvf = neurovascular foramen; nvt = neurovascular tract; plp = posterolateral process; sal = supralveolar lamina; sep = septum; sgj = sutural grove for jugal; vgv = vomer groove. Scale bar = 10 mm.

by a rugose flange on the maxilla for the lateral ramus of the palatine (Figs. 5–8; 11.2, 11.3, coronal section A). A slot opening dorsally from the neurovascular tract surrounds the lateral and anterior margins of this flange (Fig. 11.1; 11.2, 11.3, coronal sections A, B).

The antorbital fossa is walled laterally and ventrally by the supralveolar lamina and medially by the medial lamina (Figs. 7, 8, 11). The posterior region of the antorbital fossa is located anterior to the flange for the lateral ramus of the palatine and lateral to the internal antorbital fenestra (Fig. 11.1, 11.2; 11.2, 11.3, coronal sections B, C). In this posterior region of the antorbital fossa, the neurovascular tract forms an internalized duct separated from the antorbital fossa by a thin septum (Fig. 11.3, coronal section C). This septum thickens in the midregion of the antorbital fossa and the neurovascular tract appears to divide into dorsal and ventral moieties (Fig. 11.3, coronal section D). In the anteriormost region of the antorbital fossa, the neurovascular tract and the antorbital fossa merge (Fig. 11.2, 11.3, coronal sections E, F). The neurovascular tract forms a dorsally opening channel on the ventral floor of the antorbital fossa. The anteriormost end of the antorbital fossa terminates at the ascending ramus (Fig. 11.1, 11.2). From this point, the neurovascular tract continues anteriorly and bifurcates to exit at two anterior maxillary foramina within a shallow anterolateral fossa, dorsal to the anteroventral process (Figs. 5, 7, 8; 11.2, 11.3, coronal sections G, H). The neurovascular tract is separated medially from the alveoli by a septum through which foramina pass (e.g., Fig. 11.3, coronal sections B, H).

Two slot-like foramina penetrate the anterolateral margin of the ascending ramus and extend posteroventrally to communicate with the merged region of the neurovascular tract and the anteriormost region of the antorbital fossa (Fig. 11.2, 11.3,

https://doi.org/10.1017/jpa.2018.95

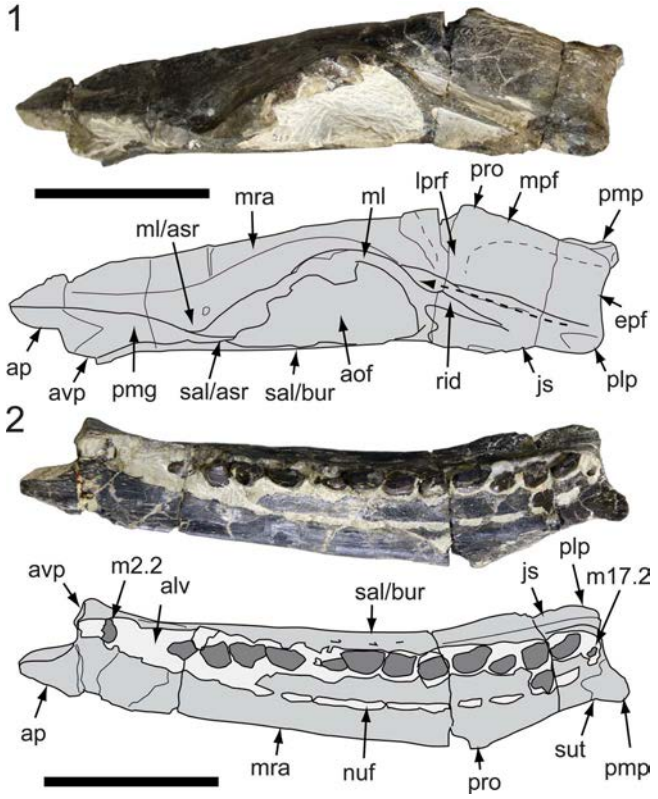

Figure 9. *Camptosaurus dispar* Marsh, 1879, left maxilla and schematics (YPM VP 1886) in dorsal (**1**) and ventral (**2**) views. Dashed arrow in (**1**) indicates presumed dorsal path of the neurovascular tract; dashed lines indicate approximate margins of the palatine facet. alv = alveolus; aof = antorbital fossa; ap = anterior (premaxillary) process; asr = ascending ramus; avp = anteroventral process; bur = buccal ridge; epf = ectopterygoid flange; js = jugal shelf; lprf = sutural flange for the lateral palatine ramus; m# = maxillary tooth position (from anterior end) and replacement number; ml = medial lamina; mpf = medial palatine facet; mra = maxillary ramus; nuf = nutrient foramen; plp = posterolateral process; pmg = premaxillary groove; pmp = posteromedial process; pro = protuberance; rid = ridge; sal = supralveolar lamina; sut = sutural margin. Scale bars = 50 mm. Image (**1**) by A. Heimer, courtesy of YPM. Image (**2**) by S. Hochgraf, courtesy of YPM.

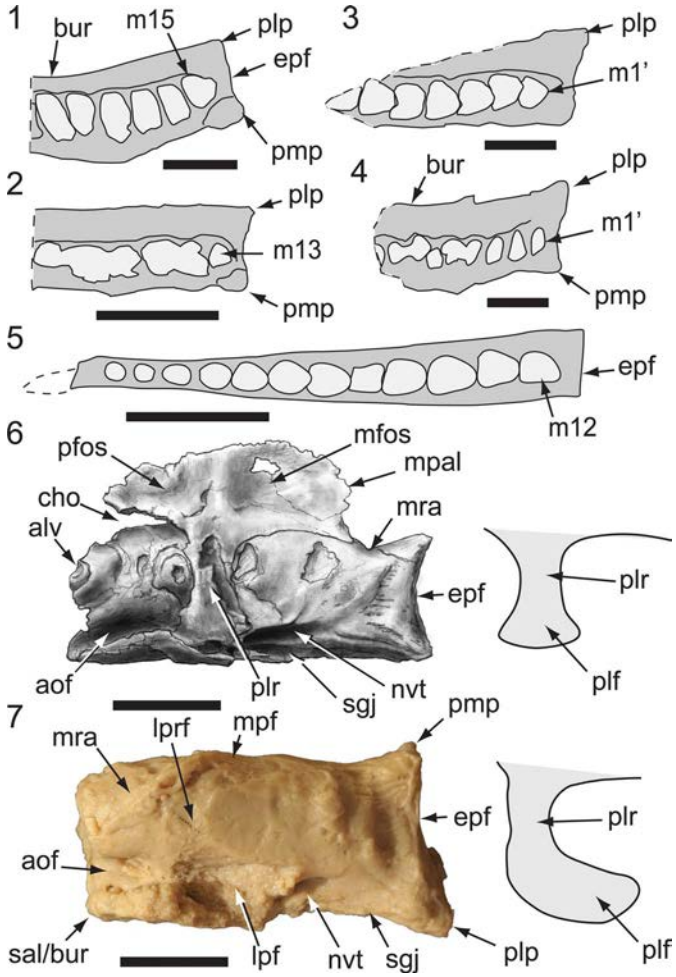

Figure 10. Comparisons of *Galleonosaurus dorisae* n. gen. n. sp.: (**1–4**) schematics of holotype of *G. dorisae* n. gen. n. sp. (NMV P229196) (**1**), *G. dorisae* n. gen. n. sp. (NMV P209977) (**2**), *Atlascopcosaurus loadsi* Rich and Rich, 1989 (NMV P157390) (**3**), and original *Atlascopcosaurus loadsi* holotype (NMV P166409) (**4**), posterior maxillary regions in ventral view, showing extent of the posteromedial processes; (**5**) schematic of holotypic maxilla of *Leaellynasaura amicagraphica* Rich and Rich, 1989 (NMV P185991) in ventral view showing shapes of the alveolar and posterior margins; (**6, 7**) illustration of *G. dorisae* n. gen. n. sp. (NMV P186440) (**6**) and cast of the original *Atlascopcosaurus loadsi* holotype (NMV P166409) (**7**) in dorsal view, with schematics showing difference in the shape of the lateral palatine rami/sutural facets. alv = alveolus; aof = antorbital fossa; bur = buccal ridge; cho = choana; epf = ectopterygoid flange of maxilla; lpf = lateral palatine flange on maxilla; lprf = facet for the lateral ramus of the palatine; m# = maxillary tooth position (from anterior end) and replacement number; m#' = maxillary tooth position (from posterior end) and replacement number; mfos = muscular fossa on palatine; mpal = medial palatine ala; mpf = facet for medial palatine flange on maxilla; mra = maxillary ramus; nvt = neurovascular tract; pfos = pneumatic fossa on palatine; plp = posterolateral process; plf = palatine lateral flange; plr = palatine lateral ramus; pmp = posteromedial process; sal = supralveolar lamina; sgj = sutural grove for jugal. Scale bars = 10 mm.

between coronal sections F–H). These slot-like foramina are walled medially by the medial lamina, which in this region is exceedingly thin (<100 μm). A small foramen that exits laterally on the ascending ramus communicates with the uppermost of the two slot-like foramina (Fig. 11.2, 11.3, coronal section G). A further small foramen extends from the anterior end of the antorbital fossa dorsally to the neurovascular tract to exit laterally on the ascending ramus (Fig. 11.2, 11.3, between coronal sections F, G). Apart from the aforementioned foramina of the neurovascular tract, ~13 additional neurovascular foramina penetrate the supralveolar lamina to communicate with the neurovascular tract. The ventralmost of these foramina (Fig. 11.2, 11.3, between coronal sections B–F) pass ventrally to the antorbital fossa to communicate directly with the neurovascular tract.

The dorsal maxillary trough extends anteriorly on the dorsal surface of the maxilla, from the region of the internal antorbital fenestra and onto the dorsal surface of the premaxillary process (Figs. 5, 7, 8; 11.2, 11.3, coronal sections D–H). The antorbital fossa and dorsal maxillary trough are separated by the medial lamina. The central portion of the medial lamina extends dorsally as a thin sheet of bone (~1.2 mm thick). Sutural striae on the medial surface of the lamina suggest the region of contact with the medial lamina of the lacrimal, as in *Leaellynasaura amicagraphica* (see Herne, 2014, fig. 5.8). Viewed dorsally (Fig. 5), the medial lamina on the holotype bows medially at its midpoint, partly encroaching on the dorsal maxillary trough. The degree of medial bowing is greater in the smallest maxillae (NMV P209977, P212845; Figs. 7, 8), which in this aspect, approaches the condition in *Camptosaurus dispar* (YPM VP 1886: Fig. 9). However, bowing of the medial lamina

https://doi.org/10.1017/jpa.2018.95

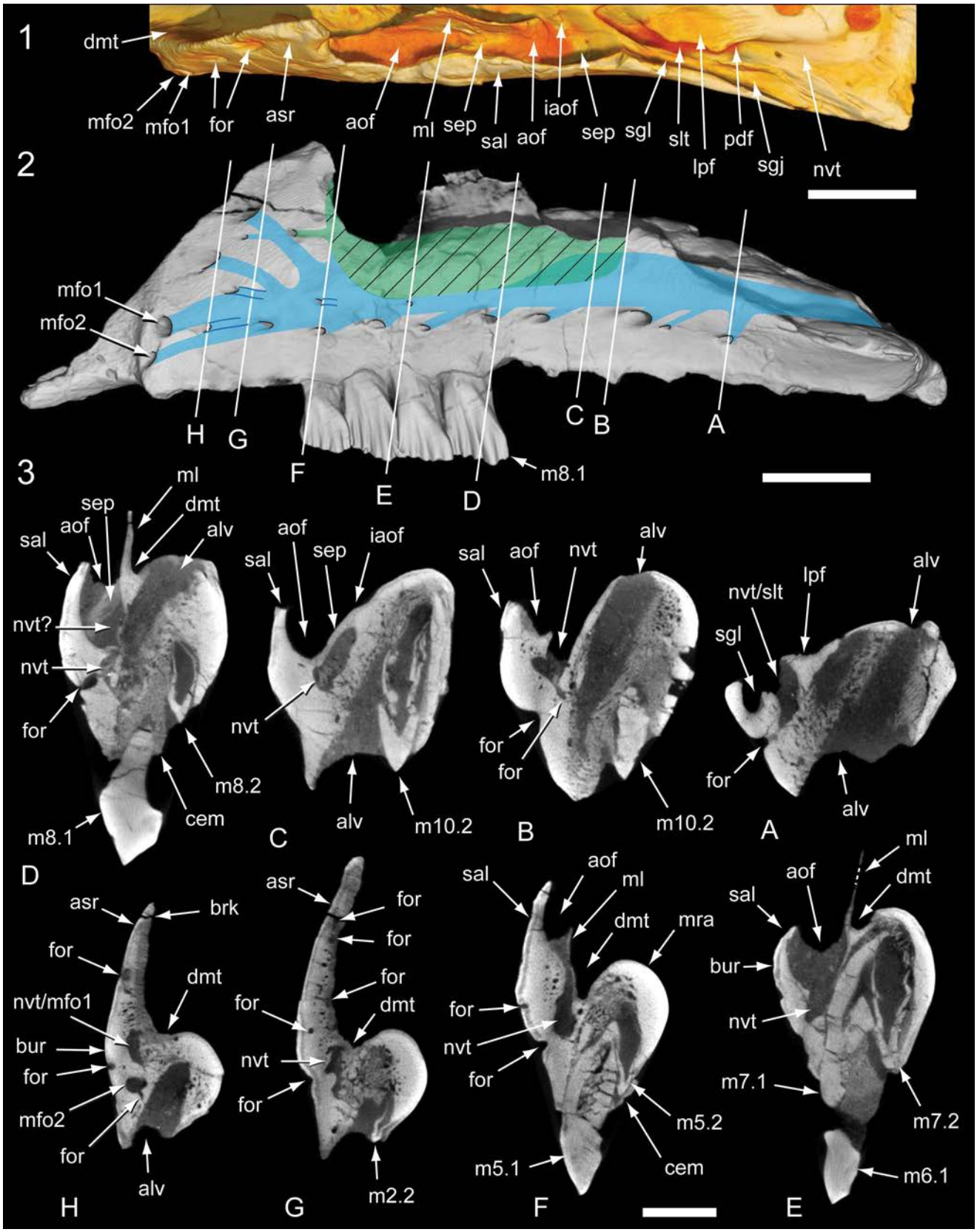

Figure 11. Internal anatomy of the *Galleonosaurus dorisae* n. gen. n. sp. holotypic left maxilla (NMV P229196) from µCT scans: (**1**) antorbital region in dorsal view; (**2**) maxilla in lateral view with schematic overlay showing internal locations of the antorbital fossa (in green; ventral extent, cross-hatching) and neurovascular tract (in blue); (**3**) coronal sections through maxilla as indicated in (**2**). alv = alveolus; aof = antorbital fossa; asr = ascending ramus of maxilla; brk = breakage; bur = buccal ridge; cem = cementum; dmt = dorsal maxillary trough; for = foramen; iaof = region of internal antorbital fenestra; lpf = lateral palatine facet and flange on maxilla; m# = maxillary tooth position (from anterior end) and replacement number; mfo# = anterior maxillary foramen (1 = dorsal branch; 2 = ventral branch); ml = medial lamina; mra = maxillary ramus; nvt = neurovascular tract; nvt? = uncertain dorsal moity of neurovascular tract; pdf = posterodorsal foramen of the maxilla; sal = supralveolar lamina; sep = septum; sgj = sutural groove for jugal; sgl = sutural groove for lacrimal; slt = slot. Scale bars: 10 mm (**1, 2**); 5 mm (**3**).

https://doi.org/10.1017/jpa.2018.95

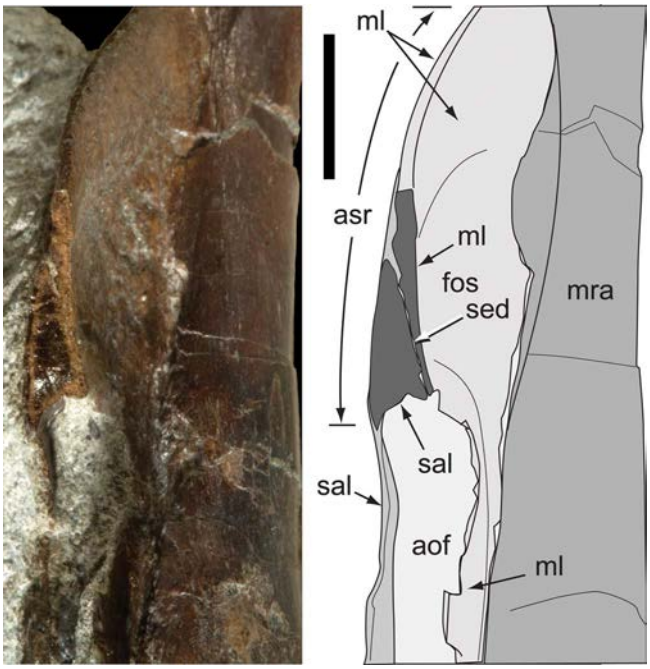

Figure 12. *Galleonosaurus dorisae* n. gen. n. sp., holotypic left maxilla (NMV P229196) in dorsal view and schematic showing broken surface (dark shading) of the ascending ramus and separation of the supralveolar and medial laminae indicated by a seam of sediment infill. aof = antorbital fossa; asr = ascending ramus of maxilla; fos = fossa; ml = medial lamina of maxilla; mra = maxillary ramus; sed = host sediment infill; sal = supralveolar lamina. Scale bar = 10 mm.

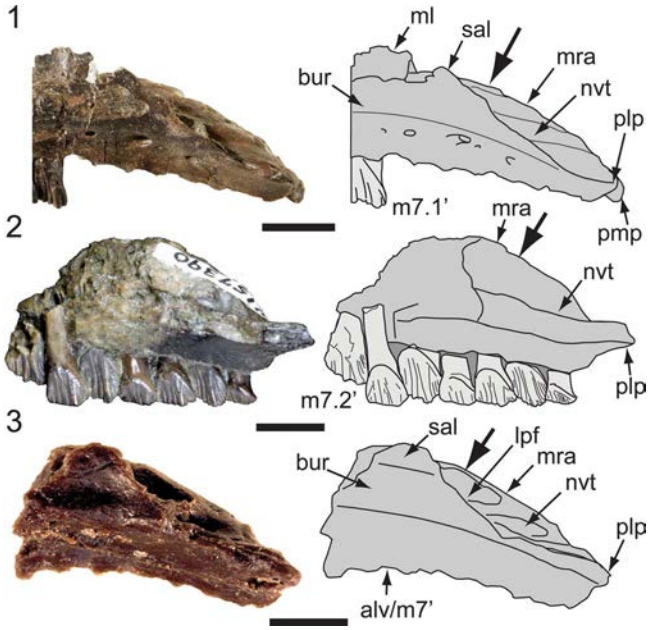

Figure 13. Comparisons of Victorian ornithopod maxillae in lateral view and schematics, showing dorsalmost extent of the maxillary ramus (indicated by large arrows): (**1**) *Galleonosaurus dorisae* n. gen. n sp., holotypic left maxilla (NMV P229196); (**2**) *Atlascopcosaurus loadsi* Rich and Rich, 1989, left maxilla (NMV P157390); (**3**) cast of original holotypic left maxilla of *Atlascopcosaurus loadsi* (NMV P166409). alv = alveolus; bur = buccal ridge; lpf = lateral palatine flange of maxilla; m#' = maxillary tooth position (from posterior end) and replacement number; ml = medial lamina of maxilla; mra = maxillary ramus; nvt = neurovascular tract; plp = posterolateral process of maxilla; pmp = posteromedial process of maxilla; sal = supralveolar lamina of maxilla. Scale bars = 10 mm.

in the latter taxon is greater and more posteriorly positioned. A gap in the medial lamina between the anterior ascending ramus and its central region (Fig. 5) could indicate the presence of an anterior internal antorbital fenestra ('promaxillary fenestra' of Carpenter, 1992; Witmer, 1997) as in *Heterodontosaurus tucki* Crompton and Charig, 1962 (Norman et al., 2011) and *Hypsilophodon foxii* (see Galton, 1974), or alternatively, could have resulted from breakage.

Palatine.—Viewed dorsoventrally (Fig. 6), the ala of the palatine forms a reniform, posteroventrally sloping sheet of bone that projects medially from the medial maxillary flange, which tightly adjoins the maxilla. Viewed medially, the maxillary flange has a boot-shaped profile (Fig. 6.4, 6.10). The medial ala slopes posteroventrally and fails to rise dorsally above the level of the maxillary ramus. Viewed anteriorly, the medial ala is horizontally oriented (Fig. 6.6, 6.11), as in *Leaellynasaura amicagraphica* (see Herne, 2014, figs 5.6, 5.7) and differs from the angled to subvertical orientation of the alae in *Muttaburrasaurus langdoni* Bartholomai and Molnar, 1981 (unpublished data, Herne, 2018), *Hypsilophodon foxii* (Fig. 14), styracosternans, *Tenontosaurus tilletti* (see Thomas, 2015), and *Thescelosaurus neglectus* Gilmore, 1913 (Boyd, 2014). Viewed dorsally, the choanal margin is anterolaterally concave and the posterolateral margin of the flange in contact with the maxilla is laterally concave (Fig. 6.1, 6.7). The choana coincides with the internal antorbital fenestra, as in other ornithopods (Witmer, 1997). A transverse ridge, posterior to the choana ('postchoanal strut' of Witmer, 1997), crosses the dorsal surface of the palatine body (Fig. 6.1, 6.7). A deep muscular fossa is developed posterior to the strut, as in *H. foxii* (Fig. 14), and a shallower pneumatic fossa is developed anterior to the strut (see Witmer, 1997), as in *Lesothosaurus diagnosticus* (see Porro et al., 2015, fig. 8A, D). The pneumatic fossa is reportedly absent in *Heterodontosaurus tucki* (see Norman et al., 2011) and among ornithopods, also absent in at least *H. foxii* and *Iguanodon bernissartensis* Boulenger, 1881 (Witmer, 1997), *Tenontosaurus tilletti* (see Thomas, 2015, fig. 14), and the hadrosaurid *Edmontosaurus regalis* Lambe, 1917 (Heaton, 1972, figs. 2, 5). A strap-like lateral ramus extends over the convex dorsal surface of the maxilla and a hatchet-shaped, dorsoventrally compressed flange is developed at the end of the lateral ramus. This flange is accommodated in the sutural flange on the maxilla (Figs. 5–8, 11.1; 11.3, coronal section A), coinciding with the medial face of the lacrimal (see below), and most likely the anteriormost end of the jugal.

Lacrimal.—A small, plate-like fragment of bone adjoining the maxilla in NMV P186440 (Fig. 6) is interpreted as the posteroventral portion of the left lacrimal. The irregular ventral edge of the fragment locates in the sutural slot on the maxilla anterior to the margin for the jugal. The lacrimal slightly overlaps the sutural edge laterally on the maxilla. The anterolateral surface of the lacrimal is slightly scalloped.

Maxillary dentition.—The crowns and roots have en echelon emplacement relative to the long axis of the tooth row and the erupted crowns are imbricated (Figs. 5, 6, 15), as in all

https://doi.org/10.1017/jpa.2018.95

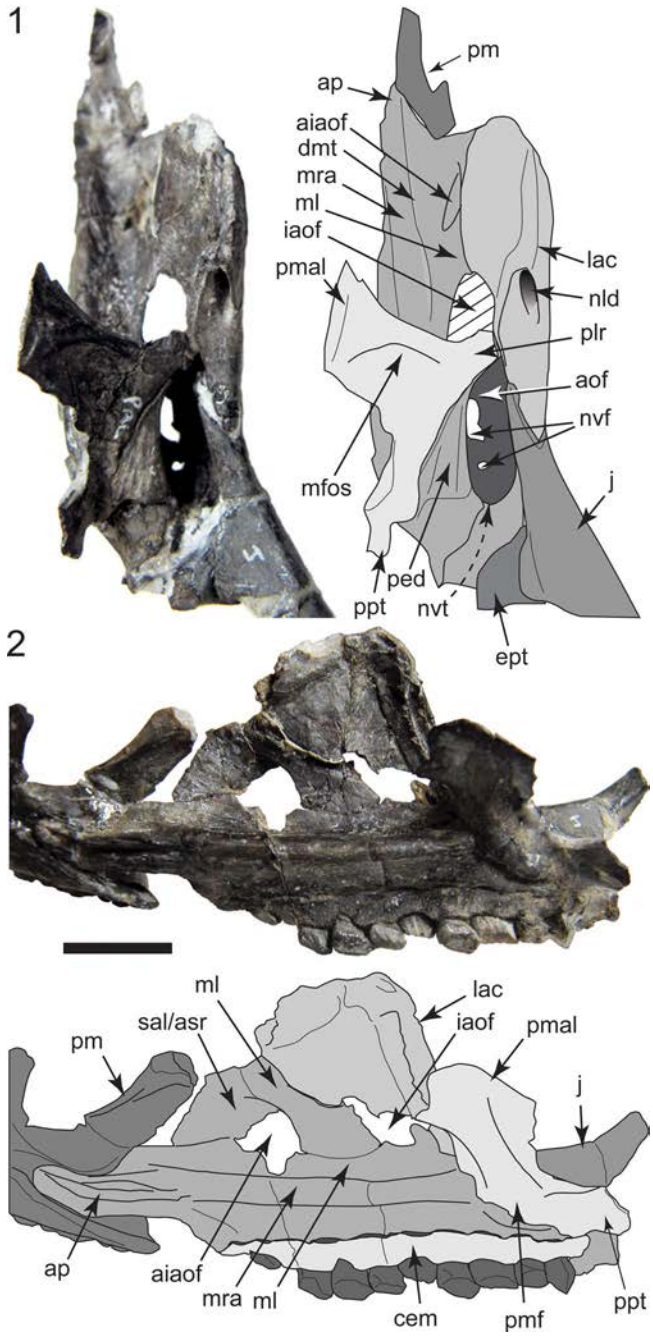

Figure 14. *Hypsilophodon foxii* Huxley, 1870, partial right cranium (NHMUK R2477) and schematics in oblique posterodorsal (1) and medioventral (2) views. Cross-hatching in (**1**) indicates missing supralveolar lamina bordering the antorbital fenestra; dashed arrow indicates entrance of the posterodorsal foramen of the neurovascular tract. aiaof = anterior (accessory) internal antorbital fenestra; aof = antorbital fossa; ap = anterior process of maxilla; asr = ascending ramus of maxilla; cem = cementum; dmt = dorsal maxillary trough; ept = ectopterygoid; iaof = internal antorbital fenestra; j = jugal; lac = lacrimal; mfos = muscular fossa of palatine; ml = medial maxillary lamina; mra = maxillary ramus; nld = nasolacrimal duct; nvf = neurovascular foramina; nvt = neurovascular tract; ped = pedestal; plr = palatine lateral ramus; pm = premaxilla; pmal = palatine medial ala; pmf = palatine maxillary flange; ppt = pterygoid process of the palatine; sal = supralveolar lamina. Scale bar = 10 mm (**2**; for scale in **1**, refer to **2**).

ornithischians (e.g., Porro et al., 2011, 2015). Viewed labially, the distal margins of the crowns mostly overlap the mesial margins of the adjacent crowns. This pattern of overlap is reversed on some crowns (Fig. 15). The roots taper toward their distal ends and are roughly ovoid in section (Fig. 16). The axis of the root is straight. However, the lingual margin of the root on the teeth in the middle of the tooth row forms a marked S-shaped bend extending dorsally from its base at the cingulum (Fig. 16.4). As a result, mesiolingual and distolingual fossae are formed that accommodate developing crowns of the abutting tooth families. Twisting of the root shaft also aligns the broad mesial and distal surfaces of the roots with the oblong, obliquely angled alveoli (Fig. 5.4). The resorption facets on the roots follow the profile of the apical margins of the successively developing crowns (Fig. 15). At full-length, the roots reach the dorsal surface of the maxillary ramus (Fig. 16). Tooth replacement is posterior to anterior with a Zahnreihe spacing ('Z-spacing,' sensu Edmund, 1960) of 1.65 suggested (calculated at M7–M8 on the holotype; based on methods of Osborn, 1975, fig. 1).

The largest maxillary crowns are in the posterior region of the tooth row. However, the two posteriormost teeth are reduced (Fig. 17), as in most ornithopods. At M8 on the holotype, the ratio of apicobasal depth/mesiodistal width is 1.8 (Fig. 17.4), noting that that the unworn depth of the crown would have been greater. The unworn crowns are spatulate and asymmetrical in labiolingual profile. Wear facets on the worn (working) crowns form a continuous occlusal surface, which slopes at ~ 45° to the root axis, in mesiodistal view (Figs. 5; 11.3, coronal section D; 15). Labially and lingually, the basal region forms a deep V-shaped cingular vertex, offset mesially relative to the central axis of the root (Figs. 15–17). Lingually, the cingulum forms a smooth base lacking bounding ridges. Labially, the cingulum forms the mesial and distal bounding ridges (Figs. 15–17). The mesial bounding ridge is straight and vertically oriented. The distal bounding ridge is longer than the mesial, obliquely sloping from the vertex and arcuate toward its apical end. The primary ridge, developed labially, is arcuate (mesially concave/distally convex), strongly offset to the distal third of crown surface, and merges with the distal bounding ridge, distal to the cingular vertex (Figs. 15–17). On many of the crowns, a shallow labial furrow is formed at the point of confluence with the primary ridge, as in *Leaellynasaura amicagraphica* (Fig. 17). On some crowns, the primary ridge is slightly undercut by the narrow distal paracingular fossa, as in *Atlascopcosaurus loadsi* and *Muttaburrasaurus* sp. (QM F14921). Labially, the secondary apicobasal ridges are closely abutting. Four stronger ridges are developed mesial to the primary ridge (Figs. 15–17). The ridge closest to the primary ridge is convergent with the latter. Two finer secondary ridges are developed in the paracingular fossa distal to the primary ridge (Figs. 15–17). These distal ridges merge with the inside margin of the mesial bounding ridge. Tertiary ridges are additionally developed on the surface of the primary and secondary ridges (Fig. 15.1), as in *Mantellisaurus atherfieldensis* (Hooley, 1925) (Norman, 1986). Narrow apicobasal ridges, separated by channels, are developed on the lingual crown surfaces (Fig. 15). These ridges merge with the smooth crown base. The distal ends of all secondary ridges terminate apically in a transversely oriented, blade-like denticle. The stronger, mesial secondary ridges additionally form tridenticulate mamillated cusps (Fig. 15.3), as in *Nanosaurus agilis* Marsh, 1877 (Bakker et al., 1990; Carpenter and Galton, 2018).

https://doi.org/10.1017/jpa.2018.95

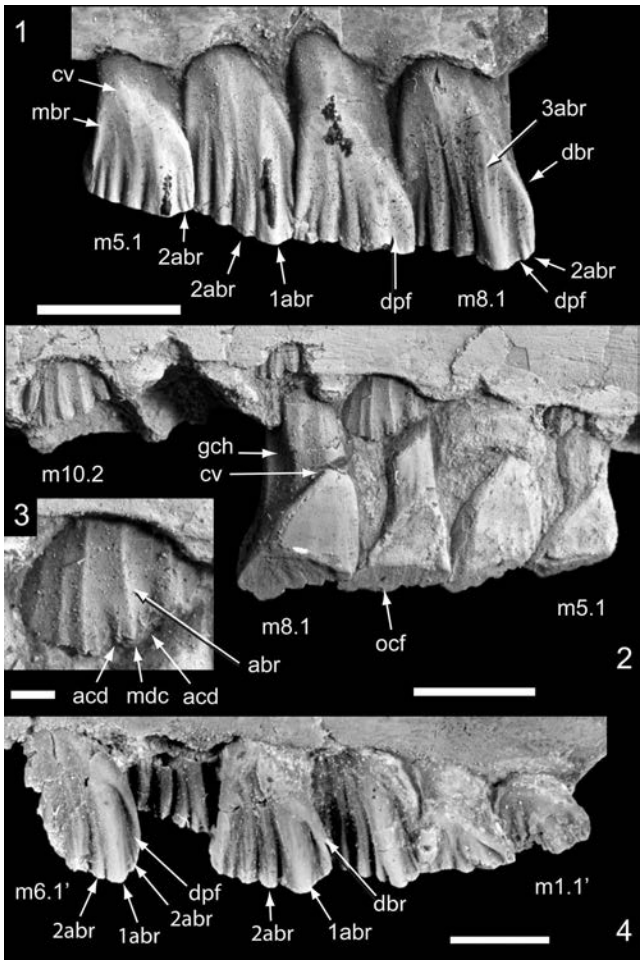

Figure 15. Maxillary dentition of *Galleonosaurus dorisae* n. gen. n. sp.: (**1, 2**) holotypic left dentition (NMV P229196) in labial (**1**) and lingual (**2**) views; (**3**) enlargement of maxillary tooth (m7.2) in (**2**); (**4**) left dentition of NMV P186440 in labial view. 1abr = primary apicobasal ridge; 2abr = secondary apicobasal ridge; 3abr = tertiary apicobasal ridge; abr = apicobasal ridge (see definition, Table 1); acd = accessory denticle; cv = cingular vertex; dbr = distal bounding ridge; dpf = distal paracingular fossa; gch = growth channel/fossa; m# = maxillary tooth position (from anterior end) and replacement number; m#' = maxillary tooth position (from posterior end) and replacement number; mbr = mesial bounding ridge; mdc = median denticle; ocf = occlusal facet. Scale bars: 5 mm (**1, 2, 4**); 1 mm (**3**).

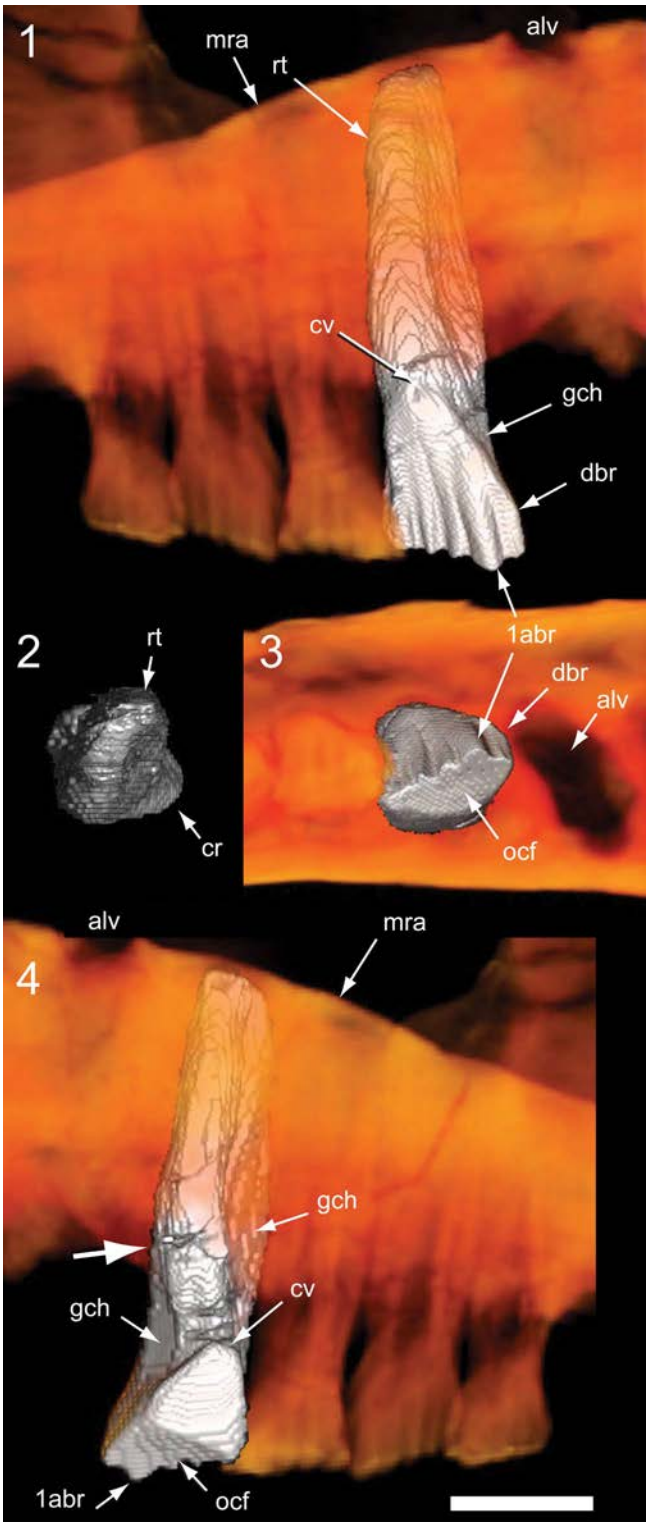

Figure 16. Maxillary dentition of *Galleonosaurus dorisae* n. gen. n. sp., digital 3D model of holotypic maxillary tooth m8 (NMV P229196) derived from µCT scans in labial (**1**), dorsal (**2**), apical (**3**), and lingual (**4**) views. Larege arrow in (**4**) indicates sinuous bend on the lingual margin of the root. 1abr = primary apicobasal ridge; alv = alveolus; cr = crown; cv = cingular vertex; dbr = distal bounding ridge; gch = growth channel/fossa; mra = maxillary ramus; ocf = occlusal facet; rt = root. Scale bar = 5 mm.

Variation.—Among the four maxillae with complete alveoli, the number of alveoli varies (Figs. 4, 5, 7, 8). The holotype (NMV P229196) and midsized maxilla (NMV P208178) each have 15 alveoli, and the smaller maxillae (NMV P209977, P212845) each have 13 and 14? (15?) alveoli, respectively. In NMV P209977, a protuberance at the anterior end of the alveolar margin, within the anteroventral process, is interpreted as a blind, developing alveolus (Fig. 7). In NMV P212845 (with 14 or 15 alveoli), the anteriormost alveolus is small and contains a germ tooth. This developing tooth is in the same position as the protuberance on NMV P209977 (Fig. 8). As a result of the abrupt kink on the maxillae of the holotype (NMV P229196), NMV P212845, and possibly in P208178, the posterior portion of the ramus is posterolaterally deflected (Figs. 5, 8). The kink, however, is lacking on NMV P209977 and P186440 (Figs. 6, 7). Therefore, although noting limitations in sample size, the kink is both present and absent on maxillae of larger and smaller sizes. We postulate that the presence and absence of the kink is due to dimorphic rather than ontogenic variation. The dorsal surface of the maxillary

https://doi.org/10.1017/jpa.2018.95

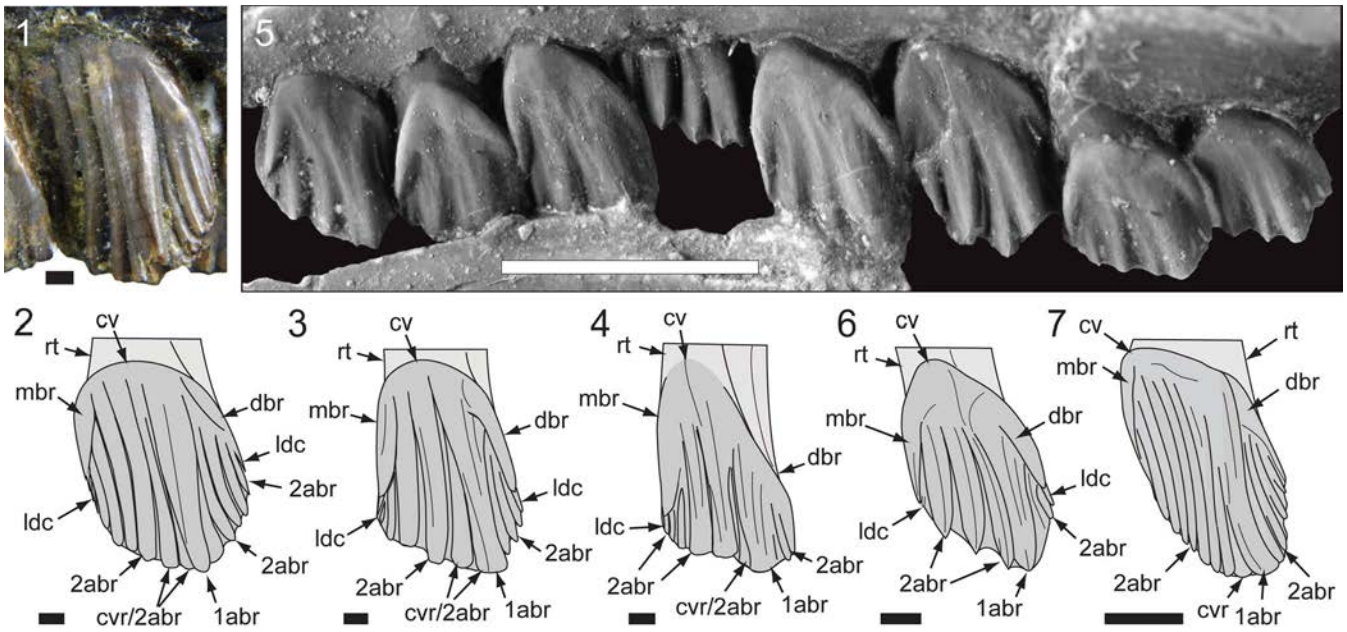

Figure 17. Comparisons of Australian ornithopod maxillary tooth crowns in left labial view: (**1, 2**) *Atlascopcosaurus loadsi* Rich and Rich, 1989 (NMV P157390), m5' (counted from posterior end) and schematic (**2**); (**3**) Victorian ornithopodan maxillary morphotype 4 (cf. *Atlascopcosaurus loadsi*; NMV P208133), schematic of right m3' (reversed; counted from posterior end); (**4**) *Galleonosaurus dorisae* n. gen. n. sp., schematic of holotypic (NMV P229196) m8; (**5, 6**) *Leaellynasaura amicagraphica* Rich and Rich, 1989, holotypic (NMV P185991) m5–m12 with schematic of m9 (**6**); (**7**) *Muttaburrasaurus* sp. (QM F14921), schematic of left ~m4' (counted from posterior end). 1abr = primary apicobasal ridge; 2abr = secondary apicobasal ridge; cv = cingular vertex; cvr = convergent (secondary) ridge; dbr = distal bounding ridge; ldc = lingulate denticle; mbr = mesial bounding ridge; rt = root. Scale bars: 10 mm (**7**); 5 mm (**5**); 1 mm (**1–4, 6**).

Table 2. Measurements (in mm) of Victorian ornithopod maxillary specimens. APL1 = anteroposterior length of maxillary ramus (without anterior process); APL2 = anteroposterior length of the dentulous maxillary portion (extent of alveoli); APL3 = anteroposterior length of anterior (premaxillary) process; DVDR = greatest dorsoventral depth of maxillary ramus; TVW1 = greatest transverse width of maxillary ramus; TVW2 = transverse width of ramus at fifth alveolus; TVW3 = narrowest transverse width of ramus; + = measurement incomplete. In incomplete specimens (NMV P166409, P157390, P208133), the alveoli are counted from the posterior end of the ramus.

Specimen	Alveoli	APL1	APL2	TVW1 (alveolus where measured) and % of ramus length	DVDR (alveolus where measured)	TVW2, and % of ramus length	APL3	TVW3 (alveolus where measured)
Atlascopcosaurus loadsi Rich & Rich, 1989								
NMV P166409 (holotype)	9+	36.0+	–	17.0, –	17.0	–	–	–
NMV P157390	7+	45.0+	–	–	18.0	–	–	–
Galleonosaurus dorisae n. gen. n. sp.								
NMV P229196 (holotype)	15	60.0	54.0	13.5 (m11), 22%	12.5 (m10)	9.0, 15%	9.8	7.0 (m2)
NMV P208178	15	44.5	41.0	9.8 (m12), 22%	9.0 (m10)	5.0, 11%	6.0	5.0 (m2–5)
NMV P186440	7+	35.0	–	12.8, –	14.6	–	–	–
NMV P209977	13	35.6	31.5	7.7 (m10), 22%	7.4 (m9)	5.7, 16%	3.0+	5.0 (m2)
NMV P212845	14	37.0	34.5	9.0 (m11), 24%	7.0 (m10)	6.9, 19%	3.0+	4.8 (m2)
Leaellynasaura amicagraphica Rich & Rich, 1989								
NMV P185991 (holotype)	12	27.0	24.5	4.0 (m9), 15%	4.0 (m9)	2.0, 7%	–	1.8 (m4)
Victorian ornithopod maxillary morphotype 4 (cf. *Atlascopcosaurus loadsi*)								
NMV P208133	6+		–	–	–	–	–	–

ramus on the small maxilla NMV P209977 differs from the other maxillae by forming a pyramid-shaped peak (compare Figs. 5–8). On the other maxillae, including the similarly sized NMV P212845, the surface is smoothly convex. This variation is also incongruent to maxillary size and could be dimorphic. The reasons for dimorphism are unknown. Subspecies variation seems possible, particularly given that the fossil assemblage of the Flat Rocks Sandstone is time-averaged. Sexual dimorphism is also possible, although extremely difficult to assess (see Mallon, 2017). Minor variation is apparent among the observable tooth crowns, although secondary ridge numbers appear uniform. The distal paracingular fossa excavates the distal bounding ridge on the crowns of NMV P186440 to a greater degree than on the holotype (Fig. 15).

Etymology.—dorisae, in recognition of Doris Seegets-Villiers for her geological, palynological, and taphonomic work on the Flat Rocks fossil vertebrate locality.

Materials.—Flat Rocks Sandstone: NMV P212845, partial left maxilla lacking erupted dentition; NMV P208178, partial left maxilla with erupted dentition; NMV P208113, worn right

https://doi.org/10.1017/jpa.2018.95

maxillary tooth; NMV P208523, worn left maxillary tooth; and NMV P209977, partial left maxilla, lacking erupted dentition. The Caves: NMV P186440, posterior portion of left maxilla, left palatine, and fragment of left lacrimal.

Remarks.—The maxilla of *Galleonosaurus dorisae* n. gen. n. sp. possesses several traits typically shared with noniguanodontian neornithischians, including: (1) extensive excavation of the maxilla by the antorbital fossa; (2) articulation of the ectopterygoid restricted to the posterior margin of the maxilla; (3) a single replacement cheek tooth per tooth family; (4) shallow medial inset of the premaxillary process on the maxilla; (5) absence of channel on the anterior ascending ramus of the maxilla for the premaxilla; (6) an obtuse anterior margin on the maxilla; and (7) the lack of contact between the jugal and the external antorbital fenestra by insertion of the lacrimal (as indicated on NMV P186440; Fig. 6). These traits are apparent in neornithischians such as *Heterodontosaurus tucki* (see Norman et al., 2011), *Hypsilophodon foxii* (see Galton, 1974), *Lesothosaurus diagnosticus* (see Porro et al., 2015), and *Changchunsaurus parvus* (see Jin et al., 2010). However, an extensive antorbital fossa is also present in the rhabdodontids (e.g., *Zalmoxes robustus* [NHMUK R3395; unpublished data, Herne, 2009; see also Nopcsa, 1904, table 2; Weishampel et al., 2003]) and basal dryomorphans (e.g., *Camptosaurus dispar* [YPM VP 1886, Fig. 9] and *Dysalotosaurus lettowvorbecki* [see Janensch, 1955; Galton, 1983; Hübner and Rauhut, 2010]). Like *Galleonosaurus dorisae* n. gen. n. sp., the premaxillary process on the maxilla of *Muttaburrasaurus langdoni* lacks strong medial inset (unpublished data, Herne and Nair, 2018). However, as in styracosternans, the premaxillary process in *M. langdoni* is dorsally elevated and a deep channel for the premaxilla is developed on the posterodorsally sloping anterior margin of the anterior ascending ramus (e.g., Norman 2004; Gasulla et al., 2014).

The maxilla of *Galleonosaurus dorisae* n. gen. n. sp. differs from that of *Atlascopcosaurus loadsi* by having a less protrusive posterolateral process and a shallower posterior slope on the dorsal surface of the maxillary ramus leading from the dorsal summit of the maxillary ramus to the ectopterygoid shelf. The maxilla of *Galleonosaurus dorisae* n. gen. n. sp. differs from that of *Leaellynasaura amicagraphica* by having greater lateral concavity of the maxillary alveolar axis and deeper buccal emargination. The number of alveoli in the largest complete maxillae of *Galleonosaurus dorisae* n. gen. n. sp. (up to 15) is greater than that currently known in *L. amicagraphica* (12 in the holotype, NMV P185991). However differing numbers of alveoli between these two taxa could be due to differing stages of ontogeny. On three of the five maxillary specimens currently assigned to *Galleonosaurus dorisae* n. gen. n. sp., the posterior third of the maxilla deflects posterolaterally outward at an abrupt kink (see Variation, above). The kinked form is regarded herein as a potential autapomorphy, with its absence on some maxillae interpreted as dimorphic variation.

The neurovascular tract in *Galleonosaurus dorisae* n. gen. n. sp. is separated from the posterior region of the antorbital fossa by a septum (see coronal section F in Fig. 11.3), which is potentially autapomorphic; however, this region has not been described in adequate detail in most ornithischians to fully confirm its uniqueness. In contrast to *Galleonosaurus dorisae* n. gen. n. sp., the neurovascular tract of *Hypsilophodon foxii* merges with the antorbital fossa. In *Galleonosaurus dorisae* n. gen. n. sp., the ventrolateral neurovascular foramina bypass the antorbital fossa to directly connect the neurovascular tract (Fig. 11.3, coronal sections B–F). These foramina in *H. foxii* (NHMUK R1477; Fig. 14), and most likely *Zalmoxes robustus* (NHMUK R3395; unpublished data, Herne, 2009), penetrate the supralveolar wall to directly enter the antorbital fossa. A similar condition is described in *Changchunsaurus parvus* and *Jeholosaurus shangyuanensis* (see Barrett and Han, 2009; Jin et al., 2010). In *Mantellisaurus atherfieldensis*, the neurovascular tract is separated from its reduced antorbital fossa and restricted to the region between the internal and external antorbital fenestra (see Witmer, 1997, fig. 11B). Similar morphology is likely in *Tenontosaurus tilletti* (see Thomas, 2015). In this aspect, separation of the neurovascular tract and posterior region of the antorbital fossa in *Galleonosaurus dorisae* n. gen. n. sp. appears closer to that of the nonrhabdodontid iguanodontians than to the condition in *H. foxii* and basal neornithischians. Future investigation of this region in other ornithischians could prove phylogenetically informative.

In *Hypsilophodon foxii* (NHMUK R1477; Fig. 14) and *Tenontosaurus tilletti* (see Thomas, 2015), the size of the posterodorsal neurovascular foramen relative to the dorsal surface of the maxilla is substantially larger than in *Galleonosaurus dorisae* n. gen. n. sp. (Figs. 6–8, 10, 11). The relatively small foramen in *Galleonosaurus dorisae* n. gen. n. sp. more closely resembles the condition in *Camptosaurus dispar* (YPM VP 1886; Fig. 9) and *Mantellisaurus atherfieldensis* (see Witmer, 1997, fig. 11B). The two slot-like foramina on the anterolateral margin of the anterior ascending ramus in *Galleonosaurus dorisae* n. gen. n. sp. (Fig. 5) that communicate with the neurovascular tract have not been previously described in any other ornithischian. Bifurcation of the neurovascular tract in the maxilla forming two anterior exits is also unique. For example, in *Tenontosaurus tilletti* (see Thomas, 2015) and *Zephyrosaurus schaffi* Sues, 1980 (Sues, 1980), a single maxillary foramen is reported within the anteroventral fossa. However, there is the possibility that dual foramina in other ornithischians have been previously overlooked.

In *Galleonosaurus dorisae* n. gen. n. sp., the anterior region of the antorbital fossa is partitioned from the internal nasal cavity by the medial lamina of the maxilla (Figs. 8, 11, 12) as in basal neornithischians (e.g., *Jeholosaurus shangyuanensis* [see Barrett and Han, 2009]), basal dryomorphans (e.g., *Dryosaurus elderae* Carpenter and Galton, 2018 [see Galton, 1983], *Dysalotosaurus lettowvorbecki* [see Janensch, 1955; Hübner and Rauhut, 2010, p. 4], and *Camptosaurus dispar* [YPM VP 1886]), and possibly the rhabdodontid *Zalmoxes robustus* (suggested on the incomplete left maxilla, NHMUK R3395). However, in *Tenontosaurus tilletti* (see Thomas, 2015, figs. 10, 19) and styracosternans (e.g., *Iguanodon bernissartensis* [see Witmer, 1997, fig. 11B]), the medial lamina fails to partition the antorbital fossa. Similarly, in *Hypsilophodon foxii* (NHMUK R2477), the medial lamina of the maxilla is absent along the posterior margin of the ascending ramus and as a result, the anterior region of the antorbital fossa opens into the nasal cavity through the anterior (accessory) internal antorbital fenestra (Fig. 14.2).

https://doi.org/10.1017/jpa.2018.95

Therefore, among ornithopods, the form of the medial lamina in *Galleonosaurus dorisae* n. gen. n. sp. appears closer to basal dryomorphans than to *H. foxii* and *Tenontosaurus tilletti*.

The presence of a well-developed dorsal maxillary trough, as in *Galleonosaurus dorisae* n. gen. n. sp., is uncertain in *Atlascopcosaurus loadsi* and *Leaellynasaura amicagraphica*. A dorsal maxillary trough has been reported in *Zalmoxes robustus* (NHMUK R4901; Weishampel et al., 2003), although this region in NHMUK R4901 is obscured by matrix. However, on another maxilla of *Z. robustus* (NHMUK R3395; unpublished data, Herne, 2009), the dorsal maxillary trough is absent because the maxilla is strongly excavated by the antorbital fossa (see also Nopcsa, 1904, table 2.3). In comparison to *Galleonosaurus dorisae* n. gen. n. sp., the dorsal maxillary trough is shallow in *Tenontosaurus tilletti* (see Thomas, 2015, figs. 14, 17) and *Hypsilophodon foxii* (NHMUK R2477; Fig. 14) and absent in *Camptosaurus dispar*. In the last taxon, the medial lamina of the maxilla markedly bulges medially to accommodate a transversely broad antorbital fossa (Fig. 9). Bulging of the medial lamina is also developed on the maxillae of *Galleonosaurus dorisae* n. gen. n. sp., in particular, in the smaller maxillae (NMV P209977, P212845; Figs. 7.2, 8.2, 8.3), but not to the extent observed in *Camptosaurus dispar*.

The lateral ramus of the palatine in *Galleonosaurus dorisae* n. gen. n. sp. is horizontally oriented and strap-like and expands laterally to form a flange (Figs. 6, 10). The hatchet-shaped form of the lateral palatine flange is a potential autapomorphy of the taxon. The lateral flange on the palatine is received in an anteroposteriorly oriented sutural facet on the dorsal surface of the maxilla posterior to the antorbital fossa (Figs. 5–8, 11). This facet on the maxilla for the palatine forms the dorsal surface of the flange that overlies the neurovascular tract (Figs. 5, 7, 8, 11.1; 11.2, 11.3, coronal section A)—morphology shared with *Atlascopcosaurus loadsi* (Fig. 10.6, 10.7) and possibly *Leaellynasaura amicagraphica*—and might be unique to these taxa. A lateral palatine flange is also postulated for *Atlascopcosaurus loadsi* (Fig. 10), as indicated by the facet on the dorsal surface of the maxilla as mentioned. However, in contrast to the hatchet-shaped flange on the lateral ramus of the palatine in *Galleonosaurus dorisae* n. gen. n. sp., that of *Atlascopcosaurus loadsi* was likely to have been asymmetrically expanded in the posterior direction (Fig. 10). As in *Galleonosaurus dorisae* n. gen. n. sp., the lateral palatine ramus in *Camptosaurus dispar* (YPM VP 1886) would have been horizontally oriented, as suggested by a rugose facet on the dorsal surface of its maxilla (Fig. 9). However, unlike in *Galleonosaurus dorisae* n. gen. n. sp., a facet on the maxilla for a lateral flange of the palatine is not apparent. The lateral ramus of the palatine in *Jeholosaurus shangyuanensis* is reportedly horizontally oriented (Barrett and Han, 2009), as in *Galleonosaurus dorisae* n. gen. n. sp., but differs in being hook-like. Unlike in *Galleonosaurus dorisae* n. gen. n. sp., the lateral rami on the palatines of *Hypsilophodon foxii* (NHMUK R2477; Fig. 14) and *Tenontosaurus tilletti* (see Thomas, 2015) form thickened, dorsolaterally directed struts, which adjoin dorsally raised pedestals on their maxillary rami. The distal ends of these rami lack an expanded flange. A lateral ramus on the palatine is absent in *Thescelosaurus neglectus* (see Brown et al., 2011; Boyd, 2014) and styracosternans (e.g., Horner, 1992). This region currently lacks detailed description in dryosaurids and ornithischians in general, thus inhibiting more extensive comparisons.

The maxillae of *Galleonosaurus dorisae* n. gen. n. sp. suggest that new alveoli developed at the anterior end of the tooth row during ontogeny, which is consistent with the pattern of development interpreted in *Dysalotosaurus lettowvorbecki* (see Hübner and Rauhut, 2010), *Jeholosaurus shangyuanensis* (see Barrett and Han, 2009), and *Heterodontosaurus tucki* (see Norman et al., 2011). The sinuous lingual margin on the maxillary tooth roots in *Galleonosaurus dorisae* n. gen. n. sp. is not presently reported in any other ornithischian (Fig. 16).

Galleonosaurus dorisae n. gen. n. sp. possesses a combination of seven maxillary crown features, which include: (G1) spatulate, asymmetrical crowns, resulting from having markedly V-shaped labial and lingual cingular vertices offset mesially relative to the central root axis and the primary ridge (developed labially) offset to distal third of the crown surface; (G2) the primary ridge on some crowns slightly undercut by the distal paracingular fossa; (G3) the distal bounding ridge developed labially being longer and more sloping than the mesial bounding ridge, which is relatively straight and vertical; (G4) secondary ridges, developed labially, closely abutting the ridges distal to the primary ridge more finely developed than those mesially; (G5) secondary ridges developed lingually, with mesiodistally narrow crests; (G6) the primary ridge and secondary ridges mesial to the primary ridge, terminating apically in mamillated, tridenticulate cusps; and (G7) apical crown margins lacking the development of multiple unsupported lingulate denticles.

Nearly all of the aforementioned maxillary crown features (G1–7) in *Galleonosaurus dorisae* n. gen. n. sp. are shared with *Atlascopcosaurus loadsi*, *Leaellynasaura amicagraphica*, and *Muttaburrasaurus* spp. (see comparisons, Fig. 17). However, specific differences are apparent among these taxa. Whereas the cingular vertex on the labial crown surfaces of *Galleonosaurus dorisae* n. gen. n. sp., *L. amicagraphica*, and *Muttaburrasaurus* spp. are V-shaped and mesially offset (in part, crown feature G1), the labial cingular vertex on the *Atlascopcosaurus loadsi* crowns is U-shaped and more centrally positioned. However, the lingual vertex on the *Atlascopcosaurus loadsi* crowns is V-shaped and mesially offset, as in *Galleonosaurus dorisae* n. gen. n. sp. The base of the primary ridge on the crowns of *Galleonosaurus dorisae* n. gen. n. sp., *Atlascopcosaurus loadsi*, and *Muttaburrasaurus* spp. merges more distally with the distal bounding ridge than on the crowns of *L. amicagraphica* (Fig. 17). On crowns of similar size, those of *Galleonosaurus dorisae* n. gen. n. sp. differ from those of *Atlascopcosaurus loadsi* by having fewer secondary ridges mesial to primary ridge (four ridges compared with six) and fewer, more finely developed, secondary ridges distal to primary ridge (two ridges compared with four). In secondary ridge number and development, the crowns of *L. amicagraphica* are closer to those of *Galleonosaurus dorisae* n. gen. n. sp. than to those of *Atlascopcosaurus loadsi*. The number of secondary ridges on the maxillary crowns of *Muttaburrasaurus* spp., mesial to the primary ridge, is substantially greater (~11 ridges) than on the crowns of the Victorian taxa. However, the number of secondary ridges in the distal paracingular fossa on the crowns of *Muttaburrasaurus* sp. (QM F14921; four ridges) is comparable to that in *Atlascopcosaurus loadsi*. Tridenticulate mamillated cusps on the crowns of *Galleonosaurus dorisae* n. gen. n. sp.

https://doi.org/10.1017/jpa.2018.95

(crown feature G6; Fig. 15) are shared with the holotype of *Atlascopcosaurus loadsi* (NMV P166409), and are unknown on the crowns of *L. amicagraphica* and *Muttaburrasaurus* spp. Tridenticulate marginal cusps have previously been reported only in the Late Jurassic Laurentian neornithischian *Nanosaurus agilis* ('multicuspid cusps' of Carpenter and Galton, 2018).

Most of the maxillary crown features in *Galleonosaurus dorisae* n. gen. n. sp. are also shared with the Argentinian ornithopods *Gasparinisaura cincosaltensis* (MUCPv 208; unpublished data, Herne, 2008) and *Talenkauen santacrucensis* Novas, Cambiaso, and Ambrosio, 2004 (based on Cambiaso, 2007, fig. 17). These include having: (1) spatulate crowns (Fig. 3.3c) with V-shaped cingular vertices and asymmetrical form, resulting from distal offset of the primary ridge (crown feature G1; noting that mesial offset of the cingular vertices is uncertain); (2) closely abutting secondary ridges developed labially, eliminating space for ridge-free paracingular fossae with finer secondary ridges developed distal to the primary ridge (crown feature G4); (3) the primary ridge slightly undercut by the distal paracingular fossa (crown feature G2); and (4) the absence of multiple unsupported lingulate denticles along the apical margins of the crowns (crown feature G7). Apicobasal ridges are also developed on the lingual crowns of *Talenkauen santacrucensis* (crown feature G5), but these are presently unknown in *Gasparinisaura cincosaltensis*.

Cambiaso (2007) described the maxillary dentition of *Anabisetia saldiviai* Coria and Calvo, 2002, suggesting that the maxilla of the holotype (MCF-PVPH-74; see Coria and Calvo, 2002) possessed two crown morphologies, one larger and one smaller. In agreement with Cambiaso (2007), the presence of two crown morphologies on the fragmentary holotypic maxilla (unpublished data, Herne, 2008) confirms that the maxillary dentition of *Anabisetia saldiviai* is unusually heterodont. Importantly, *Anabisetia saldiviai* shares several maxillary crown features with *Galleonosaurus dorisae* n. gen. n. sp. On the larger crown form (see Cambiaso, 2007): (1) the primary ridge is undercut by the distal paracingular fossa (crown feature G2); (2) the crown profile is spatulate (crown feature G1, in part, although not asymmetrical in form); (3) apicobasal ridges are possibly present on the lingual crown surface (crown feature G5); (4) mamillated marginal cusps are present (crown feature G6, in part, noting that fully-extending, lingual secondary ridges are absent, and the development of tridenticulate cusps unknown); and (5) multiple unsupported marginal lingulate denticles are absent (crown feature G7). However, the larger crown form of *Anabisetia saldiviai* also shares with dryomorphans (e.g., *Dryosaurus* spp. and *Mantellisaurus atherfieldensis* [see Galton, 1983; Norman, 1986]) relatively smooth mesial and distal paracingular fossae flanking a sharp-crested primary ridge; this is not present on the crowns of *Galleonosaurus dorisae* n. gen. n. sp. The smaller maxillary crown form in *Anabisetia saldiviai* shares with *Galleonosaurus dorisae* n. gen. n. sp.: (1) a spatulate asymmetrical form, with a mesially offset V-shaped cingular vertex and a distally positioned primary ridge (see also Cambiaso, 2007; crown feature G1, noting that the presence of a mesially offset vertex on the lingual crown surface is unknown; that is undercut by a narrow distal paracingular fossa [crown feature G2]); and (2) closely abutting, round-crested secondary ridges (Cambiaso, 2007) mesial to the primary ridge (crown feature G4, noting that secondary ridges distal to the primary ridge appear absent).

The maxillary crown features shared between *Galleonosaurus dorisae* n. gen. n. sp., other Victorian ornithopods, *Muttaburrasaurus* spp., and the Argentinian ornithopods, as mentioned, suggest that these taxa could be closely related. Moreover, the crown features differ from those of *Tenontosaurus* spp. and dryomorphans (e.g., Galton, 1983; Norman 1986; Thomas, 2015), in which the crowns are rhomboidal (diamond-shaped or lanceolate; Fig. 3.3d), the mesial and distal paracingular fossae are smooth (i.e., ridge-free) or have channels between the secondary ridges, and multiple unsupported lingulate denticles are present along the apical margins.

As a concept of tooth replacement efficiency in the mature stages of all reptiles, a Z-spacing of 1.75–2.5 indicates that at least three teeth are in a favorable functioning state within a sequence of eight tooth positions (following Osborn, 1975). The estimated Z-spacing in the holotype of *Galleonosaurus dorisae* n. gen. n. sp. of 1.65 is slightly less than the lowest replacement timing (i.e., 1.75) suggested by Osborn (1975). However, because the value we calculated is based solely on alveolar positions M7–M8 on the holotype, the amount of Z-spacing in *Galleonosaurus dorisae* n. gen. n. sp. is inconclusive.

In summary, the overall morphology of the maxilla, dentition, and palatine suggest tht *Galleonosaurus dorisae* n. gen. n. sp., *Atlascopcosaurus loadsi*, and *Leaellynasaura amicagraphica* are closely related. Apart from these taxa, closer affinities between *Galleonosaurus dorisae* n. gen. n. sp., *Anabisetia saldiviai*, *Gasparinisaura cincosaltensis*, *Muttaburrasaurus* spp., and *Talenkauen santacrucensis* are suggested by shared features of the dentition. However, the larger maxillary crown form in *Anabisetia saldiviai* also suggests morphology shared with dryomorphans. The lack of an anterior groove on the anterior margin of the maxilla for the premaxilla and the shallow medial inset of the premaxillary process are features consistent with nondryomorphan neornithischians. However, the kinked shape of the maxilla in *Galleonosaurus dorisae* n. gen. n. sp. (in dorsoventral view), and the relatively small size of the posterodorsal neurovascular foramen relative to the maxillary ramus, resemble features in *Camptosaurus dispar* (Figs. 5, 8, 9, 11). These features suggest that *Galleonosaurus dorisae* n. gen. n. sp. might be closer to basal dryomorphans than to both *Hypsilophodon foxii* (NHMUK R2477; Fig. 14) and the basal iguanodontian *Tenontosaurus tilletti* (based on Thomas, 2015, fig. 12), in which the posterodorsal neurovascular foramen is comparatively large. Further investigations that compare the dorsal and internal structures of the maxilla in more neornithischians are likely to be phylogenetically informative.

Genus *Atlascopcosaurus* Rich and Rich, 1989

Type species.—*Atlascopcosaurus loadsi* Rich and Rich, 1989; Point Lewis and Dinosaur Cove in the Otway region of Victoria, southeastern Australia; lower Albian of the Eumeralla Formation in the Otway Basin.

cf. *Atlascopcosaurus loadsi* (Rich and Rich, 1989)
Figures 17.3, 18; Table 2

Occurrence.—Flat Rocks locality in the Inverloch region of Victoria, southeastern Australia (Fig. 1); Flat Rocks

https://doi.org/10.1017/jpa.2018.95

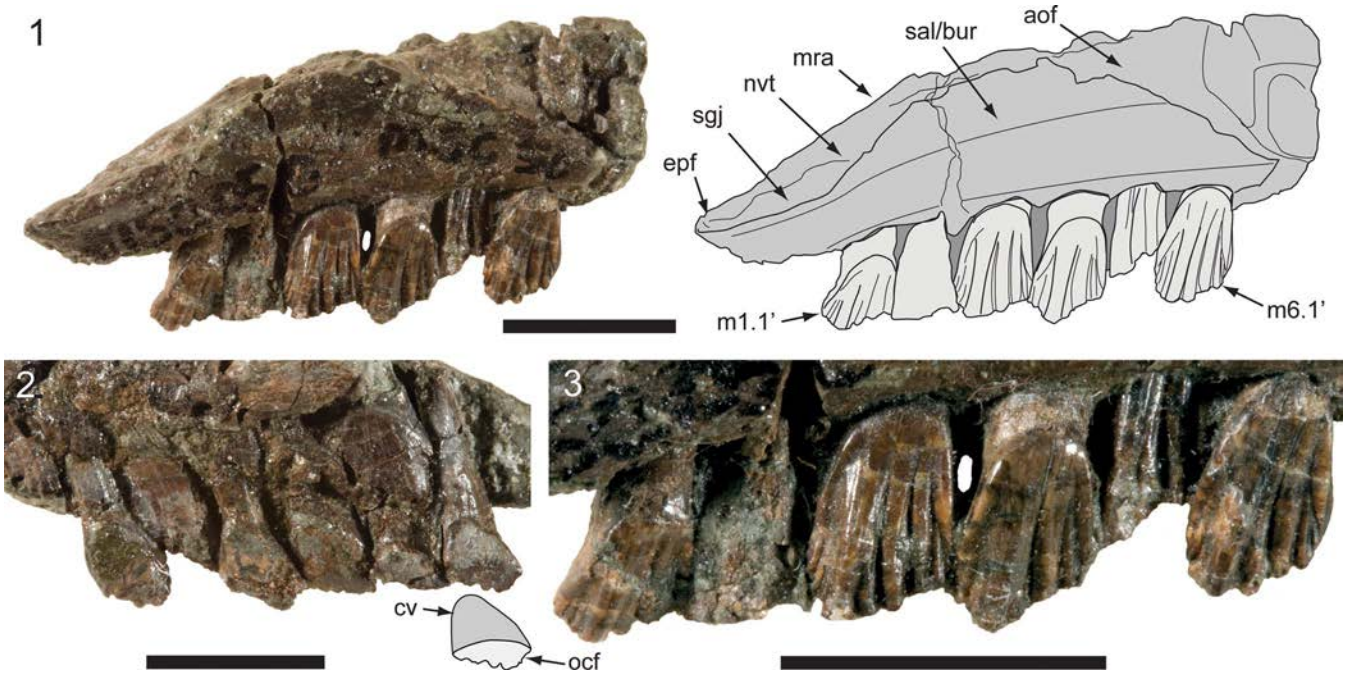

Figure 18. Victorian ornithopodan maxillary morphotype 4 (cf. *Atlascopcosaurus loadsi* Rich and Rich, 1989) from the Flat Rocks Sandstone in the Wonthaggi Formation, southeastern Australia: (**1**) right maxilla (NMV P208133) in lateral view; (**2, 3**) maxillary dentition in lingual (**2**) and labial (**3**) views, with schematic of crown surface in (**2**). aof = antorbital fossa; bur = buccal ridge; cv = cingular vertex; epf = ectopterygoid flange on maxilla; m#' = maxillary tooth position (from posterior end) and replacement number; mra = maxillary ramus; nvt = neurovascular tract; ocf = occlusal facet; sal = supralveolar lamina; sgj = sutural groove for jugal. Scale bars = 10 mm.

Sandstone, upper Barremian of the Wonthaggi Formation in the Gippsland Basin.

Materials.—NMV P208133, partial right maxilla with erupted dentition.

Remarks.—The maxilla NMV P208133 (Fig. 18) is referred to cf. *Atlascopcosaurus loadsi* based on features of the maxillary tooth crowns shared with *Atlascopcosaurus loadsi* from the Eumeralla Formation. The maxilla is hereafter termed 'Victorian ornithopod maxillary morphotype 4' (VOM4). As in *Atlascopcosaurus loadsi*, the maxillary crowns of VOM4 have a U-shaped labial cingular vertex and strongly developed secondary apicobasal ridges labially in the distal paracingular fossa (Fig. 17). The crowns of *Galleonosaurus dorisae* n. gen. n. sp. differ from those of VOM4 by having: (1) a V-shaped cingular vertex on the labial crown surface; (2) greater mesial offset of the labial cingular vertex; (3) merger between the primary and distal bounding ridge more distally offset; and (4) secondary ridges, distal to the primary ridge, more weakly developed (see the listed combination of maxillary crown features in Remarks for *Galleonosaurus dorisae* n. gen. n. sp.). VOM4 possesses four strongly developed secondary ridges mesial to the primary ridge, as in *Galleonosaurus dorisae* n. gen. n. sp., and at least three secondary ridges distal to the primary ridge, as in *Atlascopcosaurus loadsi* (Fig. 17). Although incomplete, the dorsoventral depth of the maxillary ramus in NMV P208133 appears more like that of *Galleonosaurus dorisae* n. gen. n. sp. than of *Atlascopcosaurus loadsi*, particularly the referred maxilla NMV P157390, in which the dorsal peak of the ramus is comparatively higher (compare Figs. 13 and 18). Thus, from the morphology available, VOM4 (NMV P208133) appears intermediate to *Atlascopcosaurus loadsi* and *Galleonosaurus dorisae* n. gen. n. sp. Nonetheless, we consider features of the maxillary tooth crowns closer to those of *Atlascopcosaurus loadsi*.

Genus *Qantassaurus* Rich and Vickers-Rich, 1999

Type species.—*Qantassaurus intrepidus* Rich and Vickers-Rich, 1999 from the Flat Rocks Sandstone, Victoria, southeastern Australia, by original designation.

Qantassaurus intrepidus Rich and Vickers-Rich, 1999
Figures 19, 20.1, 20.3–20.5; Tables 3, 4

1999 *Qantassaurus intrepidus* Rich and Vickers-Rich, p. 175, fig. 9.

Holotype.—NMV P199075, almost complete dentary from the Wonthaggi Formation, Victoria, Australia.

Diagnosis.—Small-bodied ornithopod characterized by a combination of six features, including three potential autapomorphies (*): (1*) dentary markedly foreshortened (ratio of greatest dorsoventral height from ventral margin to alveolar margin/total tooth row length ≅ 0.6); (2*) dorsoventral depth of the lateral alveolar parapet higher than the portion of dentary ramus ventral to the buccal ridge (ratio of alveolar

https://doi.org/10.1017/jpa.2018.95

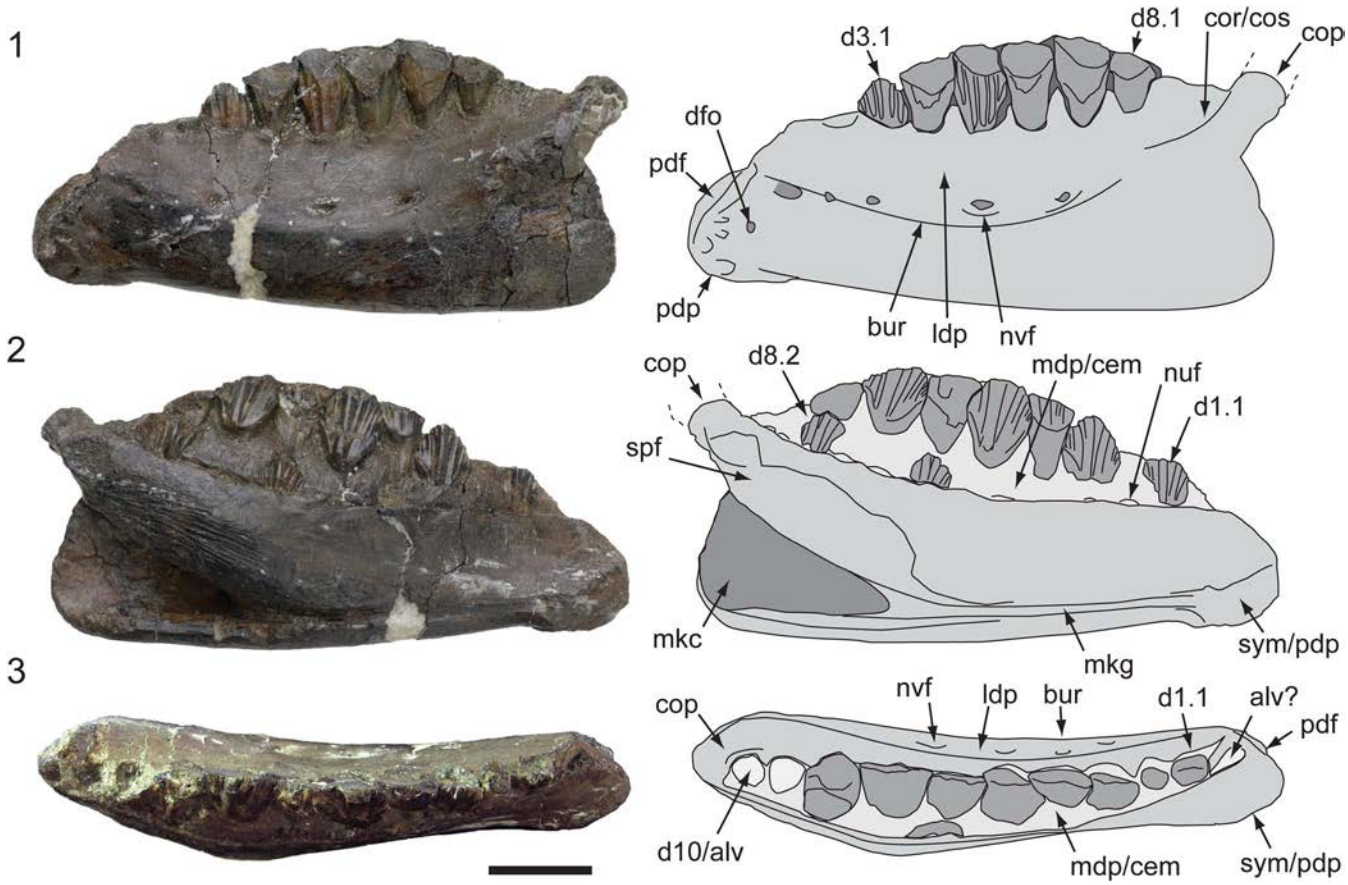

Figure 19. *Qantassaurus intrepidus* Rich and Vickers-Rich, 1999, holotypic left dentary (NMV P199075) and schematics from the Flat Rocks Sandstone in the Wonthaggi Formation, southeastern Australia, in lateral (**1**), medial (**2**), and dorsal (**3**) views. alv = alveolus; bur = buccal ridge; cem = cementum; cop = coronoid process; cor = coronoid ridge; cos = coronoid shelf; d# = dentary tooth position (from anterior end) and replacement number; dfo = anterior dentary foramen; ldp = lateral dentary parapet; mdp = medial dentary parapet; mkc = Meckelian canal (fossa); mkg = Meckelian groove; nuf = nutrient foramen; nvf = neurovascular foramen; pdf = predentary facet; pdp = predentary process; spf = splenial facet; sym = symphyseal surface. Scale bar = 10 mm. Images (**1, 2**) courtesy of Museums Victoria.

parapet height/height ventrally to buccal ridge ≅ 1.8); (3*) line of the buccal ridge deeply concave and offset ventrally relative to the line of the coronoid ridge; (4) level of the lateral alveolar parapet markedly elevated relative to the coronoid ridge and shelf; (5) occlusal margin on the dentary teeth markedly convex; and (6) ventral margin of the dentary ramus convex over its length as far as the symphyseal margin. (Amended from the original work of Rich and Vickers-Rich, 1999).

Occurrence.—Flat Rocks locality in the Inverloch region of Victoria, southeastern Australia (Fig. 1); Flat Rocks Sandstone, upper Barremian of the Wonthaggi Formation in the Gippsland Basin.

Description.—(Amended from that of Rich and Vickers-Rich, 1999 with some information by the original authors only repeated where new context is considered necessary.) The taxon is known only from a single dentary with almost complete dentition (Figs. 19, 20). Two previously referred dentaries (NMV P198962, P199087; Rich and Vickers-Rich, 1999) are removed and assigned herein to *Qantassaurus* ? *intrepidus* (Fig. 21). The predentary and coronoid processes are degraded and incomplete. The two posteriormost erupted teeth are missing. Ten alveoli are present (sensu Rich and Vickers-Rich, 1999), however, a small, anterior, triangular, matrix-filled pit suggests an eleventh alveolus could be present, but it is yet unconfirmed. Viewed dorsally (Fig. 19.3), the alveolar margin is shallowly concave laterally, and the buccal emargination depth (measured midway along the tooth row) roughly equals the labiolingual width of a single crown. Viewed lateromedially, the occlusal margin is markedly convex (Fig. 20.1), with the greatest depth of the dentition (taken from the anteroposterior cord along the tooth row) ~16% of the total tooth row length. The buccal ridge forms a deeply concave margin, the line of which is separated from and depressed ventrally to the line of the coronoid ridge (Fig. 19). The lateral dental parapet (= buccal shelf) forms a dorsoventrally deep fossa between the buccal ridge and the alveolar margin, as in *Dysalotosaurus lettowvorbecki* (see Janensch, 1955, table 11), *Zalmoxes robustus* (NHMUK R3407, although not R3392), and *Owenodon hoggii* Owen, 1874 (NHMUK R2998). The lateral dental parapet is distinctly elevated dorsally relative to the coronoid shelf (Fig. 19), as in *Dysalotosaurus lettowvorbecki* (see Janensch, 1955, table 11). Five ovate neurovascular foramina penetrate the lateral dental parapet. The ventral margin of the dentary is

https://doi.org/10.1017/jpa.2018.95

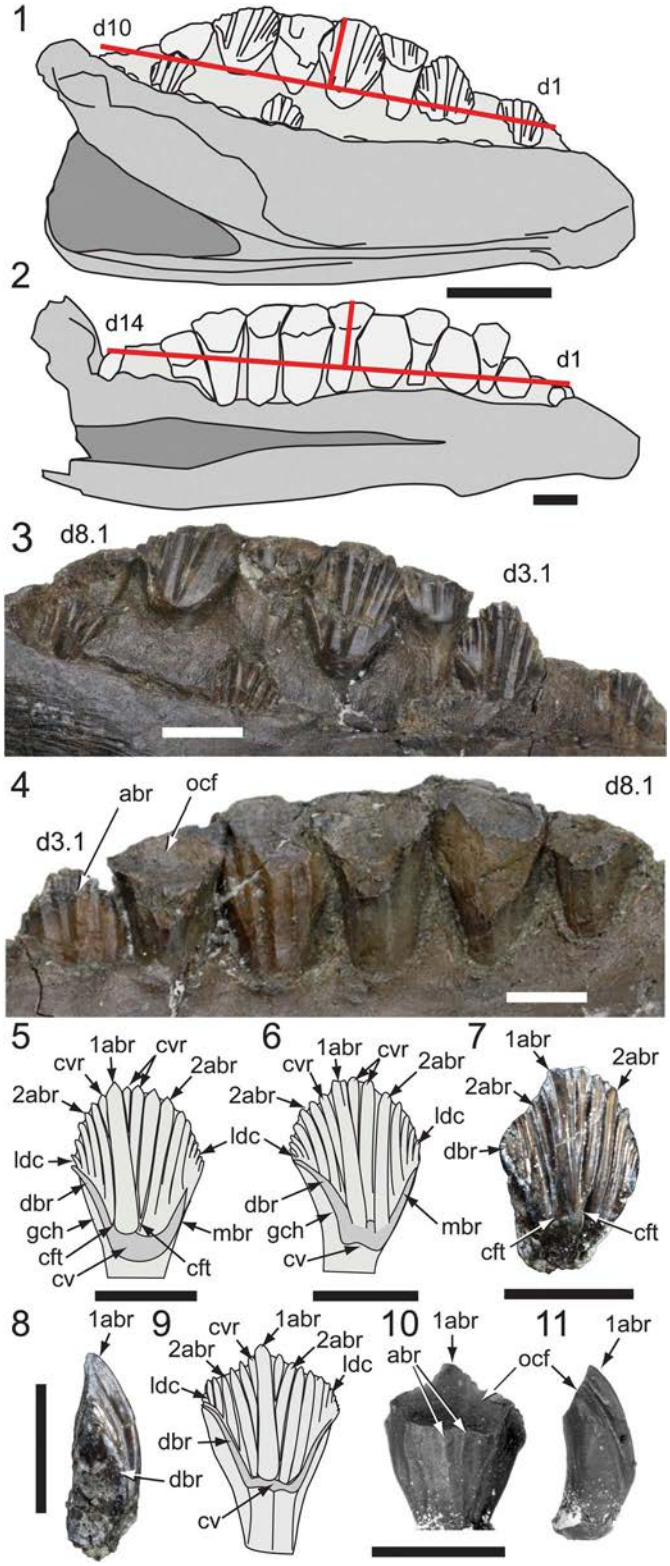

Figure 20. Dentition of *Qantassaurus intrepidus* Rich and Vickers-Rich, 1999 and comparisons: (**1, 2**) schematics of dentary occlusal margin profiles in medial view of *Q. intrepidus* (NMV P199075) (**1**) and *Owenodon hoggii* Owen, 1874 (NHMUK R2998, holotype) (**2**); (**3, 4**) holotypic left dentition of *Q. intrepidus* (NMV P199075) in lingual (**3**) and labial (**4**) views (images courtesy of Museums Victoria); (**5, 6**) schematics showing lingual ornamentation of unworn left dentary tooth d5.1 in *Q. intrepidus* (NMV P199075) (**5**) and unworn isolated left dentary tooth (NMV P177934) from the Eumeralla Formation referred to *Atlascopcosaurus loadsi* Rich and Rich, 1989 (**6**) (Rich and Vickers-Rich, 1989, fig. 11B); (**7, 8**) unworn left dentary tooth (NMV P186426) from the Eumeralla Formation in lingual (**7**) and labial (**8**) views; (**9–11**) right worn dentary tooth of *Kangnasaurus coetzeei* Haughton, 1915 (SAM-PK-2732; reversed) showing schematic of lingual ornamentation (**9**) (from image courtesy of K. Poole) and labial (**10**) and distal (**11**) views of cast (NMV P197995). Lines in (**1, 2**) indicate tooth row length and depth. 1abr = primary apicobasal ridge; 2abr = secondary apicobasal ridge; abr = apicobasal ridge; cft = cleft; cv = cingular vertex; cvr = convergent (secondary) ridge; d# = dentary tooth position (from anterior end) and replacement number; dbr = distal bounding ridge; gch = growth channel; ldc = lingulate denticle; mbr = mesial bounding ridge; ocf = occlusal facet. Scale bars: 10 mm (**1–2, 9–11**); 5 mm (**3–8**).

https://doi.org/10.1017/jpa.2018.95

Table 3. Measurements (in mm) of Victorian ornithopod dentary specimens. APL1 = total anteroposterior length of ramus; APL2 = anteroposterior length of alveolar margin; CPA = angle of coronoid process relative to alveolar margin; DVD1 = dorsoventral depth from lateral alveolar margin at midtooth row to ventralmost point; DVD2 = dorsoventral depth of dentary and dentition at midtooth row; TVWR = transverse width of ramus at midtooth row; + = measurement incomplete; [e] = estimation.

Specimen	Alveoli	APL1	APL2	DVD1	DVD2	TVWR	CPA
Qantassaurus intrepidus Rich and Vickers-Rich, 1999							
NMV P199075 (holotype)	10	55.0	47.0	13.0	25.5	10.5	–
Victorian ornithopod dentary morphotype 2 (*Q. intrepidus*?)							
NMV P199087	8+	44+	–	–	–	–	–
NMV P198962	10	59.0	44.0	17.0	?	10.5	70°
Victorian ornithopod dentary morphotype 3 (Ornithopoda indet.)							
NMV P199135	12–13	68.0	–	–	19.0	–	–
NMV P228408	13	41.0	34.0	9.8	14.0[e]	6.0	45°
NMV P231182	13	91.0	62.0	18.5[e]	–	–	45°

Table 4. Percentage of dentary depth against tooth row length for selected ornithopods. ALTR = total anteroposterior length of tooth row; DVD = greatest dorsoventral depth of dentary and dentition from ventral margin to occlusal margin (exclusive of coronoid process); DVD/ALTR = percentage of the dentary depth to tooth row length. All measurements in mm.

Specimen (side of jaw) and tooth position of DVD	ALTR	DVD	DVD/ALTR
Qantassaurus intrepidus Rich and Vickers-Rich, 1999 NMV P199075 (left), d7	47.0	28.2	60.0%
Zalmoxes shqiperorum Weishampel et al., 2003 UBB NVZ1-1 (left), d7 (Godefroit et al., 2009, fig. 9)	147.0	73.5	50.0%
Dysalotosaurus lettowvorbecki Pompeckj, 1920 MB.R.1365 (right), d7 (Janensch, 1955, table 11)	65.0	32.0	49.0%
Dryosaurus altus Marsh, 1878 CM 3392 (right), d8	62.0	29.0	46.8%
Owenodon hoggii Owen, 1874 NHMUK R2998 (right), d10	108.0	48.0	44.4%
Victorian ornithopod dentary morphotype 3 NMV P199135 (right), d8	46.7	20.5	42.8%
Victorian ornithopod dentary morphotype 3 NMV P228408 (left), d9	34.0	14.0	41.2%
Camptosaurus dispar Marsh, 1879 YPM VP 1886 (left), d5	156.0	62.0	39.7%
Mantellisaurus atherfieldensis (Hooley, 1925) RBINS R57 and NHMUK R5764 (right, composite), d11 (Norman, 1986, fig. 19)	205.0	64.0	31.2%

convex up to the symmetrically triangular predentary process. The facet for the caudolateral process of the predentary is grooved and the anterior dentary foramen is approximately in the middle of the predentary process (Fig. 19). The dorsomedial surface of the predentary process is spout-shaped.

Laterally (Fig. 19.1), the alveolar and ventral margins are convergent, as in *Talenkauen santacrucensis*, *Hypsilophodon foxii*, *Dryosaurus* spp. (in agreement with Agnolin et al., 2010), *Dysalotosaurus lettowvorbecki* (see Janensch, 1955, table 11), and *Thescelosaurus neglectus* (see Galton, 1997, fig. 1). Medially (Fig. 19.2), the dorsal and ventral margins of the dentary ramus (taken as the region between the medial groove and the ventral margin) are also convergent, as in *Dysalotosaurus lettowvorbecki* (see Janensch 1955, fig. 12) and, provisionally, *Talenkauen santacrucensis* (see Cambiaso, 2007, fig. 15) and *Owenodon hoggii* (see Norman and Barrett, 2002, fig. 2). In contrast, these margins are divergent anteriorly in at least *H. foxii* (based on Galton, 1974, fig. 10), *Tenontosaurus tilletti* (see Thomas, 2015, fig. 47), and possibly *Thescelosaurus neglectus* (see Galton, 1997, fig. 1). The greatest dorsoventral height of the dentary and dentition is ~60% of the tooth row length. In this aspect, the dentary of *Qantassaurus intrepidus* is higher than in the other ornithopods compared herein (Table 4). Cementum forming the medial dental parapet encasing the erupted and developing crowns dorsally to the medial groove (Fig. 19.2) is distinguished by a slightly pitted texture. Elongate nutrient foramina distributed along the medial groove align with the tooth families. The triangular medial opening of the Meckelian canal forms an included angle of ~30°. The opening pinches out posterior to the middle of the dentary, and anterior to this point, a narrow Meckelian groove continues onto the dorsal surface of the predentary process (Fig. 19.2). The surface for the splenial/prearticular is slightly depressed with anteroposteriorly oriented striae. Dorsal to the splenial surface, another, smaller sutural surface with finer striae likely adjoined the coronoid.

Dentition.—Only a single replacement crown is present per tooth family, as in basal ornithopods and basal iguanodontians (Norman, 2004; Norman et al., 2004). The complete morphology of the root is uncertain. Viewed lingually, the crowns are spatulate and mesiodistally expanded relative to the roots (Fig. 20.3). The cingulum is more strongly developed lingually than labially. Labially, the cingular vertex is deeply V-shaped (Fig. 20.4), however, on most of the crowns (where observable), the cingular base merges with the root. Lingually,

https://doi.org/10.1017/jpa.2018.95

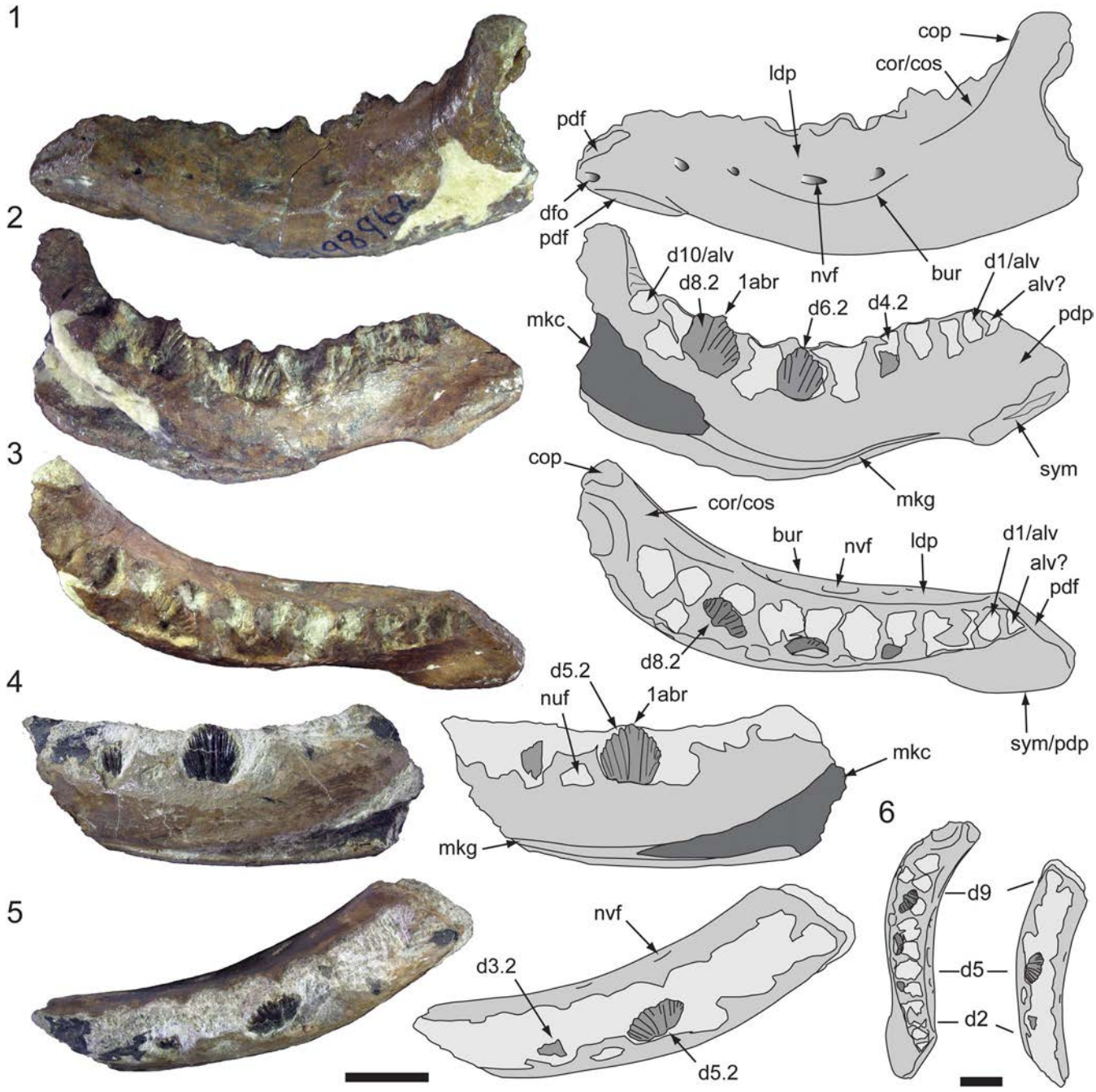

Figure 21. Victorian ornithopodan dentary morphotype 2 (*Qantassaurus ?intrepidus* Rich and Vickers-Rich, 1999) from the Flat Rocks Sandstone in the Wonthaggi Formation, southeastern Australia: (**1–3**) left dentary (NMV P198962) and schematics in lateral (**1**), medial (**2**), and dorsal (**3**) views; (**4, 5**) right dentary (NMV P199087) and schematics in lingual (**4**) and dorsal (**5**) views; (**6**) schematic size comparison between NMV P198962 and P199087 (reversed) in dorsal view. 1abr = primary apicobasal ridge; alv = alveolus; bur = buccal ridge; cop = coronoid process; cor = coronoid ridge; cos = coronoid shelf; d# = dentary tooth position (from anterior end) and replacement number; dfo = anterior dentary foramen; ldp = lateral dentary parapet; mkc = Meckelian canal (fossa); mkg = Meckelian groove; nuf = nutrient foramen; nvf = neurovascular foramen; pdf = predentary facet; pdp = predentary process; sym = symphyseal surface. Scale bars = 10 mm.

the mesial and distal bounding ridges converge to form a V-shaped cingular vertex (Fig. 20.3). The outer margins of the mesial and distal bounding ridges are convex and concave, respectively. The largest unworn crowns are midway along the tooth row. Measured lingually, the apicobasal depth of the largest observable crown (d5) is ~1.4 times its mesiodistal width. A continuous occlusal margin is formed. Lingually, the primary ridge is weakly developed, offset distally relative to the central axis of the crown, and has predominantly parallel margins that expand only slightly at the ridge base (Fig. 20.3, 20.5). The lingual margin of the primary ridge is apicobasally straight and the slightly expanded base of the ridge protrudes lingually from the cingulum. Clefts are formed between the primary ridge and the mesial and distal bounding ridges. Lingually, up to six lingulate denticles are developed in a cluster on the mesialmost margin, apically to the mesial

https://doi.org/10.1017/jpa.2018.95

bounding ridge, and a similar number of lingulate denticles are developed in the equivalent position on the distal margin. Six secondary ridges are developed on the mesial lobe, three of which are convergent with the primary ridge, and five ridges are developed on the distal lobe, one of which is convergent with the primary ridge. The pattern of ridge development appears consistent among the crowns. Apicobasal ridges, developed labially, have sharp crests and are separated by channels.

Remarks.—A foreshortened dentary (sensu Rich and Vickers-Rich, 1999), dorsoventrally high lateral dental parapet, and a markedly convex occlusal margin are distinctive features of *Qantassaurus intrepidus* (Figs. 19, 20). The foreshortened dentary of *Q. intrepidus*, quantified by the dorsoventral dentary depth (at its deepest point along the tooth row) of 60% of the tooth row length, is greater than in the other ornithopods compared herein, with the depth in *Zalmoxes shqiperorum* Weishampel et al., 2003 closest (Table 4). Among cerapods, dorsoventrally deep dentaries are also present in basal neoceratopsians, such as *Bagaceratops rozhdestvenskyi* Maryanska and Osmolska, 1975 (Alifanov, 2003, fig. 3a) and *Archaeoceratops oshimai* Dong and Azuma, 1997 (You and Dodson, 2003). The dorsoventrally high lateral dental parapet results from a deeply concave buccal ridge, a highly convex occlusal margin, and dorsally highset dentition (Figs. 19, 20). Marked ventral depression of the buccal ridge, relative to the coronoid ridge, differs from that in other ornithopods in which these ridges are less offset or roughly continuous. The highset dentition results from marked dorsal elevation of the dental parapet relative to the line of the coronoid shelf, as in *Dysalotosaurus lettowvorbecki* (see Janensch, 1955, table 11). Marked dorsal convexity of the occlusal margin closely resembles the margin in *Owenodon hoggii* (NHMUK R2998; Fig. 20.1, 20.2). The uniformly convex ventral margin on the dentary lacking recurvature anteriorly toward the symphyseal margin, also resembles the dentaries of *Z. shqiperorum* (Godefroit et al., 2009) and some basal neornithischians (e.g., *B. rozhdestvenskyi*; Alifanov, 2003, fig. 3a) and differs from those in most other ornithopods, in which the ventral margin is concave or sinuous and procurved toward the symphyseal margin (in, e.g., *Hypsilophodon foxii* [see Galton, 1974] and *Thescelosaurus neglectus* [see Boyd, 2014]).

The apicobasally tall, spatulate dentary crowns of *Qantassaurus intrepidus*, possessing closely abutting, basally convergent secondary ridges lingually, and apicobasal ridges labially with the primary ridge offset distally, are a combination of features resembling the crowns of *Talenkauen santacrucensis* (see Cambiaso, 2007, fig. 17) and the dryosaurid *Kangnasaurus coetzeei* Haughton, 1915 (SAM-PK-2732; Fig. 20.5, 20.9; see also Cooper, 1985). The *Q. intrepidus* crowns differ from the subtriangular crowns (Fig. 3.3a) of noncerapodan neornithischians, e.g., *Changchunsaurus parvus*, *Jeholosaurus shangyuanensis*, *Orodromeus makelai* Horner and Weishampel, 1988, and *Thescelosaurus neglectus*—taxa that also have a prominent apicobasal swelling on the crowns, rather than a primary ridge, and fully extending apicobasal ridges on the crowns are lacking (following Jin et al., 2010). The dentary crowns of the rhabdodontids, *Zalmoxes robustus* and *Z. shqiperorum*, differ from those of *Q. intrepidus* in being proportionally larger relative to the dentary, having higher, triangular apical peaks, and a greater number of apicobasal ridges (Weishampel et al., 2003; Godefroit et al., 2009). The dentary crowns of *Hypsilophodon foxii* (NHMUK R2477) and *Tenontosaurus tilletti* (see Thomas, 2015) differ by having relatively vertical secondary ridges separated by channels, multiple unsupported lingulate marginal denticles, and a more strongly developed primary ridge. The crowns of dryomorphans (e.g., *Bayannurosaurus perfectus* Xu et al., 2018 [Xu et al., 2018, fig. 2], *Camptosaurus dispar* [YPM VP 1886], *Dryosaurus altus* Marsh, 1878 [YPM VP 1876], and other iguanodontians [Mantell, 1848; Fanti et al., 2016]), with the exception of *K. coetzeei*, differ from those of *Q. intrepidus* by having multiple lingulate marginal denticles on the apical crown margins, sparsely developed lingual apicobasal ridges on comparatively smooth mesial and distal paracingular fossae, and smooth labial crown surfaces. The crowns of *Tenontosaurus tilletti* (see Thomas, 2015, fig. 23), styracosternans (Godefroit et al., 2012), and *Z. robustus* (NHMUK R3407), further differ from those of *Q. intrepidus* by having lingually facing lingulate denticles developed on an everted marginal lip. Mesial facing denticles also appear to be lacking on the crowns of *Dryosaurus altus* (YPM VP 1876).

On the labial surfaces of the dentary crowns in *Qantassaurus intrepidus*, narrow apicobasal ridges, separated by channels, resemble those in *Hypsilophodon foxii* (NHMUK R2477), *Zalmoxes shqiperorum* (see Godefroit et al., 2009, fig. 11B), and possibly *Kangnasaurus coetzeei* (SAM-PK-2732). Two isolated dentary teeth from the Eumeralla Formation (NMV P177934, previously referred to *Atlascopcosaurus loadsi* by Rich and Rich, 1989, fig. 11B; and NMV P186426) also resemble the crowns of *Q. intrepidus* (Fig. 20.6–20.8), suggesting that *Q. intrepidus* or a *Q. intrepidus*-like ornithopod had also been present in the lower Albian of the Eumeralla Formation. One of the aforementioned isolated crowns (NMV P177934) demonstrates a similar degree of apicobasal convexity on the lingual surface of the crown as in *Q. intrepidus*, in distal view (Fig. 20.8). Furthermore, convexity of the crown surfaces in *Q. intrepidus* and NMV P177934 also resemble those of the partly worn *K. coetzeei* crown (Fig. 20.11), which is ~50% larger than the Victorian crowns.

Qantassaurus ?*intrepidus* Rich and Vickers-Rich, 1999
Figure 21; Table 3

Occurrence.—Flat Rocks locality in the Inverloch region of Victoria, southeastern Australia (Fig. 1); Flat Rocks Sandstone, upper Barremian of the Wonthaggi Formation in the Gippsland Basin.

Materials.—NMV P198962, incomplete left dentary lacking erupted dentition; NMV P199087, right dentary fragment lacking erupted dentition.

Remarks.—The dentaries assigned herein to *Qantassaurus* ? *intrepidus* are hereafter termed 'Victorian ornithopodan dentary morphotype 2' (VOD2). In this context, *Q. intrepidus*

https://doi.org/10.1017/jpa.2018.95

is VOD1. The more complete of the two dentaries (NMV P198962) is similar in size to the *Q. intrepidus* holotype. As in *Q. intrepidus*, 10 alveoli are present (see NMV P198962; Fig. 21), and a small, triangular alveolus could be developed anteriorly, but its presence is uncertain. The dentary is strongly bowed in both mediolateral and dorsoventral views. The lateral margin is markedly concave and the medial margin is strongly convex. In contrast, curvature on the *Q. intrepidus* dentary is comparatively shallow (Fig. 19). The medial margin on VOD2 (NMV P198962) is smoothly convex, which differs from *Q. intrepidus* in which a distinct kink is evident. In mediolateral view, the coronoid process is angled at 70° relative to the anteroposterior axis of the alveolar margin, as in *Q. intrepidus*, and its distal end is slightly expanded and rounded (Fig. 21). The medioventral surface adjacent to the symphyseal margin is depressed by a shallow fossa that could have accommodated the ventrolateral process of the predentary. The symmetrically triangular predentary process resembles those of *Dysalotosaurus lettowvorbecki*, *Hypsilophodon foxii*, *Tenontosaurus tilletti*, and *Zalmoxes robustus* (Janensch, 1955; Galton, 1974; Weishampel et al., 2003; Thomas, 2015), and contrasts with the comparatively asymmetrical form in ankylopollexians, e.g., *Camptosaurus dispar* (YPM VP 1886) and *Mantellisaurus atherfieldensis* (see Norman, 1986), in which the dorsal facet is longer than the relatively horizontal ventral facet. The shape of the VOD2 crowns and their ornamentation resemble those of *Q. intrepidus*.

As originally described by Rich and Vickers-Rich (1999, p. 175), the left dentary (NMV P198962) was considered to differ from that of the *Qantassaurus intrepidus* holotype by having a "bloated" appearance, which according to these authors, potentially resulted from a pathological condition. However, the incomplete right dentary (NMV P199087), originally referred to *Q. intrepidus* (see Rich and Vickers-Rich, 1999), has morphology closer to NMV P198962 (Fig. 21.6) than to the *Q. intrepidus* holotype. The dentary (NMV P199087) appears to be slightly larger than in NMV P198962 and, therefore, is unlikely to pertain to the same individual. Thus, NMV P198962 and P199087 confirm the presence of two VOD2 individuals, based on comparable morphology differing from that of the *Q. intrepidus* holotype. VOD2 could represent dimorphism among *Q. intrepidus* or alternatively a separate taxon.

Ornithopoda indet.
Figures 22–24.6; Table 3

Occurrence.—Flat Rocks locality in the Inverloch region of Victoria, southeastern Australia (Fig. 1); Flat Rocks Sandstone, upper Barremian of the Wonthaggi Formation in the Gippsland Basin.

Materials.—NMV P199135, complete but degraded right dentary with partial dentition; NMV P208506, worn left dentary tooth with root; NMV P210049, worn, incomplete left dentary tooth; NMV P228408, complete left dentary with partial dentition; NMV P231182, incomplete, degraded right dentary, lacking coronoid process and dentition; and NMV P208192, incomplete, degraded right dentary with partial dentition.

Remarks.—The dentaries are hereafter referred to as 'Victorian ornithopodan dentary morphotype 3' (VOD3). They have up to 13 alveoli, contrasting with 10 in *Qantassaurus intrepidus* and VOD2. Viewed lateromedially, the ventral margin is shallowly convex in the posterior half and slightly procurved ventrally toward the symphyseal margin (Fig. 22). On the smaller dentaries (Fig. 22), the alveolar margin is slightly concave in the posterior half and the anterior portion procurved toward the predentary process. However, on the largest dentary (NMV P231182; Fig. 23), the margin is dorsally concave over its length. The predentary process is symmetrically triangular, as in *Q. intrepidus* and VOD2, with the dorsal and ventral facets for the predentary slightly concave and grooved. Viewed dorsally, the dentary ramus and alveolar margins are laterally concave/medially convex and the line of the anterior alveoli is convergent with the lateral margin of the dentary (Figs. 22–23). The posteriormost alveolus is anteromedial to the base of the coronoid process. Although the dorsalmost portions of the lateral alveolar parapets on the two dentaries are missing, the parapet was unlikely to have been elevated dorsally to the extent evident in *Q. intrepidus*. The coronoid process, best preserved on NMV P228408, is anteroposteriorly narrow and angled at ~45° relative to the alveolar margin. The coronoid processes on the dentaries of *Q. intrepidus* and VOD2 are more steeply angled (~ 70°; Figs. 19, 21). The dorsal end of the coronoid process is slightly expanded and rounded and is located dorsally above the apical level of the dentition (Fig. 22). The posteriorly directed medial coronoid cusp forms a small shelf at the base of the coronoid process (Fig. 22.3). The anteroposterior length of the coronoid process head is ~ 8% of the total alveolar length. In contrast, this ratio is almost double (~ 15%) in VOD2 (NMV P198962; Fig. 21.1, 21.2). Laterally, the short coronoid ridge merges with the lateral dentary parapet (Figs. 22, 23). The buccal ridge is smoothly rounded and lacking the ventral depression present in *Q. intrepidus* and VOD2 (Figs. 19, 21). The anterior dentary foramen is located centrally on the premaxillary process and a row of four neurovascular foramina penetrates the lateral alveolar parapet roughly corresponding to the line of the coronoid ridge (Figs. 22, 23). Two smaller foramina are posterior and slightly ventral to the anterior dentary foramen. Two further foramina form a row dorsally near the anterior end of the alveolar margin. Medially, the alveolar groove differentiates the medial dental parapet and the dentary ramus (Fig. 22.3). Nutrient foramina within the groove correspond to the alveoli. The Meckelian canal forms an elongate triangular opening in the posterior half of the dentary (Figs. 22, 23). The angle of the Meckelian canal opening of 15° is half that of *Q. intrepidus* and VOD2 (~ 30°). A narrow Meckelian groove continues anteriorly and extends onto the dorsomedial surface of the predentary process adjacent to the symphyseal margin. The dentary is more elongate than that of *Q. intrepidus* and VOD2 (Table 4).

Most of the erupted teeth are missing on the dentaries that retain dentition (NMV P199135, P208192 [not figured], P228408) and only the apical regions of some unerupted crowns

https://doi.org/10.1017/jpa.2018.95

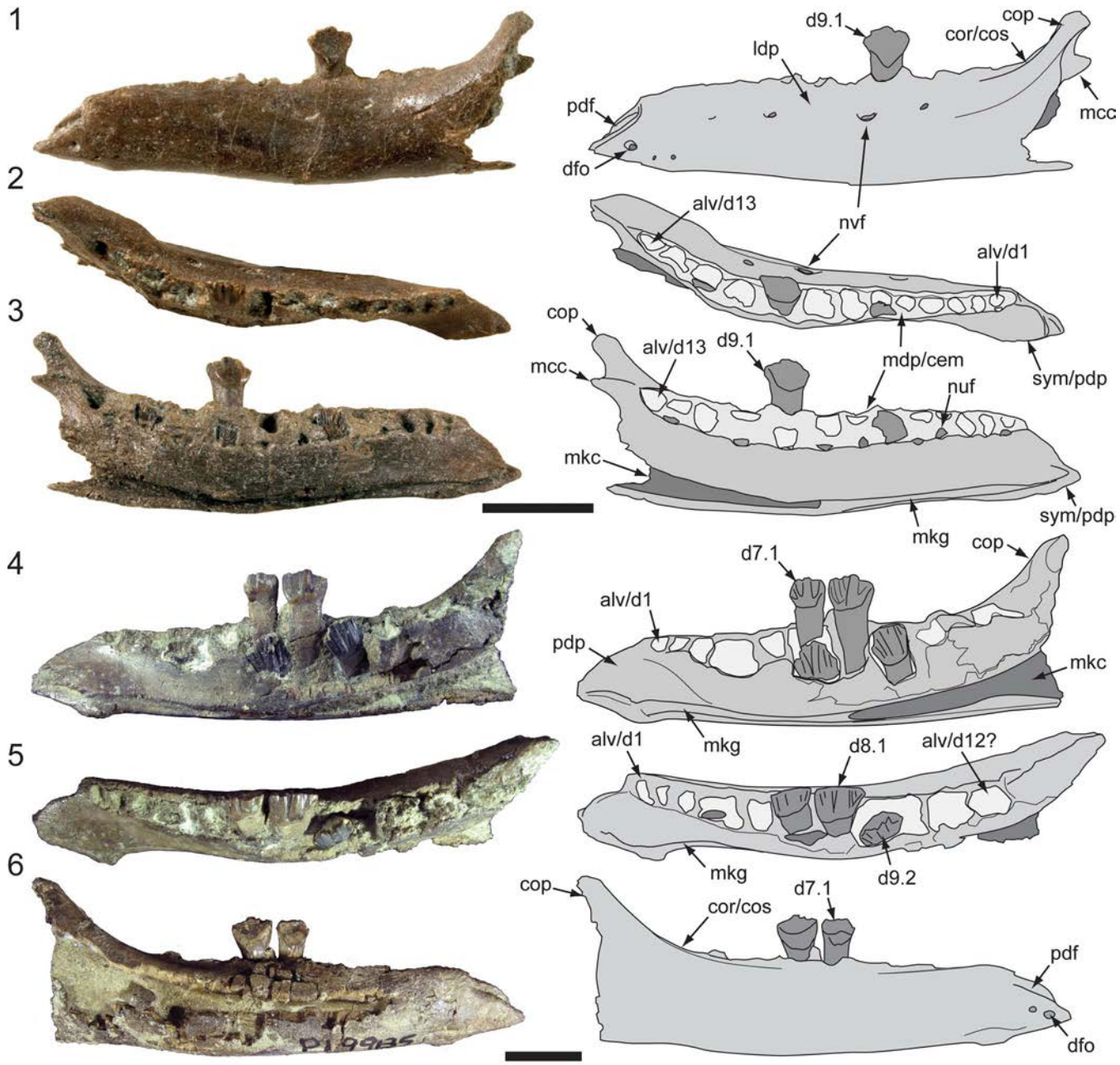

Figure 22. Victorian ornithopodan dentary morphotype 3 (Ornithopoda indet.) from the Flat Rocks Sandstone in the Wonthaggi Formation, southeastern Australia: (**1–3**) left dentary (NMV P228408) and schematics in lateral (**1**), dorsal (**2**), and medial (**3**) views; (**4–6**) right dentary (NMV P199135) and schematics in lateral (**4**), dorsal (**5**), and medial (**6**) views. alv = alveolus; cem = cementum; cop = coronoid process; cor = coronoid ridge; cos = coronoid shelf; d# = dentary tooth position (from anterior end) and replacement number; dfo = anterior dentary foramen; ldp = lateral dentary parapet; mcc = medial coronoid cusp; mdp = medial dentary parapet; mkc = Meckelian canal (fossa); mkg = Meckelian groove; nuf = nutrient foramen; nvf = neurovascular foramen; pdf = predentary facet; pdp = predentary process; sym = symphyseal surface. Scale bars = 10 mm.

are exposed (Figs. 22, 24). The isolated teeth provide additional information although none are without wear. The root is swollen with a roughly rectangular section, as in *Zalmoxes* (Weishampel et al., 2003; Godefroit et al., 2009) and on some teeth forms a slight constriction near the crown base. The lingual surface of the root has a slight depression (Fig. 24). The roots of *Qantassaurus intrepidus* and VOD2 teeth cannot be presently compared with VOD3, because none are exposed and isolated teeth have not been categorically identified. Lingually, the cingulum is distinct from the root (Fig. 24). Although a complete unworn crown is presently unknown, the collection of specimens indicates that the crown is spatulate, with a mesiodistal width approximately equalling the apicobasal depth (Fig. 24.6). In contrast, the crowns of *Q. intrepidus* are relatively taller apicobasally, with a deeper basal region (Fig. 20.5). Lingually, the mesial and distal bounding ridges on the crowns of VOD3 form an asymmetrically U-shaped to shallowly W-shaped cingular vertex, with the cingulum mesiobasally sloping (Fig. 24). On some crowns, the base of the mesial bounding ridge is bulbous. The primary ridge, present lingually, expands

https://doi.org/10.1017/jpa.2018.95

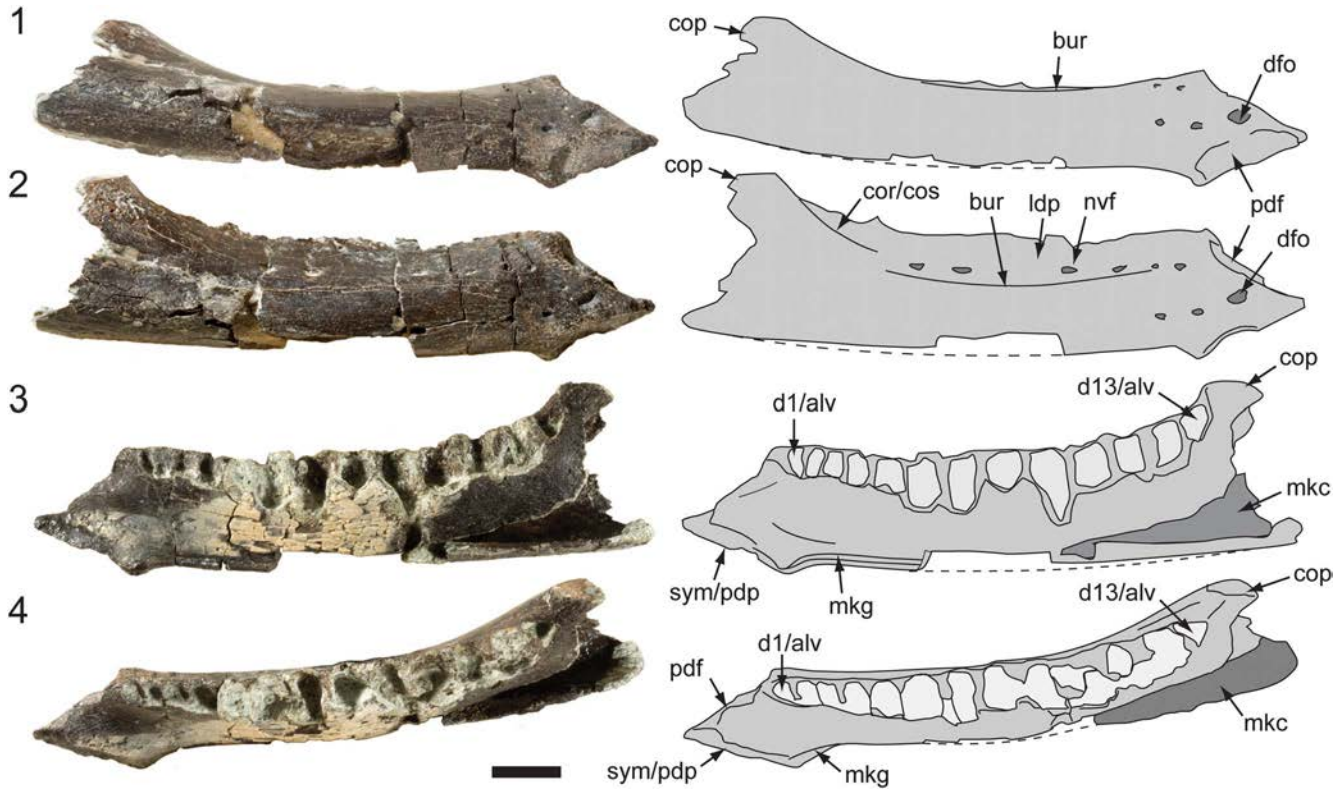

Figure 23. Victorian ornithopodan dentary morphotype 3 (Ornithopoda indet.), right dentary (NMV P231182) and schematics in ventral (**1**), lateral (**2**), medial (**3**), and dorsal (**4**) views. Dashed lines in (**2–4**) indicates damaged ventral margin. alv = alveolus; bur = buccal ridge; cop = coronoid process; cor = coronoid ridge; cos = coronoid shelf; d# = dentary tooth position (from anterior end) and replacement number; dfo = anterior dentary foramen; ldp = lateral dentary parapet; mkc = Meckelian canal (fossa); mkg = Meckelian groove; nvf = neurovascular foramen; pdf = predentary facet; pdp = predentary process; sym = symphyseal surface. Scale bar = 10 mm.

toward its base and is offset distally from the central axis of the crown. The primary ridge on many of the crowns is obliquely oriented and roughly parallels the distal bounding ridge. On some crowns, clefts are formed between the primary ridge and the mesial and distal bounding ridges, as in *Q. intrepidus* (Figs. 20.5, 24.6). The lingual secondary ridges are closely abutting. Five are developed on the mesial lobe, two of which are convergent with the primary ridge, and at least three are developed on the distal lobe, with at least one convergent with the primary ridge. At least one lingulate denticle is further developed on the mesialmost apical margin, and one lingulate denticle also developed on the equivalent distal margin. Apicobasal ridges separated by channels are developed on the labial crown surfaces of the isolated crowns (NMV P208526, P210049; Fig. 24.5, 24.6), as in *Q. intrepidus*.

The crowns of VOD3 resemble those of an isolated ornithopod tooth (QM F52774; Fig. 24.7) described by Hocknull and Cook (2008) from the upper Albian of the Winton Formation in central-western Queensland. Although originally reported as a right maxillary tooth, the morphology of QM F52774 is consistent with a right dentary tooth.

Variation.—The largest of the VOD3 dentaries (NMV P231182; Fig. 23) differs from the other dentaries (NMV P199135, P208192 [not figured], P228408; Fig. 22) by having more anteriorly divergent alveolar and ventral margins. In this aspect, the alveolar margin on NMV P231182 is more concave than on the other dentaries. The posteromedial end of the symphyseal margin on NMV P231182 forms a bulbous process, not present on the other dentaries. If of the same taxon, variation between NMV P231182 and the other VOD3 dentaries could result from age-related dimorphism, however, taxonomic variation is also possible.

Phylogenetic analysis

Dataset and search methods.—The phylogenetic relationships of Australian ornithopods were assessed in TNT 1.5 (Goloboff and Catalano, 2016) using the dataset of Dieudonné et al. (2016) in a substantially modified form. Two principal search methodologies, 'traditional' equal weighting (EW) and implied weighting (IW), were employed. Implied weighting methodology seeks to reduce the effect of homoplastic information in the dataset and acts to produce a consensus with comparatively fewer polytomies (Goloboff, 2014; Congreve and Lamsdell, 2016; Goloboff et al., 2018). The degree of down-weighting in an IW analysis is governed by a chosen concavity constant (k) (Goloboff, 1993). The outcome of the search is dependent on the amount of homoplasy inherent in the data (Goloboff, 2014) and size of the dataset (Goloboff et al., 2018). A concavity constant of k = 7.00 was applied to the implied weighted search in this work (see Text S1 for further details). Because recent assessments of ornithischian phylogeny have produced highly unresolved

https://doi.org/10.1017/jpa.2018.95

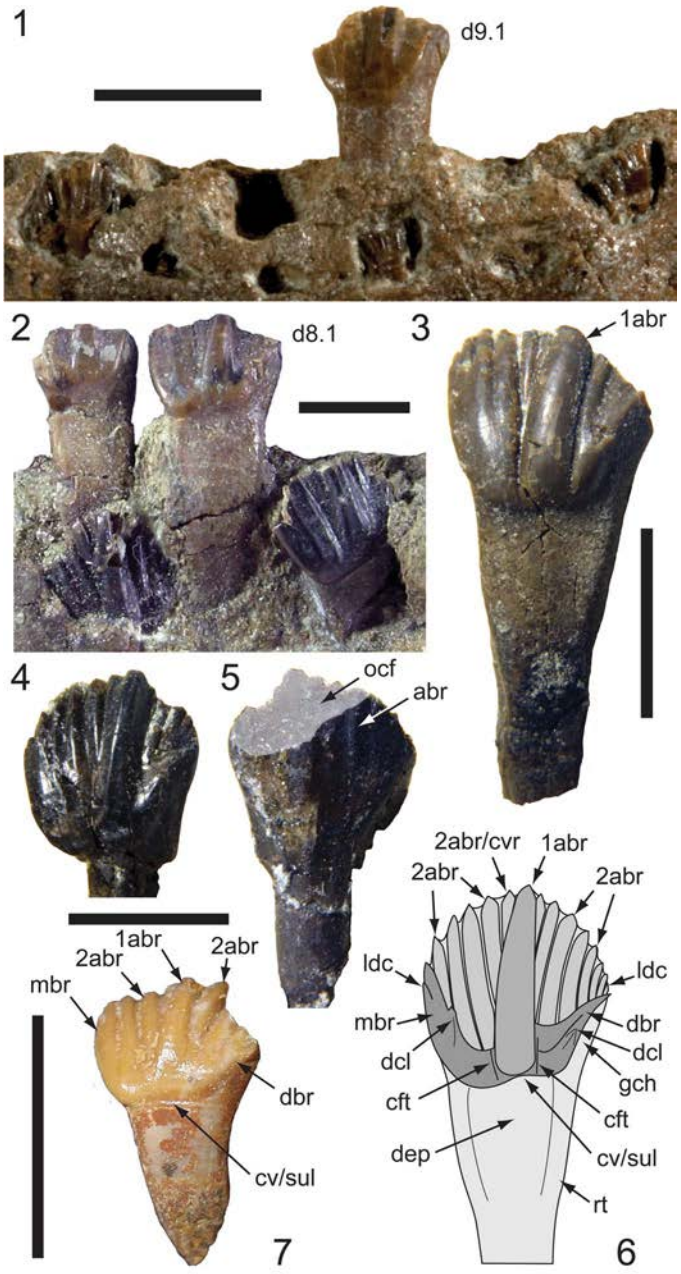

Figure 24. Dentition of Victorian ornithopodan dentary morphotype 3 (Ornithopoda indet.), with comparisons: (**1**) left dentition of NMV P228408 (reversed) in lingual view; (**2**) right dentition of NMV P199135 in lingual view; (**3**) isolated left tooth NMV P208506 (reversed) in lingual view; (**4, 5**) isolated left tooth NMV P210049 (reversed) in lingual (**4**) and labial (**5**) views with schematic shading shown on occlusal facet in (**5**); (**6**) schematic right dentary tooth of Victorian ornithopodan dentary morphotype 3, based on composite of specimens at a midtooth row position; (**7**) isolated right dentary tooth, QM F52774, of an indeterminate neornithischian from the Winton Formation, central western Queensland. 1abr = primary apicobasal ridge; 2abr = secondary apicobasal ridge; abr = apicobasal ridge; cft = cleft; cv = cingular vertex; cvr = convergent (secondary) ridge; d# = dentary tooth position (from anterior end) and replacement number; dbr = distal bounding ridge; dcl = denticle; dep = depression; gch = growth channel; ldc = lingulate denticle; mbr = mesial bounding ridge; ocf = occlusal facet; rt = root; sul = sulcus. Scale bars = 5 mm.

strict consensus results based on generally similar underlying character data (e.g., Butler et al., 2008, 2011; Boyd, 2015; Madzia et al., 2018), it was expected that new analyses with highly incomplete taxa would produce similarly poor results, if not worse resolution. To this end, the application of IW is a result-optimization procedure and in this respect, akin to supplementary analyses (e.g., maximum agreement subtrees, reduced consensus) utilized in other works, which typically follow retrieval of a strict consensus. However, unlike such methods, an IW search has the advantage of utilizing the full dataset without a posteriori pruning of taxa, and accordingly, its consensus tree is directly comparable to a 'traditional' EW strict consensus tree (i.e., allowing a one-on-one comparison).

Character matrix.—A previous attempt to assess the phylogeny of Australian ornithopods within the dataset of Dieudonné et al. (2016; 288 characters) obtained poor resolution (Herne et al., 2018, supplemental data). To revivify this dataset, we revised character codings, amended several character scores, and augmented the dataset with new characters. From the original dataset, 34 characters were deleted and 48 novel or replacement characters were added (all modifications are detailed in the character list; see Text S2). Revision of the dataset was undertaken in Mesquite v. 3.40 (Maddison and Maddison, 2009), with inapplicable states actively scored as '–' rather than '?' (Brazeau, 2011). The resulting dataset comprised 302 active characters, all of which were unordered (including multistate characters that were ordered in previous works). Several of the compound characters in the original dataset were recoded into multiple contingent characters (via contingent coding methods, Forey and Kitching, 2000; Brazeau, 2011). In highly incomplete fossil taxa, it is seldom known if a multistate morphology naturally transforms step-wise and linearly (Hauser and Presch, 1991). Thus, all remaining compound multistate characters were set as unordered, because ordering characters without in-depth a priori evolutionary understanding of that morphology (e.g., using genetic data) potentially imposes incorrect assumptions.

Operational taxonomic units (OTUs).—The dataset comprises 56 terminal taxa, with *Herrerasaurus ischigualastensis* Reig, 1963 set as the outgroup. In addition to the original OTUs in the Dieudonné et al. (2016) dataset, new OTUs included *Diluvicursor pickeringi* (see Herne et al., 2018), *Galleonosaurus dorisae* n. gen. n. sp., *Leaellynasaura amicagraphica* (see Rich and Rich, 1989), *Owenodon hoggii* (see Norman and Barrett, 2002; Galton, 2009), *Qantassaurus intrepidus* (see Rich and Vickers-Rich, 1999), and five marginocephalians (*Homalocephale calathocercos* Maryanska and Osmolska, 1974, *Stegoceras validum* Lambe, 1902, *Goyocephale lattimorei* Perle, Maryanska, and Osmolska, 1982, *Liaoceratops yanzigouensis* Xu et al., 2002, and *Protoceratops andrewsi* Granger and Gregory, 1923 [Gilmore, 1924; Brown and Schlaikjer, 1940; Maryanska and Osmolska, 1974; Perle et al., 1982; Galton and Sues, 1983; Xu et al., 2002; Tanoue et al., 2009; He et al., 2018]). The addition of the marginocephalians arose out of the need to stabilize Cerapoda, identified as a problematically volatile node within a previous analysis (Herne et al., 2018). *Othnielosaurus consors* Marsh, 1894 was replaced by *Nanosaurus agilis* with

https://doi.org/10.1017/jpa.2018.95

augmented scores following recent systematic revision (Carpenter and Galton, 2018), whereas '*Dryosaurus altus*' was relabelled *Dryosaurus* spp., after establishment of the new species *Dryosaurus elderae*. Following re-evaluation of *Pisanosaurus mertii* Casamiquela, 1967 as a potential nondinosaurian (Agnolín and Rozadilla, 2018), this taxon was removed.

Heuristic searches.—The analyses (EW, IW) were conducted with the maximum tree space pre-set to 200,000 and zero-length branches collapsed. These each comprised 1,000 tree bisection and reconnection replicates, with 10 trees held per replicate. The strict consensus from EW was augmented by standard bootstrap and Bremer values (see details in Text S1). Bootstrapping comprised 1,000 pseudoreplications, reported as 'frequency distribution' values (rather than 'absolute frequencies') to factor-in resampling that contradicts recovered clades in the consensus (Goloboff et al., 2003). Bremer support was calculated by running the TNT script 'bremer.run,' surveying trees up to five steps longer than the most parsimonious tree (MPT). Node support for the IW strict consensus utilized symmetric resampling ($p = 33$), which provides a more appropriate support measure for a weighted analysis than bootstrapping (Goloboff et al., 2003). Symmetric resampling comprised 1,000 pseudoreplications that were also reported as frequency distributions. Because of the way in which the IW MPT tree-fit measure is yielded, the resulting IW Bremer support values are reported as fractions rather than as integers (Text S1).

Consensus methods.—Maximum agreement subtrees were obtained to present the more resolved 'backbone' topologies for each search following the removal of taxa considered unstable, via their conflicting positions (Kitching et al., 1998). Further identification of wildcard taxa was made by applying an iterative reduced positional congruence index (PCR; Pol and Escapa, 2009) to the MPTs arising from each search. This procedure iteratively prunes taxa considered unstable, via their scored characters, while reporting successive improvements in the resolution of the consensus tree. Iterative PCR was assessed with the implementation of the original script ('iterPCR.run') available in TNT 1.5 (Goloboff and Szumik, 2015).

Heuristic search and reduced consensus results.—Under EW, 814 MPTs were recovered, with tree lengths of 932 steps, with the resulting EW strict consensus tree being 1,103 steps in length (Fig. 25.1). Under IW, 26 MPTs were recovered, each with a best score (IW fit length) of 55.92 and tree length of 933 steps. The resulting IW strict consensus tree (Fig. 25.2) was 951 steps long (tree fit length 57.06). For both analyses, the consistency index is 0.37 and the retention index is 0.63. The EW strict consensus returned poor results in the relationships among almost all neornithischian OTUs (Fig. 25.1; see Text S1 for definitions). In the IW strict consensus tree, the predominantly Cretaceous Gondwanan neornithischians of interest to this work are recovered as nonclypeodontan (= 'basal') ornithopods, however, as part of a broad polytomy (Fig. 25.2).

Efforts to retrieve a useful underlying topology with the raw EW trees using either method of determining a reduce consensus (i.e., agreement subtrees or iterative PCR) produced insufficient results. The maximum agreement subtree excluded a large number of OTUs (22), critically taxa of interest to this work, whereas iterative PCR produced more inferior results with most neornithischian OTUs unstable (Text S1). However, the maximum agreement subtree arising from the MPTs of the initial IW search pruned only two OTUs with unstable positions (*Qantassaurus intrepidus* and *Diluvicursor pickeringi*; Fig. 26.1). As a consequence of the excluded taxa, the basal ornithopod polytomy in the IW strict consensus became resolved as a clade of entirely Gondwanan OTUs—the Elasmaria (see Text S1 for definition)—that is sister to the remaining ornithopods (Clypeodonta). Iterative PCR of the IW MPTs also identified *Q. intrepidus* and *Diluvicursor pickeringi* as wildcard taxa (see Text S1 for details), and in effect corroborated the 'backbone' topology (IW maximum agreement subtree) of ornithopods.

Taking forward these results, an IW re-analysis of the dataset, with the iterative PCR wildcard taxa excluded a priori, produced seven MPTs, the strict consensus of which recovered an internally-unresolved Elasmaria within Ornithopoda as the sister clade to Clypeodonta (Fig. 26.2). When only *Qantassaurus intrepidus* was excluded, a similar overall topology was produced, differing only by its more internally resolved elasmarian node (Fig. 26.3). The differences between these topologies and the IW agreement subtree, and even to the original strict consensus, resulted from changes in the resolution of the elasmarian OTUs. Clearly, the stability of the elasmarian node, when recovered, was determined largely by the composition of the taxa retained. It is unsurprising that the majority of the pruned neornithischian OTUs, using either EW or IW method, are those associated with > 85% missing data (Text S1). Although obvious, it should not be understated how improved support for the lineages of interest will only be achieved when more complete materials become available.

Major neornithischian clades and interrelationships.—The IW strict consensus tree (Figs. 25.2, 26.2) is the most resolved and provides our preferred hypothesis for the discussion of neornithischian interrelationships that follows. *Lesothosaurus diagnosticus* was recovered as the basalmost branching neornithischian, below *Agilisaurus louderbacki* Peng, 1990, *Hexinlusaurus multidens* He and Cai, 1983, and *Yandusaurus hongheensis* He, 1979. A major split among more nested neornithischians occurs between Cerapoda and an unnamed clade that comprises taxa closer to *Thescelosaurus neglectus*. The Late Jurassic taxon *Nanosaurus agilis* diverges at the base of this latter clade and is the sister taxon to an entirely Cretaceous subgroup of taxa comprising the East Asian and largely North American clades Jeholosauridae and Thescelosauridae, respectively (Han et al., 2012; Brown et al., 2013). Within Cerapoda, Marginocephalia and its internal branches are well supported (Text S1), however, the interrelationships of taxa at the base of Ornithopoda are weakly supported. *Parksosaurus warreni* Parks, 1926 is recovered as the basalmost ornithopod, which contrasts to some previous analyses in which *P. warreni* was recovered allied to *Thescelosaurus neglectus* outside of Cerapoda

https://doi.org/10.1017/jpa.2018.95

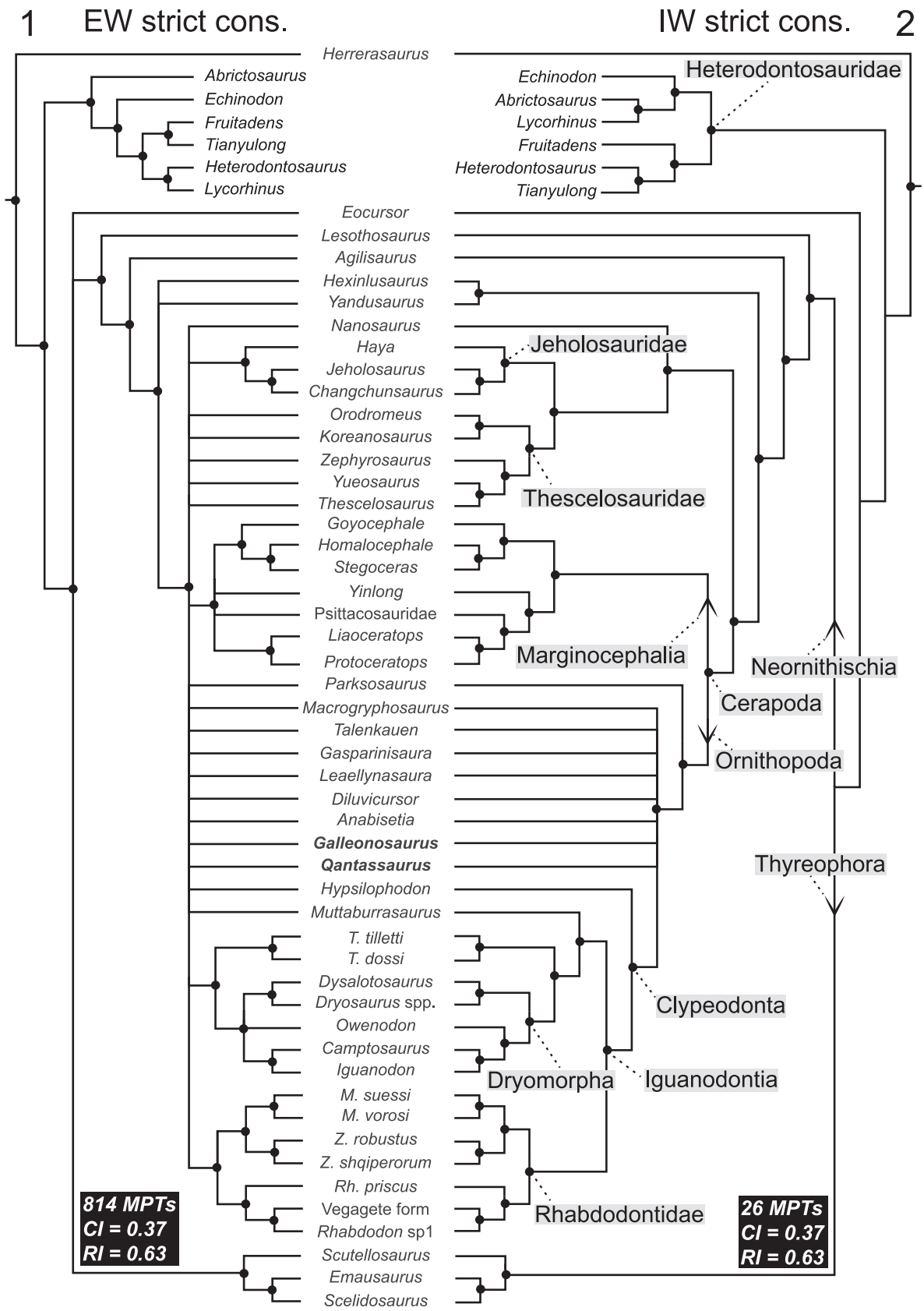

Figure 25. Strict consensus cladograms, showing the relationships of *Galleonosaurus dorisae* n. gen. n. sp. and *Qantassaurus intrepidus* Rich and Vickers-Rich, 1999: (**1**) tree derived from EW analysis (814 MPTs); (**2**) tree derived from IW analysis (26 MPTs). For phylogenetic definitions of labelled nodes and stems, see Text S1. For Bremer and bootstrap support values accompanying each search, see Text S1. M = *Mochlodon*; Rh = *Rhabdodon*; T = *Tenontosaurus*; Z = *Zalmoxes*.

https://doi.org/10.1017/jpa.2018.95

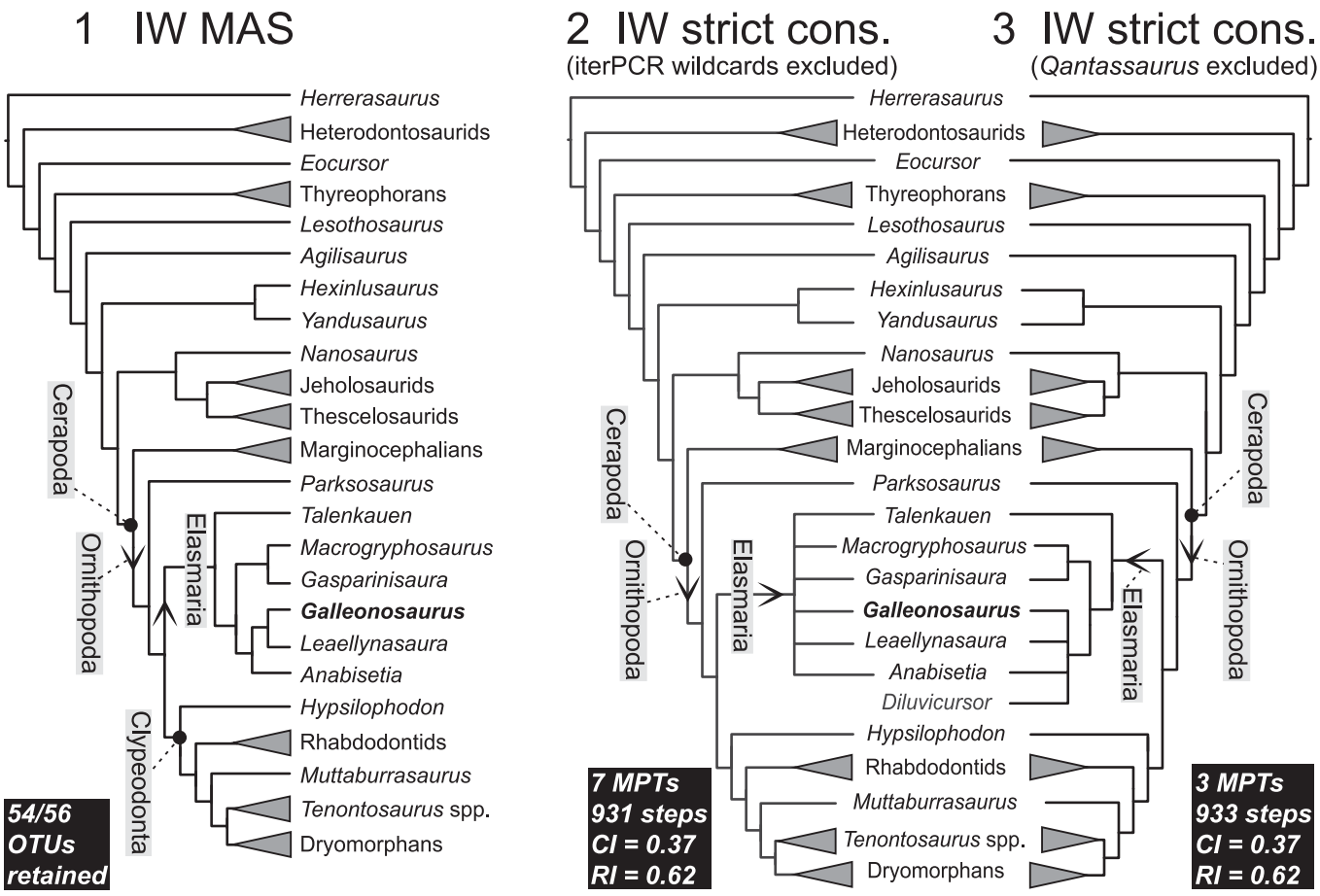

Figure 26. Reduced consensus topologies, showing the relationships of *Galleonosaurus dorisae* n. gen. n. sp.: (**1**) maximum agreement subtree derived from 26 original IW MPTs (2 OTUs pruned: *Qantassaurus* and *Diluvicursor*); (**2**) strict consensus tree derived from IW analysis following a priori exclusion of wildcard taxa indicated by iterative PCR (i.e., *Qantassaurus* and *Diluvicursor*); (**3**) strict consensus tree derived from IW analysis following a priori exclusion of *Qantassaurus* only. For simplicity, clades peripheral of the region of interest, as labelled in Fig. 25.2, were collapsed (they did not vary in taxic composition between the analyses). For phylogenetic definitions, see Text S1.

(Brown et al., 2013; Boyd, 2015). The remaining ornithopods form an unnamed polytomy, which comprises all eight Cretaceous Victorian and South American OTUs and the clade Clypeodonta (Fig. 25.2). This last clade is split between *Hypsilophodon foxii* and the remaining taxa attributable to Iguanodontia. Rhabdodontidae forms the sister clade to all other iguanodontians, comprising the progressively more nested lineages of *Muttaburrasaurus langdoni*, *Tenontosaurus* spp., and Dryomorpha. Notably, *M. langdoni* is not allied with rhabdodontids (contra Dieudonné et al., 2016), limiting the latter group to a European Cretaceous distribution.

The interrelationships of the Victorian and South American taxa included in the analysis are further revealed by the reduced consensus results (Fig. 26). Excluding *Qantassaurus intrepidus* as a wildcard, these taxa are recovered in the clade Elasmaria. Within this assemblage of taxa, *Talenkauen santacrucensis* regularly appeared to be the basalmost branch, and sister to the remaining taxa (Fig. 26.1, 26.3). *Galleonosaurus dorisae* n. gen. n. sp. clusters with *Leaellynasaura amicagraphica*, *Anabisetia saldiviai*, and *Diluvicursor pickeringi* (when included) as the sister taxon to *Gasparinisaura cincosaltensis* and *Macrogryphosaurus gondwanicus* Calvo, Porfiri, and Novas, 2007 (Fig. 26.3).

Discussion

Validity and distribution of the Victorian ornithopod taxa.—*Galleonosaurus dorisae* n. gen. n. sp., from the upper Barremian Wonthaggi Formation, is the fourth Victorian ornithopod named from cranial remains and the third described from the maxilla (Figs. 4–9, 27; Table 5). The two other Victorian taxa known from their maxillae, *Atlascopcosaurus loadsi* (Figs. 10, 13) and *Leaellynasaura amicagraphica*, are from the younger, early Albian Eumeralla Formation to the west of the Wonthaggi Formation (Figs. 1.2, 27; Table 5). Ornithopods of the Eumeralla and Wonthaggi formations could be separated by ~ 12–17 Myr (based on dating of the Eumeralla Formation by Korasidis et al. [2016] and revised dating of the Wonthaggi Formation by B. Wagstaff [personal communication, 2018]). The third-named ornithopod from Victoria, *Qantassaurus intrepidus* from the Wonthaggi Formation (Fig. 27; Table 5), is known only from its dentary. However, at least two isolated teeth from the Eumeralla Formation (NMV P177934, P186426) also resemble those of *Q. intrepidus* (Fig. 20.5–20.8). It is of note that one of these teeth (NMV P177934) was originally assigned to *Atlascopcosaurus loadsi* (Rich and Rich, 1989, fig. 11B).

https://doi.org/10.1017/jpa.2018.95

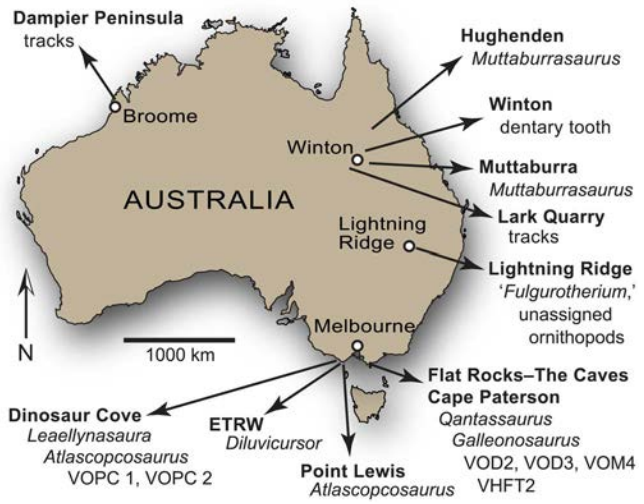

Figure 27. Australian ornithopod occurrences: ETRW = Eric the Red West; VHFT2 = Victorian Hypsilophodontid Femur Type 2; VOD2 = Victorian ornithopod dentary morphotype 2; VOD3 = Victorian ornithopod dentary morphotype 3; VOM4 = Victorian ornithopod maxilla morphotype 4; VOPC1 = Victorian ornithopod postcranium 1 (NMV P185992/P185993); VOPC2 = Victorian ornithopod postcranium 2 (NMV P186047). See Table 5 for associated information on ornithopod occurrences.

Galleonosaurus dorisae n. gen. n. sp. shares a combination of seven maxillary tooth crown features with *Atlascopcosaurus loadsi* and *Leaellynasaura amicagraphica* (Fig. 17) that suggest a close relationship between these three taxa (i.e., maxillary crowns features G1–7 in Remarks under *Galleonosaurus dorisae* n. gen. n. sp.). Most of the maxillary crown features of *Galleonosaurus dorisae* n. gen. n. sp. are also shared with the large-bodied Albian ornithopod from Queensland, *Muttaburrasaurus* spp. (Fig. 17). The phylogenetic relationships of *Muttaburrasaurus* spp. and the Victorian ornithopods will be discussed further below. It is notable that the tridenticulate mamillated cusps developed on the crowns of *Galleonosaurus dorisae* n. gen. n. sp. and *Atlascopcosaurus loadsi* have been previously reported in *Nanosaurus agilis* (Bakker et al., 1990; Carpenter and Galton, 2018). Tridenticulate cusps, however, are unknown on the maxillary crowns of *L. amicagraphica* and *Muttaburrasaurus* spp.

The maxilla of *Galleonosaurus dorisae* n. gen. n. sp. differs from that of *Leaellynasaura amicagraphica* by having: (1) deeper buccal emargination; (2) greater lateral concavity along the tooth row, with distinct outturning of the anterior alveoli; (3) a smoother buccal ridge, as opposed to sharply rounded; and (4) a stronger primary ridge, more distally offset on the labial crown surface (Figs. 5, 7, 8, 17). In addition, the largest specimens of *Galleonosaurus dorisae* n. gen. n. sp. also have a greater number of maxillary teeth than the *L. amicagraphica* holotype (15 compared to 12), although this difference could be attributable to ontogeny (e.g., Barrett and Han, 2009) because the *L. amicagraphica* holotype is almost certainly a juvenile (see also Rich and Rich, 1989). *Galleonosaurus dorisae* n. gen. n. sp. differs from *Atlascopcosaurus loadsi* by having: (1) a dorsoventrally lower maxillary ramus, (2) lesser protrusion of posterolateral process on the maxilla, (3) a more broadly rounded buccal ridge, (4) a symmetrically expanded flange on the lateral ramus of the palatine (rather than being asymmetrical and posteriorly expanded), (5) more finely developed secondary apicobasal ridges distal to the primary ridge, and (6) a markedly V-shaped (as opposed to U-shaped) cingular vertex on the maxillary crowns (Figs. 13, 17). These differences between *Atlascopcosaurus loadsi*, *Galleonosaurus dorisae* n. gen. n. sp., and *L. amicagraphica* support their taxonomic separation.

The two Wonthaggi Formation ornithopods—*Galleonosaurus dorisae* n. gen. n. sp., known from its maxilla, and *Qantassaurus intrepidus*, known from its dentary—are potentially synonymous. However, separation of these two Flat Rocks locality taxa is indirectly supported by the newly discovered ornithopod dentary morphotype VOD3 from the Flat Rocks site (Figs. 22–24, 27; Table 5). VOD3 is a more elongate dentary than that of *Q. intrepidus* and contains more alveoli in specimens of similar size (13 alveoli compared with 10 in *Q. intrepidus*). The presence of two distinctly differing ornithopod dentary morphotypes from the Flat Rocks deposit is therefore confirmed by VOD3, the other being *Q. intrepidus*. Importantly, we consider the number of dentary alveoli in VOD3 closer to the expected number in the presently unknown dentary of *Galleonosaurus dorisae* n. gen. n. sp., the maxilla of which has 15 alveoli. In comparable neornithischians, the number of dentary alveoli relative to the maxillary alveoli varies. The dentaries of some taxa contain more alveoli than the maxillae (e.g., 14 to 12 in *Hypsilophodon foxii* [see Galton, 1974]), some have fewer (e.g., 13 to 15 in *Jeholosaurus shangyuanensis* [see Barrett and Han, 2009] and *Dryosaurus elderae* [CM 3394], and 12 to 14 in *Dysalotosaurus lettowvorbecki* [see Janensch, 1955]) and some have an equivalent number (e.g., 20 in *Thescelosaurus neglectus* [see Boyd, 2014] and 10 in *Zalmoxes robustus* [see Weishampel et al., 2003]). Therefore, typically in neornithischians, the dentaries contain either the same number of alveoli as the maxillae, or vary up or down by approximately two alveoli. With 13 alveoli, we consider VOD3 more congruent to the 15 maxillary alveoli in *Galleonosaurus dorisae* n. gen. n. sp. than the foreshortened dentary of *Q. intrepidus*, containing 10 alveoli.

No dentary from the Eumeralla Formation is presently assignable to *Atlascopcosaurus loadsi* or *Leaellynasaura amicagraphica* (noting that dentaries originally referred to *Atlascopcosaurus loadsi* by Rich and Rich [1989] were not found in association with any of the *Atlascopcosaurus loadsi* maxillae, and for this reason cannot be confidently assigned to that taxon). Therefore, future potential synonymy between *Qantassaurus intrepidus* and either *Atlascopcosaurus loadsi* or *L. amicagraphica* cannot be ruled out. However, out of *Atlascopcosaurus loadsi* and *L. amicagraphica*, the robust dentary form of *Q. intrepidus* seems a more likely candidate for the maxilla of *Atlascopcosaurus loadsi*, which appears to be relatively more robust than the maxilla of *L. amicagraphica* (see Fig. 10). The possibility that the range of *Q. intrepidus* extends to the Eumeralla Formation is strengthened by the presence of two isolated dentary teeth (NMV P177934, P186426) from Dinosaur Cove that closely resemble the teeth of *Q. intrepidus* (Fig. 20.3–20.8).

If temporal separation of the Wonthaggi and Eumeralla formations by ~ 12 Myr was considered a parameter supporting taxic separation of the ornithopods between these formations, the question of *Q. intrepidus* validity would diminish. This view finds support from the work of Dodson (1990), who

https://doi.org/10.1017/jpa.2018.95

Table 5. Distribution of Australian ornithopods. VHFT2 = Victorian hypsilophodontid femur type 2; VOD2 = Victorian ornithopod dentary morphotype 2; VOD3 = Victorian ornithopod dentary morphotype 3; VOM4 = Victorian ornithopod maxilla morphotype 4; VOPC1 = Victorian ornithopod postcranium type 1; VOPC2 = Victorian ornithopod postcranium type 2.

Taxon	Locality	Stratum and age
Leaellynasaura amicagraphica Rich and Rich, 1989	Dinosaur Cove, Victoria	Eumeralla Formation, Otway Group, Otway Basin (lower Aptian)
Atlascopcosaurus loadsi Rich and Rich, 1989	Point Lewis and Dinosaur Cove, Victoria	Eumeralla Formation, Otway Group, Otway Basin (lower Aptian)
Ornithopoda indet. (NMV P185992/P185993 = VOPC1)	Dinosaur Cove, Victoria	Eumeralla Formation, Otway Group, Otway Basin (lower Aptian)
Ornithopoda indet. (NMV P186047 = VOPC2)	Dinosaur Cove, Victoria	Eumeralla Formation, Otway Group, Otway Basin (lower Aptian)
Diluvicursor pickeringi Herne et al., 2018	Eric the Red West, Victoria	Eumeralla Formation, Otway Group, Otway Basin (lower Aptian)
Galleonosaurus dorisae n. gen. n. sp.	Flat Rocks and The Caves, Victoria	Wonthaggi Formation, Strzelecki Group, Gippsland Basin (upper Barremian)
cf. *Atlascopcosaurus loadsi* (VOM4)	Flat Rocks, Victoria	Wonthaggi Formation, Strzelecki Group, Gippsland Basin (upper Barremian)
Qantassaurus intrepidus	Flat Rocks, Victoria	Wonthaggi Formation, Strzelecki Group, Gippsland Basin (upper Barremian)
Qantassaurus ?*intrepidus* (VOD2)	Flat Rocks, Victoria	Wonthaggi Formation, Strzelecki Group, Gippsland Basin (upper Barremian)
Ornithopoda indet. (VOD3)	Flat Rocks, Victoria	Wonthaggi Formation, Strzelecki Group, Gippsland Basin (upper Barremian)
Ornithopoda indet. (VHFT2)	Cape Paterson, Victoria	Wonthaggi Formation, Strzelecki Group, Gippsland Basin (upper Barremian)
Ornithopoda indet. (*Fulgurotherium australe* von Huene, 1932)	Lightning Ridge, New South Wales	Griman Creek Formation, Rolling Downs Group, Surat Basin (Albian)
Muttaburrasaurus langdoni Bartholomai and Molnar, 1981	Muttaburra, Queensland	Mackunda Formation, Manuka Subgroup, Rolling Downs Group, Eromanga Basin (upper Albian)
Muttaburrasaurus sp.	Hughenden, Queensland	Allaru Mudstone, Wilgunya Subgroup, Rolling Downs Group, Eromanga Basin (upper Albian)
Ornithopoda indet. (QM F52774)	Winton, Queensland	Winton Formation, Eromanga Basin (upper Cenomanian–lower Turonian)
Ornithopoda indet. (Lark Quarry tracks)	Winton, Queensland	Winton Formation, Eromanga Basin (upper Cenomanian–lower Turonian)
Ornithopoda indet. (Broome tracks)	Dampier Peninsula, Western Australia	Broome Sandstone (Valanginian–Barremian)

tentatively estimated that the mean duration of dinosaur genera might have been ~7.7 Myr. However, owing to the limited exposure of strata in the Eumeralla and Wonthaggi formations and the typically fragmentary and isolated nature of the fossils preserved, the nature of turnover and the duration of ornithopod genera across these formations is unlikely to be confidently ascertained in the immediate future.

We are presently uncertain whether the maxillary morphotype VOM4 (i.e., cf. *Atlascopcosaurus loadsi*) from the Wonthaggi Formation is categorically separable from the Eumeralla Formation genus *Atlascopcosaurus* (Figs. 17, 18). The U-shaped cingular vertex and ornamentation on the labial surfaces of the VOM4 maxillary tooth crowns are closer to those of *Atlascopcosaurus loadsi* than those of *Galleonosaurus dorisae* n. gen. n. sp. (Fig. 17). Given its older age, however, VOM4 is potentially precursory to *Atlascopcosaurus loadsi*. A further dentary form, identified in this work as VOD2 (= *Qantassaurus* ? *intrepidus*; Figs. 21, 27; Table 5), includes specimens (NMV P198962, P199087; Fig. 21) originally assigned to *Qantassaurus intrepidus* by Rich and Rich (1999). According to these authors, the 'bloated' appearance of one of the specimens (NMV P198962) was potentially indicative of a pathological condition. However, the morphological similarity between the two VOD2 specimens alternatively suggests that this bloated form is not isolated to one individual and could represent dimorphism in *Q. intrepidus*, or alternatively, a feature of a separate but closely related taxon.

Originally referred to *Leaellynasaura amicagraphica* as a part of the holotype (Rich and Rich, 1989), assignment of the partial postcranial skeleton NMV P185992/P185993 (='Victorian ornithopod postcranium type 1' [VOPC1, herein]; Herne, 2014) from Dinosaur Cove (Figs. 1.2, 27) is presently uncertain (Herne et al., 2016). These remains, as well as the second partial postcranium from the same locality (NMV P186047 ='VOPC2' [based on Herne, 2014]) could pertain to *L. amicagraphica*. However, taphonomic assessment of this locality also suggests that these two postcrania could alternatively pertain to *Atlascopcosaurus loadsi*, which has been identified at the same locality, or a separate taxon or taxa (Herne et al., 2016). *Diluvicursor pickeringi* is potentially synonymous with any one of *Atlascopcosaurus loadsi*, *L. amicagraphica*, *Galleonosaurus dorisae* n. gen. n. sp., or *Qantassaurus intrepidus*. However, synonymy could only be determined from future discoveries of anatomically overlapping materials. 'Victorian Hypsilophodontid Femur Type 2' (Rich and Rich, 1989) from Cape Paterson in the Wonthaggi Formation (Figs. 1.2, 27; Table 5) seems to represent a larger ornithopodan body form than inferred from the materials of the presently named Victorian ornithopods.

In summary, five ornithopod taxa have been named from the Early Cretaceous of Victoria (Figs. 1.2, 27; Table 5), including: *Leaellynasaura amicagraphica* and *Atlascopcosaurus loadsi* from the Eumeralla Formation, known from their maxillae; *Qantassaurus intrepidus* from the Wonthaggi Formation, known from its dentary; *Diluvicursor pickeringi* from the Eumeralla Formation, known from a partial postcranium (Herne et al., 2018); and *Galleonosaurus dorisae* n. gen. n. sp. from the Wonthaggi Formation, known from its maxilla. Synonymy between some of these taxa is possible but could only be ascertained from the discovery of more complete specimens in the future.

https://doi.org/10.1017/jpa.2018.95

Three jaw morphotypes are further identified (VOD2 [*Q.* ?*intrepidus*], VOD3 and VOM4 [cf. *Atlascopcosaurus loadsi*]). Associations between these morphotypes and the named Victorian ornithopods are presently uncertain. However, we consider that the dentary morphotype VOD3 a reasonable candidate for the presently unknown dentary of *Galleonosaurus dorisae* n. gen. n. sp. The large femoral morphotype (Victorian Hypsilophodontid Femur Type 2) potentially represents an additional taxon of Victorian ornithopod.

Phylogenetic affinities of the Victorian ornithopods.—The strict consensus tree from the initial IW searches, with all taxa included, produced a polytomy near the base of Ornithopoda, above the branch of *Parksosaurus warreni*. Following a priori removal of *Qantassaurus intrepidus*, which was identified by iterative PCR as a wildcard taxon, a Gondwanan clade was subsequently recovered (Fig. 25.2), consistent with the revised definition of Elasmaria (Text S1; see also Calvo et al., 2007) as all taxa closer to *Macrogryphosaurus gondwanicus* and *Talenkauen santacrucensis* than to *Hypsilophodon foxii* or *Iguanodon bernissartensis* (see also Rozadilla et al., 2016). Elasmaria was originally recovered within Iguanodontia (Calvo et al., 2007), but more recently as a polytomous clade of Argentinian and Antarctic nonhadrosaurian ornithopods, sister to *Gasparinisaura cincosaltensis*, which together, formed an unnamed clade nested within Ornithopoda (Rozadilla et al., 2016). The analysis by Rozadilla et al. (2016) recovered an ornithopod topology substantially differing from ours, particularly in its inclusion of *Thescelosaurus neglectus* within Ornithopoda, *Hypsilophodon foxii* as the basalmost ornithopod, and *P. warreni* and all other ornithopods as sister to the aforementioned unnamed Gondwanan clade. However, it is notable that the Antarctic taxa *Morrosaurus antarcticus* Rozadilla et al., 2016 and *Trinisaura santamartaensis* Coria et al., 2013, included in the analysis by Rozadilla et al. (2016) and recovered as elasmarians, were excluded from our analysis.

The Early Cretaceous Victorian ornithopods, *Diluvicursor pickeringi*, *Galleonosaurus dorisae* n. gen. n. sp., and *Leaellynasaura amicagraphica*, along with *Anabisetia saldiviai*, *Gasparinisaura cincosaltensis*, *Macrogryphosaurus gondwanicus*, and *Talenkauen santacrucensis* from the Late Cretaceous of Argentina, were recovered herein within Elasmaria (Fig. 26). However, this grouping was too weakly supported at present to afford definitive systematic assignment of the Victorian taxa to Elasmaria. From the time-calibrated phylogeny, generated from the IW strict consensus (Fig. 28), *Galleonosaurus dorisae* n. gen. n. sp. represents the earliest elasmarian presently known. None of the elasmarian taxa, as recovered, possessed all of the synapomorphies identified over all nodes (see Text S1). However, the following three synapomorphies possessed by the two Victorian taxa *Galleonosaurus dorisae* n. gen. n. sp. and *L. amicagraphica* are of interest to this present investigation. These include having: (1) the apical end of the primary ridge labially on the maxillary crowns offset to the distal third of the crown surface (character 308), shared with *Gasparinisaura cincosaltensis* and *Talenkauen santacrucensis*; (2) the basal vertex on the maxillary crowns offset mesially relative to the central axis of the tooth root (character 309), not shared with any other elasmarian, although possibly present in *Talenkauen*

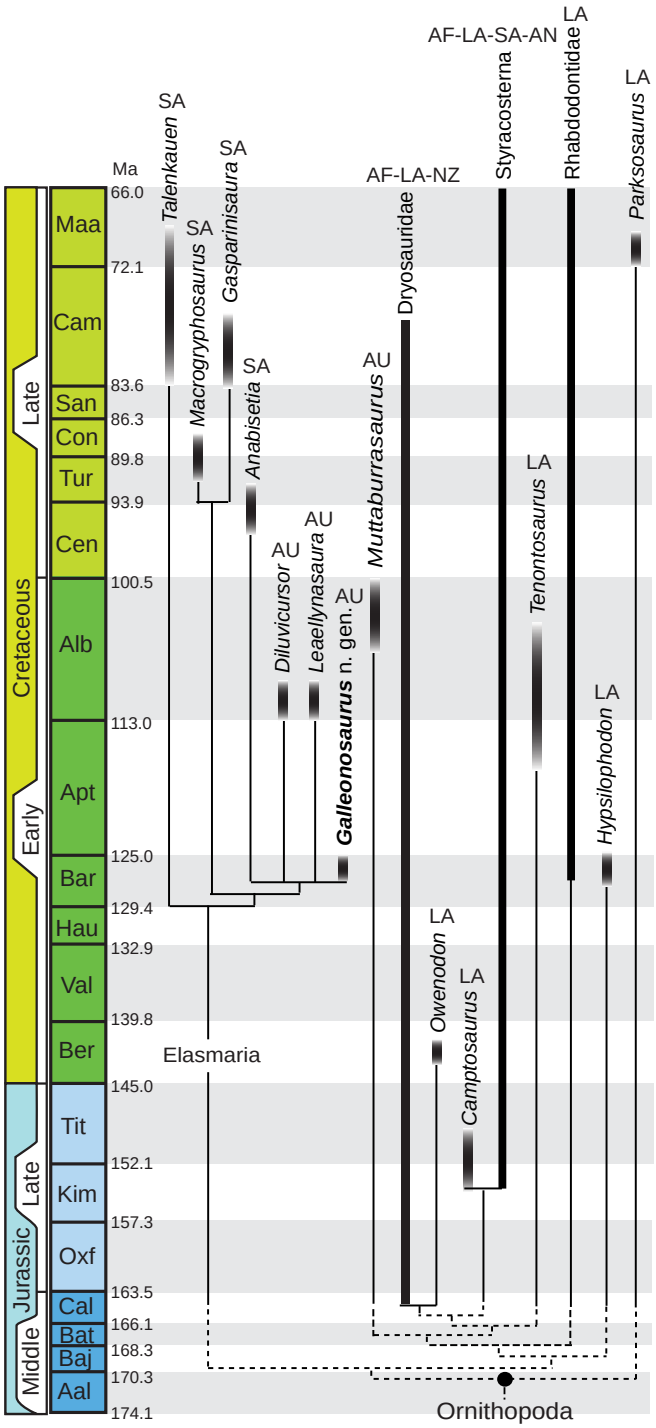

Figure 28. Time-calibrated phylogeny of the ornithopods from the IW strict consensus cladogram (Fig. 25.2). Dashed lines indicate unknown times of Pangaean branch/lineage divergences prior to the middle Callovian. Time scale based on Cohen et al. (2013). Thick lines indicate taxon (graduated shaded lines) and clade (solid lines) durations (for sources, see Text S1). Aal = Aalenian; AF = Africa; Alb = Albian; AN = Antarctica; Apt = Aptian; AU = Australia; Baj = Bajocian; Bar = Barremian; Bat = Bathonian; Ber = Berriasian; Cal = Callovian; Cam = Campanian; Cen = Cenomanian; Con = Coniacian; Hau = Hauterivian; Kim = Kimmeridgian; LA = Laurasia; Maa = Maastrichtian; NZ = New Zealand; Oxf = Oxfordian; SA = South America; San = Santonian; Tit = Tithonian; Tur = Turonian; Val = Valanginian.

santacrucensis; and (3) the apicobasal ridges labially on the maxillary crowns convergent in the direction of the primary ridge, toward the crown base (character 311), shared with

https://doi.org/10.1017/jpa.2018.95

Gasparinisaura cincosaltensis and *Talenkauen santacrucensis*. These three features, also present in *Atlascopcosaurus loadsi*, which was not included in the analysis owing to incompleteness, suggest that this taxon is likely to be an elasmarian.

In regard to the postcranially-based taxon *Diluvicursor pickeringi*, a T-shaped distal end profile on metatarsal I (character 334) is synapomorphically shared with *Anabisetia saldiviai* (see Herne et al., 2018). This feature is also present in the partial postcranium, VOPC1 (i.e., NMV P185992/P185993), from Dinosaur Cove. A further elasmarian synapomorphy, that of a proximally lunate, transversely compressed metatarsal II, at 50% or less than the width of metatarsal III (character 335), is synapomorphically shared among *Anabisetia saldiviai*, *Diluvicursor pickeringi*, and *Gasparinisaura cincosaltensis* (see Herne et al., 2018). This feature is also present in the aforementioned partial postcranium (VOPC1) and the other partial postcranium from Dinosaur Cove (VOPC2; i.e., NMV P186047).

The recovery of *Muttaburrasaurus langdoni* as a nondryomorphan iguanodontian signals a more complex history of ornithopod distributions extending to eastern Gondwana than that posed by the Gondwanan-centered Elasmaria (Fig. 28). This complexity is deepened further by the presence of an ilium (CD529) from the Campanian–Maastrichtian of New Zealand, tentatively regarded as a dryosaurid (Wiffen and Molnar, 1989; for age of specimen, see Text S1). Although dryosaurids are otherwise only known from Laurasia and Africa, this ilium strongly suggests that they also had an eastern Gondwanan distribution. Dryosaurids have not been positively identified from Australia yet, but their presence is possible. At least one isolated, although presently unassigned, ilium of an ornithischian from the Wonthaggi Formation (NMV P228444; figured by Rich, 2010, p. 16; unpublished data, Herne, 2018), possessing features resembling those in *Dryosaurus* spp., *Dysalotosaurus lettowvorbecki*, and *Valdosaurus canaliculatus* Galton, 1975, e.g., a low dorsoventral profile, a dorsoventrally 'pinched' postacetabular process, and a markedly triangular brevis shelf (see Janensch, 1955; Galton, 1981; Galton and Taquet, 1982; Barrett et al., 2011), support this possibility. However, it is important to note that these features are also present on the ilia of the elasmarians *Anabisetia saldiviai*, *Gasparinisaura cincosaltensis*, and *Macrogryphosaurus gondwanicus*.

Qantassaurus intrepidus was pruned from the secondary analyses, following its identification as wildcard. However, initial searches suggesting a basal position in Ornithopoda and comparisons of the dentary teeth indicating a close resemblance to those of *Talenkauen santacrucensis*, suggest that *Q. intrepidus* might be an elasmarian (Figs. 25.2, 28). However, the dentary teeth of *Q. intrepidus*, *Talenkauen santacrucensis* (see Cambiaso, 2007, fig. 17E, F), and the two isolated *Q. intrepidus*-like teeth from Dinosaur Cove (NMV P177934, P186426; Fig. 20) also resemble the singly known dentary tooth of *Kangnasaurus coetzeei* (Fig. 20) from the Late Cretaceous of South Africa (following de Wit et al., 1992)—a taxon that has been considered a dryosaurid (Cooper, 1985; Barrett et al., 2011). Although we did not include *K. coetzeei* in the dataset, primarily because of the problematic provenance of its materials (see also Haughton, 1915; Cooper, 1985), close resemblance among the dentary teeth of *Q. intrepidus*, *Talenkauen santacrucensis*, and the *K. coetzeei*-attributed tooth, suggests either the presence of an elasmarian in the Late Cretaceous of Africa (i.e., *K. coetzeei*), or that *Q. intrepidus* and *Talenkauen santacrucensis* might be closer to the dryosaurids than currently understood. This latter possibility finds support from the aforementioned ilium of a dryosaurid in New Zealand and the dryosaurid-like ilium from Victoria, as previously mentioned.

Some features of the dentition suggest that *Muttaburrasaurus langdoni* (and *Muttaburrasaurus* sp., QM F14921) could have closer affinities to the elasmarians than to the clypeodontans, as recovered. Firstly, multiple lingulate denticles along the apical margins of the cheek teeth (character 305) are lacking on the *Muttaburrasaurus* spp. crowns, but otherwise are present in all other clypeodontans, with the possible exception of *Kangnasaurus coetzeei*. This feature is also lacking in the elasmarians, *Anabisetia saldiviai*, *Leaellynasaura amicagraphica*, *Galleonosaurus dorisae* n. gen. n. sp., *Gasparinisaura cincosaltensis*, and *Talenkauen santacrucensis*, as well as on the dentary crowns of *Qantassaurus intrepidus*. Secondly, marked mesial offset of the cingular vertex on the maxillary tooth crowns was also recovered as autapomorphic in *M. langdoni*. However, even though the analysis failed to describe apomorphies in *L. amicagraphica* and *Galleonosaurus dorisae* n. gen. n. sp., this feature is also present in these two latter Victorian taxa. These two aforementioned features of *Muttaburrasaurus* spp. shared with elasmarians could be independently acquired, as the analysis suggests. However, we entertain the possibility that more complete data for the Victorian taxa could pull *Muttaburrasaurus* spp. and the elasmarians closer together than presently realized.

Several postcranial features variously possessed by elasmarian taxa are also possessed by the dryosaurids. Two of these features—a dorsoventrally low ilium (not included in the dataset) and a triangular brevis shelf (character 331), present in *Anabisetia saldiviai* (see Coria and Calvo, 2002), *Gasparinisaura cincosaltensis* (MCS-3; Salgado et al., 1997; unpublished data, Herne, 2008), and *Macrogryphosaurus gondwanicus* (see Calvo et al., 2007)—were mentioned above. These features are also present in the four dryosaurids, *Dryosaurus* spp., *Dysalotosaurus lettowvorbecki*, *Eousdryosaurus nanohallucis* Escaso et al., 2014, and *Valdosaurus canaliculatus* (Janensch, 1955; Galton, 1981; Escaso et al., 2014; Barrett, 2016), and also the iguanodontians *Planicoxa venenica* DiCroce and Carpenter, 2001 and *Osmakasaurus depressus* Gilmore, 1909 (Carpenter and Wilson, 2008; McDonald, 2011) not included in this study. However, it is of note that the presence of a triangular brevis shelf (character 331) was not recovered as synapomorphic in any of the clades. In addition, two further features are of interest. A deep muscle scar for the m. caudofemoralis longus on the diaphysis of the femur, markedly inset from the base of the fourth trochanter (character 256), present in *Anabisetia saldiviai* (MCF-PVPH-75; unpublished data, Herne, 2008) and a proximally lunate, transversely compressed proximoplantal portion of metatarsal II (i.e., character 335), present in *Anabisetia saldiviai*, *Diluvicursor pickeringi*, and *Gasparinisaura cincosaltensis*, are features also present in the four aforementioned dryosaurids (see also Herne et al., 2018, regarding the form of metatarsal II). The inset femoral muscle scar on the femur for the m. caudofemoralis longus is also present in *Callovosaurus leedsi* Lydekker, 1889 (Ruiz-Omeñaca et al., 2006) and *Elrhazosaurus nigeriensis* Galton and Taquet, 1982 (Galton, 2009)—taxa also

https://doi.org/10.1017/jpa.2018.95

considered to be dryosaurids. However, the three postcranial features mentioned above and included as characters in the dataset (i.e., characters 256, 331, and 335) failed to influence the recovery of taxa within Elasmaria closer to the dryosaurids, or even within Dyomorpha. Taken explicitly, the strict consensus results suggest that these postcranial features arose independently in the elasmarians and the dryosaurids.

The oldest record for the ornithopods is at least indicated by the dryosaurid *Callovosaurus leedsi* (see Ruiz-Omeñaca et al., 2006) from the middle Callovian of the Oxford Clay Formation, England (~ 165 Ma; see Fig. 28). Based on this age, both Elasmaria and *Muttaburrasaurus* spp. would have diverged from other ornithopod lineages prior to the middle Callovian (>165 Ma). This timing of divergence indicates that the origins of Elasmaria and the stem of *Muttaburrasaurus* spp. trace to Pangaea, prior to the opening of seaways between Laurasia and Gondwana in the Callovian (e.g., Iturralde-Vinent, 2006; Pindell and Kennan, 2009). The lengthy ghost lineages of Elasmaria (Fig. 28) and *Muttaburrasaurus* spp. likely reflect the poor body-fossil record of Gondwanan dinosaurs between the middle and earliest Cretaceous (e.g., Weishampel et al., 2004; Mateus, 2006, Dunhill et al., 2016).

Distribution of Australian ornithopods.—Based on newly described craniodental materials from the Flat Rocks locality, including *Galleonosaurus dorisae* n. gen. n. sp., assessment of Australian ornithopod diversity can be updated. The tooth morphology of the Victorian ornithopod dentary morphotype VOD3 resembles the isolated ornithopod tooth (QM F52774) described by Hocknull and Cook (2008, although reported as a maxillary tooth) from the Cenomanian–Turonian Winton Formation, Queensland (age based on Tucker et al., 2013; Figs. 24, 27). The similarity between these teeth suggests that the temporal and geographic range of closely related small-bodied ornithopods in eastern Australia extended from at least the upper Barremian of the Australian-Antarctic rift system to the middle Cretaceous of the Eromanga Basin, central-eastern Australia (Figs 1.3, 27). This distribution is augmented by the identification of small-bodied ornithopod body fossils from the Albian Griman Creek Formation, strata of which crop out at Lightning Ridge, northern New South Wales (Molnar and Galton, 1986; Bell et al., 2017), and small-bodied (and possibly large-bodied) ornithopod trackways at Lark Quarry in the Winton Formation (Thulborn and Wade, 1984; Romilio et al., 2013; Fig. 27). Diverse small- to large-bodied ornithopod trackways have also been described from the Valanginian–Barremian Broome Sandstone, which crops out along the coast of the Dampier Peninsula in Western Australia (Salisbury et al., 2017; Fig. 27). The only body fossils of a large-bodied ornithopod presently described from Australia are those of *Muttaburrasaurus* spp., all of which are from the late Albian Allaru Mudstone and overlying Mackunda Formation in central western Queensland (Bartholomai and Molnar, 1981; Molnar, 1996; Fig. 27). Maxillary teeth further suggest the presence of a *Muttaburrasaurus*-like ornithopod in the Griman Creek Formation at Lightning Ridge. These teeth appear to be of a size between those of the Victorian taxa (e.g., *Galleonosaurus dorisae* n. gen. n. sp.) and *Muttaburrasaurus* sp. (QM F14921), suggesting that a midsized ornithopod could have also been present in this region. Large-bodied ornithopod remains are presently unknown from the Early Cretaceous of Victoria, with the largest taxon presently represented by the femur assigned to 'Victorian Hypsilophodontid Femur Type 2' (Rich and Rich, 1989; Fig. 27). The occurrences of body fossils and tracks from the aforementioned Australian regions combined confirm that ornithopods formed a diverse fauna of dinosaurian herbivores across this continent during at least the Valanginian–Turonian (Fig. 27).

Conclusions

The identification of the new ornithopod, *Galleonosaurus dorisae* n. gen. n. sp., and three further jaw morphotypes (VOM4, VOD2, and VOD3) from the Flat Rocks locality in the upper Barremian Wonthaggi Formation complements the four previously named ornithopods from Victoria—*Atlascopcosaurus loadsi*, *Diluvicursor pickeringi*, *Leaellynasaura amicagraphica*, and *Qantassaurus intrepidus*. Although synonymy between some of these taxa is possible, *Galleonosaurus dorisae* n. gen. n. sp. and the newly identified craniodental morphotypes confirm that a highly diverse small-bodied ornithopod fauna flourished in the periodically disturbed, high-latitude, riverine floodplain environment of the Australian-Antarctic rift valley (see also Rich and Rich, 1989; Rich and Vickers-Rich, 1999, 2000; Rich et al., 2002; Herne et al., 2016, 2018).

The new dentary morphotype from the Flat Rocks Sandstone (VOD3) confirms the presence of an ornithopod with a more elongate dentary than that of *Qantassaurus intrepidus*, from the same locality, and with more alveoli in specimens of similar size (15 alveoli compared to 10). We speculate that VOD3 is a more likely candidate for the presently unknown dentary of *Galleonosaurus dorisae* n. gen. n. sp. than the dentary of *Q. intrepidus*, although this suggestion cannot be presently confirmed. The similarity between the dentary teeth of VOD3 and an isolated dentary tooth (QM F52774) discovered in the Winton Formation, central-western Queensland (Hocknull and Cook, 2008) suggests that the spatiotemporal range of potentially closely related ornithopods in eastern Australia extended from at least the upper Barremian of the Australian-Antarctic rift system to the lower Turonian of the Eromanga Basin (Figs. 1.3, 27).

The phylogenetic analysis (Figs. 25.2, 26) recovered the Victorian ornithopods *Diluvicursor pickeringi*, *Leaellynasaura amicagraphica*, and *Galleonosaurus dorisae* n. gen. n. sp. within Elasmaria (Calvo et al., 2007). In addition to the Victorian taxa, Elasmaria also comprises the Argentinian taxa *Anabisetia saldiviai*, *Gasparinisaura cincosaltensis*, *Macrogryphosaurus gondwanicus*, and *Talenkauen santacrucensis*. Increased anatomical understanding of the ornithopods recovered within Elasmaria, and particularly the Victorian ornithopods, will undoubtedly impel renewed phylogenetic assessment. The large-bodied Australian genus *Muttaburrasaurus*, however, is a nonelasmarian and was recovered within Iguanodontia. The time-calibrated phylogeny derived from the IW strict consensus tree (Fig. 28) suggests that Elasmaria and the stem of *Muttaburrasaurus langdoni* had

https://doi.org/10.1017/jpa.2018.95

their origins in Pangaea prior to the opening of seaways between Gondwana and Laurasia in the middle Callovian.

Acknowledgments

The authors acknowledge the Eastern Maar and Bunurong peoples, the Traditional Owners of the fossil sites, and pay respect to their Elders past and present. For access to specimens in their care we thank P. Barrett, R. Coria, D. Pickering, L. Salgado, K. Seymour, K. Spring, and T. Zeigler. We additionally thank D. Brinkman (YPM), P. Currie, M. Hall, D. Henry, A. Heimer, D. Herne, G. Kool (discoverer of the holotype of *Galleonosaurus dorisae* n. gen. n. sp.), L. Kool, M. Lamanna, K. Poole, T. Rich, J. Rosine, S. Salisbury, D. Schwarz, D. Seegets-Villiers, P. Vickers-Rich, B. Wagstaff, W. White, and Monash University and Museums Victoria staff and volunteers of the Dinosaur Dreaming Project. We gratefully thank the late D. Pickering for preparation of the holotype of *Galleonosaurus dorisae* n. gen. n. sp. The authors thank the reviewers P. Galton and P. Godefroit, Academic Editor H.-D. Sues and JPA editors J. Kastigar and P. Mikkelsen for their reviews and comments that greatly improved the quality this paper, and L. Marra for journal production (Cambridge University Press). Travel expenses for MCH were covered in part by a UQ Graduate School Research Travel Grant.

Accessibility of supplemental data

Data available from the Dryad Digital Repository: http://doi.org/10.5061/dryad.rm8bk77.

Supplemental data include: Table S1, list of cranial specimens observed in this study; Text S1, additional remarks on phylogenetic data and analyses in this study; Text S2, phylogenetic character list; and Supplemental Data 1, character-taxon dataset; Supplemental Data 2, CT dataset.

References

Agnolín, F.L., and Rozadilla, S., 2018, Phylogenetic reassessment of *Pisanosaurus mertii* Casamiquela, 1967, a basal dinosauriform from the Late Triassic of Argentina: Journal of Systematic Palaeontology, v. 16, p. 853–879, doi:10.1080/14772019.2017.1352623.

Agnolin, F.L., Ezcurra, M.N.D., Pais, D.F., and Salisbury, S.W., 2010, A reappraisal of the Cretaceous non-avian dinosaur faunas from Australia and New Zealand: Evidence for their Gondwanan affinities: Journal of Systematic Palaeontology, v. 8, p. 257–300, doi:10.1080/14772011003594870.

Alifanov, V.R., 2003, Two new dinosaurs of the infraorder Neoceratopsia (Ornithischia) from the Upper Cretaceous of the Nemegt Depression, Mongolian People's Republic: Paleontological Journal, v. 37, p. 524–534.

Bakker, R.T., Galton, P.M., Siegwarth, J., and Filla, J., 1990, A new latest Jurassic vertebrate fauna, from the highest levels of the Morrison Formation at Como Bluff, Wyoming, Part IV, The dinosaurs: A new *Othnielia*-like hypsilophodontid: Hunteria, v. 2, p. 8–19.

Barker, C.T., Naish, D., Newham, E., Katsamenis, O.L., and Dyke, G., 2017, Complex neuroanatomy in the rostrum of the Isle of Wight theropod *Neovenator salerii*: Scientific Reports: v. 7, p. e3749, doi:10.1038/s41598-017-03671-3.

Barrett, P.M., 2016, A new specimen of *Valdosaurus canaliculatus* (Ornithopoda: Dryosauridae) from the Lower Cretaceous of the Isle of Wight, England: Memoirs of Museum Victoria, v. 74, p. 29–48.

Barrett, P.M., and Han, F., 2009, Cranial anatomy of *Jeholosaurus shangyuanensis* (Dinosauria: Ornithischia) from the Early Cretaceous of China: Zootaxa, v. 2072, p. 31–55, doi:10.5281/zenodo.187103.

Barrett, P.M., Rich, T.H., Vickers-Rich, P., Tumanova, T.A., Inglis, M., Pickering, D., Kool, L., and Kear, B.P., 2010, Ankylosaurian dinosaur remains from the Lower Cretaceous of southeastern Australia: Alcheringa, v. 34, p. 205–217, doi:10.1080/03115511003655430.

Barrett, P.M., Butler, R.J., Twitchett, R.J., and Hutt, S., 2011, New material of *Valdosaurus canaliculatus* (Ornithischia: Ornithopoda) from the Lower Cretaceous of southern England: Special Papers in Palaeontology, v. 86, p. 131–163, doi:10.1111/J.1475-4983.2011.01076.x.

Bartholomai, A., and Molnar, R.E., 1981, *Muttaburrasaurus*, a new iguanodontid (Ornithischia: Ornithopoda) dinosaur from the Lower Cretaceous of Queensland: Memoirs of the Queensland Museum, v. 20, p. 319–349.

Behrensmeyer, A.K., 1982, Time resolution in fluvial vertebrate assemblages: Paleobiology, v. 8, p. 211–227.

Bell, P.R., Herne, M.C., and Smith, E., 2017, New ornithopods (Dinosauria) from the Lower Cretaceous Griman Creek Formation (Albian) at Lightning Ridge, NSW, Australia, *in* Seventy-seventh Annual Meeting Society of Vertebrate Paleontology, Calgary, Alberta, Canada, Meeting Program and Abstracts, p. 80.

Bengston, P., 1988, Open nomenclature: Paleontology, v. 31, p. 223–227.

Benoit, J., Manger, P.R., and Rubidge, B.S., 2016, Palaeoneurological clues to the evolution of defining mammalian soft tissue traits: Scientific Reports, v. 6, p. e25604, doi:10.1038/srep25604.

Benson, R.B.J., Rich, T.H., Vickers-Rich, P., and Hall, M., 2012, Theropod fauna from southern Australia indicates high polar diversity and climate-driven dinosaur provinciality: PLoS ONE: v. 7, p. e37122, doi:10.1371/journal.pone.0037122.

Boulenger, G.A., 1881, Sur l'arc pelvien chez les dinosauriens de Bernissart: Bulletins de l'Académie Royale des Sciences, des Lettres et des Beaux-Arts de Belgique, ser. 3, v. 1, p. 600–608.

Boyd, C.A., 2014, The cranial anatomy of the neornithischian dinosaur *Thescelosaurus neglectus*: PeerJ: v. 2, p. e669, doi:10.7717/peerj.669.

Boyd, C.A., 2015, The systematic relationships and biogeographic history of ornithischian dinosaurs: PeerJ: v. 3, p. e1523, doi:10.7717/peerj.1523.

Brazeau, M.D., 2011, Problematic character coding methods in morphology and their effects: Biological Journal of the Linnean Society, v. 104, p. 489–498, doi:10.1111/j.1095-8312.2011.01755.x.

Brown, B., and Schlaikjer, E.M., 1940, The structure and relationships of *Protoceratops*: Annals of the New York Academy of Sciences, v. 40, p. 133–266.

Brown, C.M., Boyd, C.A., and Russell, A.P., 2011, A new basal ornithopod dinosaur (Frenchman Formation, Saskatchewan, Canada), and implications for late Maastrichtian ornithischian diversity in North America: Zoological Journal of the Linnean Society, v. 163, p. 1157–1198, doi:10.1111/j.1096-3642.2011.00735.x.

Brown, C.M., Evans, D.C., Ryan, M.J., and Russell, A.P., 2013, New data on the diversity and abundance of small-bodied ornithopods (Dinosauria, Ornithischia) from the Belly River Group (Campanian) of Alberta: Journal of Vertebrate Paleontology, v. 33, p. 495–520, doi:10.1080/02724634.2013.746229.

Bryan, S.E., 2007, Silicic large igneous provinces: Episodes, v. 30, p. 20–31.

Bryan, S.E., Constantine, A.E., Stephens, C.J., Ewart, A., Schon, R.W., and Parianos, J., 1997, Early Cretaceous volcano-sedimentary successions along the eastern Australian continental margin: Implications for the break-up of eastern Gondwana: Earth and Planetary Science Letters, v. 153, p. 85–102.

Bryan, S.E., Ewart, A., Stephens, C.J., Parianos, J., and Downes, P.J., 2000, The Whitsunday Volcanic Province, central Queensland, Australia: Lithological and stratigraphic investigations of a silicic-dominated large igneous province: Journal of Volcanology and Geothermal Research, v. 99, p. 55–78, doi:10.1016/S0377-0273(00)00157-8.

Butler, R.J., Upchurch, P., and Norman, D.B., 2008, The phylogeny of the ornithischian dinosaurs: Journal of Systematic Palaeontology, v. 6, p. 1–40, doi:10.1017/S1477201907002271.

Butler, R.J., Jin, L., Jun, C., and Godefroit, P., 2011, The postcranial osteology and phylogenetic position of the small ornithischian dinosaur *Changchunsaurus parvus* from the Quantou Formation (Cretaceous: Aptian–Cenomanian) of Jilin Province, north-eastern China: Palaeontology, v. 54, p. 667–683, doi:10.1111/j.1475-4983.2011.01046.x.

Calvo, J.O., Porfiri, J.D., and Novas, F.E., 2007, Discovery of a new ornithopod dinosaur from the Portezuelo Formation (Upper Cretaceous), Neuquén, Patagonia, Argentina: Arquivos do Museu Nacional, Rio de Janeiro, v. 65, p. 471–483.

Cambiaso, A.V., 2007, Los ornitópodos e iguanodontes basales (Dinosauria, Ornithischia) del Cretácico de Argentina y Antártida [Ph.D. Thesis]: Buenos Aires, Argentina, Universidad de Buenos Aires, 411 p.

Carpenter, K., 1992, Tyrannosaurids (Dinosauria) of Asia and North America, *in* Mateer, N.J., and Chen, P., eds., Aspects of Nonmarine Cretaceous Geology: Beijing, China, China Ocean Press, p. 250–268.

Carpenter, K., and Galton, P.M., 2018, A photo documentation of bipedal ornithischian dinosaurs from the Upper Jurassic Morrison Formation, USA: Geology of the Intermountain West, v. 5, p. 167–207.

Carpenter, K., and Wilson, Y., 2008, A new species of *Camptosaurus* (Ornithopoda: Dinosauria) from the Morrison Formation (Upper Jurassic) of Dinosaur National Monument, Utah, and a biomechanical analysis of its forelimb: Annals of the Carnegie Museum, v. 76, p. 227–263.

Casamiquela, R.M., 1967, Un nuevo dinosaurio ornitisquio Triásico (*Pisanosaurus mertii*: Ornithopoda) de la Formacion Ischigualasto, Argentina: Ameghiniana, v. 5, p. 47–64.
Chiupka, J.W., 1996, Hydrocarbon play fairways of the onshore Gippsland Basin, Victoria: Melbourne, Victoria, Australia, Department of Natural Resources and Environment, Victorian Initiative for Minerals and Petroleum Report 30, 50 p.
Close, R.A., Vickers-Rich, P., Trusler, P., Chiappe, L.M., O'Connor, J.K., Rich, T.H., Kool, L., and Komarower, P., 2009, Earliest Gondwanan bird from the Cretaceous of southeastern Australia: Journal of Vertebrate Paleontology, v. 29, p. 616–619, doi:10.1671/039.029.0214.
Cohen, K.M., Finney, S.C., Gibbard, P.L., and Fan, J.-X., 2013, The ICS International Chronostratigraphic Chart: Episodes, v. 36, p. 199–204.
Congreve, C.R., and Lamsdell, J.C., 2016, Implied weighting and its utility in palaeontological datasets: A study using modelled phylogenetic matrices: Palaeontology, v. 59, p. 447–462, doi:10.1111.pala.12236.
Constantine, A.E., and Holdgate, G.R., 1993, Selwyn Symposium, Gippsland Basin Excursion Guide: Melbourne, Geological Society of Australia, Victoria Division, 20 p.
Cookson, I., and Dettmann, M.E., 1958, Some trilete spores from upper Mesozoic deposits in the eastern Australian region: Proceedings of the Royal Society of Victoria, v. 70, p. 95–128.
Cooper, M.R., 1985, A revision of the ornithischian dinosaur *Kangnasaurus coetzeei* Haughton, with a classification of the Ornithischia: Annals of the South African Museum, v. 95, p. 281–317.
Coria, R.A., and Calvo, J.O., 2002, A new iguanodontian ornithopod from Neuquén Basin, Patagonia, Argentina: Journal of Vertebrate Paleontology, v. 22, p. 503–509, doi:10.1671/0272-4634(2002)022[0503:ANIOFN]2.0.CO;2.
Coria, R.A., and Salgado, L., 1996, A basal iguanodontian (Ornithischia: Ornithopoda) from the Late Cretaceous of South America: Journal of Vertebrate Paleontology, v. 16, p. 445–457.
Coria, R.A., Moly, J.J., Reguero, M., Santillana, S., and Marenssi, S., 2013, A new ornithopod (Dinosauria; Ornithischia) from Antarctica: Cretaceous Research, v. 41, p. 186–193.
Crompton, A.W., and Charig, A.J., 1962, A new ornithischian from the Upper Triassic of South Africa: Nature, v. 196, p. 1074–1077.
de Wit, M.C.J., Ward, J.D., and Spaggiari, R., 1992, A reappraisal of the Kangnas dinosaur site, Bushmanland, South Africa: South African Journal of Science, v. 88, p. 504–507.
DiCroce, T., and Carpenter, K., 2001, New ornithopod from the Cedar Mountain Formation (Lower Cretaceous) of eastern Utah, *in* Tanke, D. H., and Carpenter, K., eds., Mesozoic Vertebrate Life: New Research Inspired by the Paleontology of Philip J. Currie: Bloomington and Indianapolis, Indiana University Press, p. 183–196.
Dieudonné, P.-E., Tortosa, T., Torcida Fernández-Baldor, F., Canudo, J.I., and Díaz-Martínez, I., 2016, An unexpected early rhabdodontid from Europe (Lower Cretaceous of Salas de los Infantes, Burgos Province, Spain) and a re-examination of basal iguanodontian relationships: PLoS ONE: v. 11, p. e0156251, doi:10.1371/journal.pone.0156251.
Dodson, P., 1990, Counting dinosaurs: How many kinds were there?: Proceedings of the National Academy of Sciences of the United States of America, v. 87, p. 7608–7612.
Dong, Z., and Azuma, Y., 1997, On a primitive neoceratopsian from the Early Cretaceous of China, *in* Dong, Z., ed., Sino-Japanese Silk Road Dinosaur Expedition: Beijing, China Ocean Press, p. 68–89.
Dunhill, A., Bestwick, J., Narey, H., and Sciberras, J., 2016, Dinosaur biogeographic structure and Mesozoic continental fragmentation: A network-based approach: Journal of Biogeography, v. 43, p. 1691–1704, doi:10.1111/jbi.12766.
Edmund, A.G., 1957, On the special foramina in the jaws of many ornithischian dinosaurs: Contributions of the Royal Ontario Museum Division of Zoology and Palaeontology, v. 48, p. 1–14.
Edmund, A.G., 1960, Tooth replacement phenomena in the lower vertebrates: Royal Ontario Museum, Contributions of the Life Sciences Division, v. 52, p. 1–190.
Escaso, F., Ortega, F., Dantas, P., Malafaia, E., Silva, B., Gasulla, J.M., Mocho, P., Narváez, I., and Sanz, J.L., 2014, A new dryosaurid ornithopod (Dinosauria, Ornithischia) from the Late Jurassic of Portugal: Journal of Vertebrate Paleontology, v. 34, p. 1102–1112, doi:10.1080/02724634.2014.849715.
Fanti, F., Cau, A., Panzarin, L., and Cantelli, L., 2016, Evidence of iguanodontian dinosaurs from the Lower Cretaceous of Tunisia: Cretaceous Research, v. 60, p. 267–274, doi:10.1016/j.cretres.2015.12.008.
Felton, E.A., 1997, A non-marine Lower Cretaceous rift-related epiclastic volcanic unit in southern Australia: The Eumeralla Formation in the Otway Basin, Part II, Fluvial systems: ASGO Journal of Australian Geology and Geophysics, v. 16, p. 731–757.
Forey, P.L., and Kitching, I.J., 2000, Experiments in coding multistate characters, *in* Scotland, R.W., and Pennington, R.T., eds., Homology and Systematics: Coding Characters for Phylogenetic analysis: London, Taylor and Francis, p. 54–80.
Galton, P.M., 1974, The ornithischian dinosaur *Hypsilophodon* from the Wealden of the Isle of Wight: Bulletin of the British Museum (Natural History), Geology, v. 25, p. 1–152.
Galton, P.M., 1975, English hypsilophodontid dinosaurs (Reptilia; Ornithischia): Palaeontology, v. 18, p. 741–752.
Galton, P.M., 1978, Fabrosauridae, the basal family of ornithischian dinosaurs (Reptilia: Ornithopoda): Paläontologische Zeitschrift, v. 52, p. 138–159.
Galton, P.M., 1981, *Dryosaurus*, a hypsilophodontid dinosaur from the Upper Jurassic of North America and Africa: Postcranial skeleton: Paläontologische Zeitschrift, v. 55, p. 271–312.
Galton, P.M., 1983, The cranial anatomy of *Dryosaurus*, a hypsilophodontid dinosaur from the Upper Jurassic of North America and East Africa, with a review of hypsilophodontids from the Upper Jurassic of North America: Geologica et Palaeontologica, v. 17, p. 207–243.
Galton, P.M., 1997, Cranial anatomy of the basal hypsilophodontid dinosaur *Thescelosaurus neglectus* Gilmore (Ornithischia: Ornithopoda) from the Upper Cretaceous of North America: Revue Paleobiologie, v. 16, p. 231–258.
Galton, P.M., 2009, Notes on Neocomian (Lower Cretaceous) ornithopod dinosaurs from England—*Hypsilophodon*, *Valdosaurus*, "*Camptosaurus*," "*Iguanodon*"—and referred specimens from Romania and elsewhere: Revue de Paléobiologie, v. 28, p. 211–273.
Galton, P.M., and Sues, H.-D., 1983, New data on pachycephalosaurid dinosaurs (Reptilia: Ornithischia) from North America: Canadian Journal of Earth Sciences, v. 20, p. 462–472.
Galton, P.M., and Taquet, P., 1982, *Valdosaurus*, a hypsilophodontid dinosaur from the Lower Cretaceous of Europe and Africa: Geobios, v. 15, p. 147–159.
Gasulla, J.M., Escaso, F., Ortega, F., and Sanz, J.L., 2014, New hadrosauriform cranial remains from the Arcillas de Morella Formation (lower Aptian) of Morella, Spain: Cretaceous Research, v. 47, p. 19–24, doi:10.1016/j.cretres.2013.10.004.
Gilmore, C.W., 1909, Osteology of the Jurassic reptile *Camptosaurus*, with a revision of the species of the genus, and descriptions of two new species: Proceedings of the United States National Museum, v. 36, p. 197–332.
Gilmore, C.W., 1913, A new dinosaur from the Lance Formation of Wyoming: Smithsonian Miscellaneous Collections, v. 61, p. 1–5.
Gilmore, C.W., 1924, On *Troodon validus*, an orthopodous dinosaur from the Belly River Cretaceous of Alberta, Canada: University of Alberta, Department of Geology, Bulletin, v. 1, p. 1–43.
Godefroit, P., Codrea, V.A., and Weishampel, D.B., 2009, Osteology of *Zalmoxes shqiperorum* (Dinosauria, Ornithopoda), based on new specimens from the Upper Cretaceous of Nălaţ-Vad (Romania): Geodiversitas, v. 31, p. 525–553, doi:10.5252/g2009n3a3.
Godefroit, P., Escuillié, F., Bolotsky, Y.L., and Lauters, P., 2012, A new basal hadrosauroid dinosaur from the Upper Cretaceous of Kazakhstan, *in* Godefroit, P., ed., Bernissart Dinosaurs and Early Cretaceous Terrestrial Ecosystems: Bloomington and Indianapolis, Indiana University Press, p. 334–358.
Goloboff, P.A., 1993, Estimating character weights during tree search: Cladistics, v. 9, p. 83–91.
Goloboff, P.A., 2014, Extended implied weighting: Cladistics, v. 30, p. 260–272, doi:10.1111/cla.12047.
Goloboff, P.A., and Catalano, S.A., 2016, TNT version 1.5, including a full implementation of phylogenetic morphometrics: Cladistics, v. 32, p. 221–238, doi:10.1111/cla.12160.
Goloboff, P.A., and Szumik, C.A., 2015, Identifying unstable taxa: Efficient implementation of triplet-based measures of stability, and comparison with Phyutility and RogueNaRok: Molecular Phylogenetics and Evolution, v. 88, p. 93–104, doi:10.1016/j.ympev.2015.04.003.
Goloboff, P.A., Farris, J.S., Källersjö, M., Oxelman, B., Ramirez, M.I., and Szumik, C.A., 2003, Improvements to resampling measures of group support: Cladistics, v. 19, p. 324–332, doi:10.1016/S0748-3007(03)00060-4.
Goloboff, P.A., Torres, A., and Arias, J.S., 2018, Weighted parsimony outperforms other methods of phylogenetic inference under models appropriate for morphology: Cladistics, v. 34, p. 407–437, doi:10.1111/cla.12205.
Granger, W., and Gregory, W.K., 1923, *Protoceratops andrewsi*, a preceratopsian dinosaur from Mongolia: American Museum Novitates, v. 72, p. 1–9.
Hall, M., and Keetley, J., 2009, Geoscience Victoria 3D Victoria, Report 2: Melbourne, Victoria, Australia, Department of Primary Industries, 75 p.
Han, F., Barrett, P.M., Butler, R.J., and Xu, X., 2012, Postcranial anatomy of *Jeholosaurus shangyuanensis* (Dinosauria, Ornithischia) from the Lower Cretaceous Yixian Formation of China: Journal of Vertebrate Paleontology, v. 32, p. 1370–1395, doi:10.1080/02724634.2012.694385.
Haughton, S.H., 1915, On some dinosaur remains from Bushmanland: Transactions of the Royal Society of South Africa, v. 5, p. 259–264.
Hauser, D.L., and Presch, W., 1991, The effect of ordered characters on phylogenetic reconstruction: Cladistics, v. 7, p. 243–265.
He, X., 1979, [A newly discovered ornithopod dinosaur *Yandusaurus* from Zigong, Sichuan], *in* Contributions to International Exchange of Geology,

Part 2 (Stratigraphy and Paleontology): Beijing, China, Geological Publishing House, p. 116–123 (in Chinese).
He, X., and Cai, K., 1983, [A new species of *Yandusaurus* (hypsilophodont dinosaur) from the Middle Jurassic of Dashanpu, Zigong, Sichuan]: Journal of the Chengdu College of Geology, suppl. 1, p. 5–14 (in Chinese).
He, Y., Makovicky, P.J., Xu, X., and You, H., 2018, High-resolution computed tomographic analysis of tooth replacement pattern of the basal neoceratopsian *Liaoceratops yanzigouensis* informs ceratopsian dental evolution: Scientific Reports: v. 8, p. 5870, doi:10.1038/s41598-018-24283-5.
Heaton, M.J., 1972, The palatal structure of some Canadian Hadrosauridae (Reptilia: Ornithischia): Canadian Journal of Earth Sciences, v. 9, p. 185–205.
Heine, C., Yeo, L.G., and Müller, R.D., 2015, Evaluating global paleoshoreline models for the Cretaceous and Cenozoic: Australian Journal of Earth Sciences, v. 62, p. 275–287, doi:10.1080/08120099.2015.1018321.
Helby, R., Morgan, R., and Partridge, A.D., 1987, A palynological zonation of the Australian Mesozoic: Memoirs of the Association of Australasian Palaeontologists, v. 4, p. 1–94.
Herne, M.C., 2009, Postcranial osteology of *Leaellynasaura amicagraphica* (Dinosauria; Ornithischia) from the Early Cretaceous of southeastern Australia [abs.]: Journal of Vertebrate Paleontology, v. 29, suppl. 3, p. 113A.
Herne, M.C., 2014, Anatomy, systematics and phylogenetic relationships of the Early Cretaceous ornithopod dinosaurs of the Australian-Antarctic rift system [Ph.D. Thesis]: Brisbane, Australia, The University of Queensland, 464 p.
Herne, M.C., Tait, A.M., and Salisbury, S.W., 2016, Sedimentological reappraisal of the *Leaellynasaura amicagraphica* (Dinosauria, Ornithopoda) holotype locality in the Lower Cretaceous of Victoria, Australia with taphonomic implications for the taxon: New Mexico Museum of Natural History and Science Bulletin, v. 71, p. 121–148.
Herne, M.C., Tait, A.M., Weisbecker, V., Hall, M., Nair, J.P., Cleeland, M., and Salisbury, S.W., 2018, A new small-bodied ornithopod (Dinosauria, Ornithischia) from an Early Cretaceous deep, high-energy river of the Australian-Antarctic rift system: PeerJ: v. 5, p. e4113, doi:10.7717/peerj.4113.
Hocknull, S.A., and Cook, A.G., 2008, Hypsilophodontid (Dinosauria: Ornithischia) from latest Albian, Winton Formation, central Queensland: Memoirs of the Queensland Museum, v. 52, p. 212.
Hooley, R.W., 1925, On the skeleton of *Iguanodon atherfieldensis* sp. nov., from the Wealden shales of Atherfield (Isle of Wight): Quarterly Journal of the Geological Society of London, v. 81, p. 1–61.
Horner, J.R., 1992, Cranial morphology of *Prosaurolophus* (Ornithischia: Hadrosauridae) with descriptions of two new hadrosaurid species and an evaluation of hadrosaurid phylogenetic relationships: Museum of the Rockies, Occassional Paper, v. 2, p. 1–119.
Horner, J.R., and Weishampel, D.B., 1988, A comparative embryological study of two ornithischian dinosaurs: Nature, v. 332, p. 256–257.
Hübner, T.R., and Rauhut, O.W.M., 2010, A juvenile skull of *Dysalotosaurus lettowvorbecki* (Ornithischia: Iguanodontia), and implications for cranial ontogeny, phylogeny, and taxonomy in ornithopod dinosaurs: Zoological Journal of the Linnean Society, v. 160, p. 366–396, doi:10.1111/j.1096-3642.2010.00620.x.
Huxley, T.H., 1870, On *Hypsilophodon foxii*, a new dinosaurian from the Wealden of the Isle of Wight: Quarterly Journal of the Geological Society of London, v. 25, p. 3–12.
Intergovernmental Committee on Surveying and Mapping, 2014, GDA94: Geocentric Datum of Australia, Technical Manual Version 2.4: Canberra, Australian Capital Territory, Commonwealth of Australia, 52 p.
Iturralde-Vinent, M., 2006, Meso-Cenozoic Caribbean paleogeography: Implications for the historical biogeography of the region: International Geology Review, v. 48, p. 791–827, doi:10.2747/0020-6814.48.9.791.
Janensch, W., 1955, Der ornithopode *Dysalotosaurus* der Tendaguruschichten: Palaeontographica (supplement 7), v. 3, p. 105–176.
Jin, L., Chen, J., Zan, S., Butler, R.J., and Godefroit, P., 2010, Cranial anatomy of the small ornithischian dinosaur *Changchunsaurus parvus* from the Quantou Formation (Cretaceous: Aptian–Cenomanian) of Jilin Province, northeastern China: Journal of Vertebrate Paleontology, v. 30, p. 196–214, doi:10.1080/02724630903412372.
Kitching, I.J., Forey, P.L., Humphries, C.J., and Williams, D.M., 1998, Cladistics: The Theory and Practice of Parsimony Analysis, 2nd edition: Oxford, UK, Oxford University Press, 228 p.
Kool, L., 2010, Dinosaur Dreaming: Exploring the Bass Coast of Victoria: Melbourne, Victoria, Australia, Monash Science Centre, 95 p.
Korasidis, V.A., Wagstaff, B.E., Gallagher, S.J., Duddy, I.R., Tosolini, A.M.P., Cantrill, D.J., and Norvick, M.S., 2016, Early angiosperm diversification in the Albian of southeast Australia: Implications for flowering plant radiation across eastern Gondwana: Review of Palaeobotany and Palynology, v. 232, p. 61–80, doi:10.1016/j.revpalbo.2016.04.005.
Lambe, L.M., 1902, On Vertebrata of the mid-Cretaceous of the North West Territory, 2, New genera and species from the Belly River Series (mid-Cretaceous): Geological Survey of Canada, Contributions to Canadian Palaeontology, v. 3, p. 23–81.
Lambe, L.M., 1917, A new genus and species of crestless hadrosaur from the Edmonton Formation of Alberta: Ottawa Naturalist, v. 31, p. 65–73.
Lydekker, R., 1889, On the remains and affinities of five genera of Mesozoic reptiles: Quarterly Journal of the Geological Society of London, v. 45, p. 41–59.
Maddison, W.P., and Maddison, D.R., 2009, Mesquite: A modular system for evolutionary analysis, ver. 3.40: Mesquite Software, Inc., http://mesquiteproject.org.
Madzia, D., Boyd, C.A., and Mazuch, M., 2018, A basal ornithopod dinosaur from the Cenomanian of the Czech Republic: Journal of Systematic Palaeontology, v. 16, p. 967–979, doi:10.1080/14772019.2017.1371258.
Mallon, J.C., 2017, Recognizing sexual dimorphism in the fossil record: Lessons from nonavian dinosaurs: Paleobiology, v. 43, p. 495–507, doi:10.1017/pab.2016.51.
Mantell, G.A., 1848, On the structure of the jaws and teeth of the *Iguanodon*: Philosophical Transactions of the Royal Society of London, v. 138, p. 183–202.
Marsh, O.C., 1877, Notice of some new vertebrate fossils: American Journal of Science, ser. 3, v. 14, p. 249–256.
Marsh, O.C., 1878, Principal characters of American Jurassic dinosaurs, Part 1: American Journal of Science, ser. 3, v. 16, p. 411–416.
Marsh, O.C., 1879, Notice of new Jurassic reptiles: American Journal of Science, ser. 3, v. 18, p. 501–505.
Marsh, O.C., 1881, Principal characters of American Jurassic dinosaurs, Part V: American Journal of Science, ser. 3, v. 21, p. 417–423.
Marsh, O.C., 1894, The typical Ornithopoda of the American Jurassic: American Journal of Science, ser. 3, v. 48, p. 85–90.
Maryanska, T., and Osmolska, H., 1974, Pachycephalosauria, a new suborder of ornithischian dinosaurs: Palaeontologia Polonica, v. 30, p. 45–102.
Maryanska, T., and Osmolska, H., 1975, Protoceratopsidae (Dinosauria) of Asia: Palaeontologia Polonica, v. 33, p. 133–182.
Mateus, O., 2006, Late Jurassic dinosaurs from the Morrison Formation (USA), the Lourinha and Alcobaca formations (Portugal), and the Tendaguru Beds (Tanzania): A comparison: New Mexico Museum of Natural History and Science Bulletin, v. 36, p. 223–231.
McDonald, A.T., 2011, The taxonomy of species assigned to *Camptosaurus* (Dinosauria: Ornithopoda): Zootaxa, v. 2783, p. 52–68.
Molnar, R.E., 1996, Observations on the Australian ornithopod dinosaur *Muttaburrasaurus*: Memoirs of the Queensland Museum, v. 39, p. 639–652.
Molnar, R.E., and Galton, P.M., 1986, Hypsilophodontid dinosaurs from Lightning Ridge, New South Wales, Australia: Geobios, v. 19, p. 231–239.
Nopcsa, F., 1900, Dinosaurierreste aus Siebenbürgen (Schadel von *Limnosaurus transsylvanicus* nov. gen. et spec.): Denkschriften der Kaiserlichen Akademie der Wissenschaften Wein, Mathematisch-Naturwissenschaftliche Klasse, v. 68, p. 555–591.
Nopcsa, F., 1904, Dinosaurierreste aus Siebenbürgen III (weitere schadelreste von *Mochlodon*): Denkschriften der Kaiserlichen Akademie der Wissenschaften Wein, Mathematisch-Naturwissenschaftliche Klasse, v. 74, p. 229–263.
Norman, D.B., 1986, On the anatomy of *Iguanodon atherfieldensis* (Ornithischia: Ornithopoda): Bulletin de l'Institut Royal des Sciences Naturelles de Belgique, Sciences de la Terre, v. 56, p. 281–372.
Norman, D.B., 2004, Basal Iguanodontia, *in* Weishampel, D.B., Dodson, P., and Osmólksa, H., eds., The Dinosauria, 2nd edition: Berkeley, University of California Press, p. 413–437.
Norman, D.B., and Barrett, P.M., 2002, Ornithischian dinosaurs from the Lower Cretaceous (Berriasian) of England: Special Papers in Palaeontology, v. 68, p. 161–189.
Norman, D.B., Sues, H.-D., Witmer, L.M., and Coria, R.A., 2004, Basal Ornithopoda, *in* Weishampel, D.B., Dodson, P., and Osmólksa, H., eds., The Dinosauria, 2nd edition: Berkeley, University of California Press, p. 393–412.
Norman, D.B., Crompton, A.W., Butler, R.J., Porro, L.B., and Charig, A.J., 2011, The Lower Jurassic ornithischian dinosaur *Heterodontosaurus tucki* Crompton & Charig, 1962: Cranial anatomy, functional morphology, taxonomy, and relationships: Zoological Journal of the Linnean Society, v. 163, p. 182–276, doi:10.1111/j.1096-3642.2011.00697.x.
Novas, F.E., Cambiaso, A.V., and Ambrosio, A., 2004, A new basal iguanodontian (Dinosauria, Ornithischia) from the Upper Cretaceous of Patagonia: Ameghiniana, v. 41, p. 75–82.
Osborn, J.W., 1975, Tooth replacement: Efficiency, patterns and evolution: Evolution, v. 29, p. 180–186.
Ostrom, J.H., 1970, Stratigraphy and paleontology of the Cloverly Formation (Lower Cretaceous) of the Bighorn Basin area, Wyoming and Montana: Bulletin of the Peabody Museum of Natural History, v. 35, p. 1–234.
Owen, R., 1842, Report on British fossil reptiles, Part 2: Report of the British Association for the Advancement of Science, Plymouth, v. 11, p. 60–204.
Owen, R., 1874, Monograph on the fossil Reptilia of the Wealden and Purbeck formations, Supplement 5, Dinosauria (*Iguanodon*) [Wealden and Purbeck]: Palaeontographical Society Monographs, v. 27, p. 1–18.

Parks, W.A., 1926, *Thescelosaurus warreni*, a new species of orthopodous dinosaur from the Edmonton Formation of Alberta: University of Toronto Studies, Geological Series, v. 21, p. 1–42.
Peng, G., 1990, [A new small ornithopod (*Agilisaurus louderbacki* gen. et sp. nov.) from Zigong, China]: Newsletter of the Zigong Dinosaur Museum, v. 2, p. 19–27 (in Chinese).
Perle, A., Maryanska, T., and Osmolska, H., 1982, *Goyocephale lattimorei* gen. et sp. n., a new flat-headed pachycephalosaur (Ornithischia, Dinosauria) from the Upper Cretaceous of Mongolia: Acta Palaeontologica Polonica, v. 27, p. 115–127.
Pindell, J.L., and Kennan, L., 2009, Tectonic evolution of the Gulf of Mexico, Caribbean and northern South America in the mantle reference frame: An update: Geological Society, London, Special Publications, v. 328, p. 1–55, doi:10.1144/SP328.1.
Pol, D., and Escapa, I.H., 2009, Unstable taxa in cladistic analysis: Identification and the assessment of relevant characters: Cladistics, v. 25, p. 515–527, doi:10.1111/j.1096-0031.2009.00258.x.
Pompeckj, J.F., 1920, Das angebliche Vorkommen und Wandern des Parietalforamens bei Dinosauriern: Sitzungsberichte der Gesellschaft Naturforschender Freunde zu Berlin, v. 1920, p. 109–129.
Poropat, S.F., Martin, S.K., Tosolini, A.-M.P., Wagstaff, B.E., Bean, L.B., Kear, B.P., Vickers-Rich, P., and Rich, T.H., 2018, Early Cretaceous polar biotas of Victoria, southeastern Australia—An overview of research to date: Alcheringa: An Australasian Journal of Palaeontology, v. 42, p. 157–229, doi:10.1080/03115518.2018,1453085.
Porro, L.B., Butler, R.J., Barrett, P.M., Moore-Fay, S.C., and Abel, R.L., 2011, New heterodontosaurid specimens from the Lower Jurassic of southern Africa and the early ornithischian dinosaur radiation: Earth and Environmental Science Transactions of the Royal Society of Edinburgh, v. 101, p. 351–366, doi:10.1017/S175569101102010X.
Porro, L.B., Witmer, L.M., and Barrett, P.M., 2015, Digital preparation and osteology of the skull of *Lesothosaurus diagnosticus* (Ornithischia: Dinosauria): PeerJ, v. 3, p. e1494, doi:10.7717/peerj.1494.
Reig, O.A., 1963, La presencia de dinosaurios saurisquios en los "estratos de Ischigualasto" (Mesotriassico superior) de las provincias de San Juan y La Rioja (Republica Argentina): Ameghiniana, v. 3, p. 3–20.
Rich, T.H., 2010, Research report, *in* Kool, L., ed., Dinosaur Dreaming 2010 Field Report: Melbourne, Victoria, Australia, Monash University, p. 16–18.
Rich, T.H., and Rich, P.V., 1989, Polar dinosaurs and biotas of the Early Cretaceous of southeastern Australia: National Geographic Society Research Reports, v. 5, p. 15–53.
Rich, T.H., and Vickers-Rich, P., 1999, The Hypsilophodontidae from southeastern Australia: National Science Museum Monographs, v. 15, p. 167–180.
Rich, T.H., and Vickers-Rich, P., 2000, Dinosaurs of Darkness: Sydney, New South Wales, Australia, Allen & Unwin, 222 p.
Rich, T.H., Vickers-Rich, P., and Gangloff, R.A., 2002, Polar dinosaurs: Science, v. 295, p. 979–980, doi:10.1126/science.1068920.
Rich, T.H., Galton, P.M., and Vickers-Rich, P., 2010, The holotype individual of the ornithopod dinosaur *Leaellynasaura amicagraphica* Rich & Rich, 1989 (late Early Cretaceous, Victoria, Australia): Alcheringa, v. 34, p. 385–396, doi:10.1080/03115518.2010.489404.
Romilio, A., Tucker, R.T., and Salisbury, S.W., 2013, Re-evaluation of the Lark Quarry dinosaur tracksite (late Albian–Cenomanian Winton Formation, central-western Queensland, Australia): No longer a stampede?: Journal of Vertebrate Paleontology, v. 33, p. 102–120, doi:10.1080/02724634.2012.694591.
Rozadilla, S., Agnolin, F.L., Novas, F.E., Aranciaga Rolando, A.M., Motta, M.J., Lirio, J.M., and Isasi, M.P., 2016, A new ornithopod (Dinosauria, Ornithischia) from the Upper Cretaceous of Antarctica and its palaeobiogeographical implications: Cretaceous Research, v. 57, p. 311–324, doi:10.1016/j.cretres.2015.09.009.
Ruiz-Omeñaca, J.I., Pereda Suberbiola, X., and Galton, P.M., 2006, *Callovosaurus leedsi*, the earliest dryosaurid dinosaur (Ornithischia: Euornithopoda) from the Middle Jurassic of England, *in* K. Carpenter, ed., Horns and Beaks: Ceratopsian and Ornithopod Dinosaurs: Bloomington and Indianapolis, Indiana University Press, p. 3–16.
Salgado, L., Coria, R.A., and Heredia, S.E., 1997, New materials of *Gasparinisaura cincosaltensis* (Ornithischia, Ornithopoda) from the Upper Cretaceous of Argentina: Journal of Paleontology, v. 71, p. 933–940.
Salisbury, S.W., Romilio, A., Herne, M.C., Tucker, R.T., and Nair, J.P., 2017, The dinosaurian ichnofauna of the Lower Cretaceous (Valanginian–Barremian) Broome Sandstone of the Walmadany area (James Price Point), Dampier Peninsula, Western Australia: Society of Vertebrate Paleontology Memoir (Journal of Vertebrate Paleontology, v. 36, supplement to 6, November 2016), v. 16, p. 1–152.
Seegets-Villiers, D., 2012, Taphonomy, palynology, dendrology and sedimentology of the Inverloch fossil site, Victoria, Australia [Ph.D. dissertation]: Melbourne, Victoria, Australia, Monash University, 173 p.
Seeley, H.G., 1888, On the classification of the fossil animals commonly named Dinosauria: Proceedings of the Royal Society of London, v. 43, p. 165–171.
Sereno, P.C., 1986, Phylogeny of the bird-hipped dinosaurs (Order Ornithischia): National Geographic Research, v. 2, p. 234–256.
Sues, H.-D., 1980, Anatomy and relationships of a new hypsilophodontid dinosaur from the Lower Cretaceous of North America: Palaeontographica Abteilung A, v. 169, p. 51–72.
Tanoue, K., You, H., and Dodson, P., 2009, Comparative anatomy of selected basal ceratopsian dentitions: Canadian Journal of Earth Sciences, v. 46, p. 425–439, doi:10.1139/E09-030.
Thomas, A.D., 2015, The cranial anatomy of *Tenontosaurus tilletti* Ostrom, 1970 (Dinosauria, Ornithopoda): Palaeontologia Electronica: v. 18, p. e37A, doi:10.26879/450.
Thompson, D.L., and Stilwell, J.D., 2010, Early Aptian (Early Cretaceous) freshwater bivalves from the Australian–Antarctic rift, southeast Victoria: Alcheringa, v. 34, p. 345–357, doi:10.1080/03115511003789023.
Thulborn, R.A., and Wade, M., 1984, Dinosaur trackways in the Winton Formation (mid-Cretaceous) of Queensland: Memoirs of the Queensland Museum, v. 21, p. 413–517.
Tosolini, A.-M.P., Mcloughlin, S., and Drinnan, A.N., 1999, Stratigraphy and fluvial sedimentary facies of the Neocomian lower Strzelecki Group, Gippsland Basin, Victoria: Australian Journal of Earth Sciences, v. 46, p. 951–970.
Tucker, R.T., Roberts, E.M., Yu, H., Kemp, A.I.S., and Salisbury, S.W., 2013, Detrital zircon age constraints for the Winton Formation, Queensland: Contextualizing Australia's Late Cretaceous dinosaur faunas: Gondwana Research, v. 24, p. 767–779, doi:10.1016/j.gr.2012.12.009.
VandenBerg, A.H.M., Cayley, R.A., Willman, C.E., Morand, V.J., Seymon, A.R., Osborne, C.R., Taylor, D.H., Haydon, S.J., McLean, M., Quinn, C., Jackson, P., and Sandford, A.C., 2006, Walhalla–Woods Point–Tallangallook special map area geological report: Melbourne, Victoria, Australia, Department of Primary Industries, Geological Survey of Victoria Report 127, 448 p.
von Huene, F.F., 1932, Die fossile Reptie-Ordung Saurischia, ihre Entwicklung und Geschichte: Monographien zur Geologie und Palaeontologie, ser. 1, v. 4, p. 1–361.
Wagstaff, B.E., and McEwen Mason, J., 1989, Palynological dating of Lower Cretaceous coastal vertebrate localities, Victoria, Australia: National Geographic Research, v. 5, p. 54–63.
Wandres, A.M., and Bradshaw, J.D., 2005, SW Pacific margin of Gondwana from conglomeratic rocks for the configuration of the New Zealand tectonostratigraphy and implications: Geological Society, London, Special Publications, v. 246, p. 179–216.
Weishampel, D.B, Jianu, C.-M., Csiki, Z., and Norman, D.B., 2003, Osteology and phylogeny of *Zalmoxes* (n. g.), an unusual euornithopod dinosaur from the latest Cretaceous of Romania: Journal of Systematic Palaeontology, v. 1, p. 65–123, doi:10.1017/S1477201903001032.
Weishampel, D.B., Barrett, P.M., Coria, R.A., Le Loeuff, J., Xu, X., Zhao, X., Sahni, A., Gomani, E.M.P., and Noto, C.R., 2004, Dinosaur distribution, *in* Weishampel, D.B., Dodson, P., and Osmólska, H., eds., The Dinosauria, 2nd ed.: Berkeley, University of California Press, p. 517–606.
Wiffen, J., and Molnar, R.E., 1989, An Upper Cretaceous ornithopod from New Zealand: Geobios, v. 22, p. 531–536.
Willcox, J.B., and Stagg, H.M.J., 1990, Australia's southern margin: A product of oblique extension: Tectonophysics, v. 173, p. 269–281.
Witmer, L.M., 1995, Homology of facial structures in extant archosaurs (birds and crocodilians), with special reference to paranasal pneumaticity and nasal conchae: Journal of Morphology, v. 225, p. 269–327.
Witmer, L.M., 1997, Craniofacial air sinus systems, *in* Currie, P.J., and Padian, K., eds., Encyclopedia of Dinosaurs: San Diego, California, Academic Press, p. 151–159.
Xu, X., Wang, X.-L., and You, H.-L., 2000, A primitive ornithopod from the Early Cretaceous Yixian Formation of Liaoning: Vertebrata PalAsiatica, v. 38, p. 318–325.
Xu, X., Makovicky, P.J., Wang, X., Norell, M.A., and You, H., 2002, A ceratopsian dinosaur from China and the early evolution of Ceratopsia: Nature, v. 416, p. 314–317.
Xu, X., Tan, Q., Gao, Y., Bao, Z., Yin, Z., Guo, B., Wang, J., Tan, L., Zhang, Y., and Xing, H., 2018, A large-sized basal ankylopollexian from East Asia, shedding light on early biogeographic history of Iguanodontia: Science Bulletin, v. 63, p. 556–563, doi:10.1016/j.scib.2018. 03.016.
You, H., and Dodson, P., 2003, Redescription of the neoceratopsian dinosaur *Archaeoceratops* and the early evolution of the Neoceratopsia: Acta Palaeontologica Polonica, v. 49, p. 261–272.
Zan, S., Chen, J., Jin, L.-Y., and Li, T., 2005, [A primitive ornithopod from the Early Cretaceous Quantou Formation of central Jilin, China]: Vertebrata PalAsiatica, v. 43, p. 182–193 (in Chinese)

Accepted: 1 November 2018